ABHISHEK MISHRA

NEURAL INFORMATION PROCESSING IN THE *DROSOPHILA* MOTION VISION PATHWAY

Graduate School of
Systemic Neurosciences
LMU Munich

Dissertation der Graduate School of Systemic Neurosciences der
Ludwig-Maximilians-Universität München

12th of October, 2022

Abhishek Mishra

Neural information processing in the Drosophila motion vision pathway

Dissertation der Graduate School of Systemic Neurosciences der
Ludwig-Maximilians-Universität München.

E-MAIL:
abhishek.mishra@bi.mpg.de

12th of October, 2022

First reviewer and supervisor
Prof. Dr. Alexander Borst

Second reviewer
Prof. Dr. Laura Busse

External reviewer
Prof. Dr. Gwyneth Card

Date of submission
12th of October, 2022

Date of Defense
13th of April, 2023

SUMMARY

Detecting the direction of image motion is an essential component of visual computation. An individual photoreceptor, however, does not explicitly represent the direction in which the image is shifting. Comparing neighboring photoreceptor signals over time is used to extract directional motion information from the photoreceptor array in the circuit downstream. To implement direction selectivity, two opposing models have been proposed. In both models, one input line is asymmetrically delayed compared to the other, followed by a non-linear interaction between the two input lines. The Hassenstein-Reichardt (HR) model proposes an enhancement in the preferred direction (PD): the preferred side signal is delayed and then amplified by multiplying it with the other input signal. In contrast, the Barlow-Levick (BL) detector proposes a null direction (ND) suppression, whereby the null side signal is delayed and the other input is divided by it. The motion information is computed in parallel ON and OFF pathways. T4 and T5 are the first direction-selective neurons found in the ON and in the OFF pathway, respectively. Four subtypes of T4 and T5 cells exist each responding selectively to one of the four cardinal directions: front-to-back, back-to-front, upwards, and downwards, respectively.

In the first manuscript, we found that both preferred direction enhancement and null direction suppression are implemented in the dendrites of all four subtypes of both T4 and T5 cells to compute the direction of motion. We, therefore, propose a hybrid model combining both PD enhancement on the preferred side and ND suppression on the null side. This combined strategy ensures a high degree of direction selectivity already at the first stage of calculating motion direction.

Further processing, in addition to synaptic mechanisms on the dendrites of T4 cells, can improve the direction selectivity of the T4 cells' output signals. Such processing might involve: 1.) transformation from voltage to calcium, and 2.) from calcium to neurotransmitter release. In the second manuscript, we used in vivo two-photon imaging of genetically encoded voltage and calcium indicators, Arclight and GCaMP6f respectively, to measure responses in *Drosophila* direction-selective T4 neurons. Comparison between Arclight and GCaMP6f signals revealed calcium signals to have a significantly higher direction selectivity compared to voltage signals. Using these recordings we built a model which transforms T4 voltage responses into calcium responses. The model reproduced experimentally measured calcium responses across different visual stimuli using various temporal filtering steps and a stationary non-linearity. These findings provided a mechanistic underpinning of the voltage-to-calcium transformation and showed how this processing step, in addition to synaptic mechanisms on the dendrites of T4 cells, enhances direction selectivity in the output signal of T4 neurons.

The two manuscripts included in this thesis are presented chronologically and were published in peer-reviewed journals.

CONTENTS

1 Introduction 1
  1.1 *Drosophila* as a model organism 1
  1.2 Tools for functional dissection of *Drosophila* neural circuits 1
    1.2.1 Targeting cell types: Gal4-UAS 1
    1.2.2 Measuring neural activity 2
    1.2.3 Manipulating neural activity 6
  1.3 Neural communication 7
    1.3.1 Electrical synapses 7
    1.3.2 Chemical synapses 7
    1.3.3 Voltage-gated ion channels 7
  1.4 The fly visual system 9
    1.4.1 The optic lobe 10
    1.4.2 Neural circuits underlying direction selectivity 12
    1.4.3 Neural algorithms underlying direction selectivity 15
  1.5 Concluding remarks 16
2 Publications 19
  2.1 A common directional tuning mechanism of *Drosophila* motion-sensing neurons in the ON and in the OFF pathway 19
  2.2 Voltage to calcium transformation enhances direction selectivity in *Drosophila* T4 neurons 37
3 Discussion 57
  3.1 Fly motion vision 57
    3.1.1 Models of motion detection 57
    3.1.2 Cellular implementation of motion vision 58
    3.1.3 Mechanism for the temporal delay 59
    3.1.4 Circuits downstream of T4 and T5 cells 61
  3.2 The effect of voltage-to-calcium transformation on the direction selectivity of T4 cells 64
  3.3 The function of the visual circuit during natural behavior 65
  3.4 Comparison with the direction-selective circuits in the mouse retina 66
  3.5 Neuronal calcium signaling 69
    3.5.1 Voltage-gated calcium channels 70
  3.6 Conclusion 71
Bibliography 73

LIST OF FIGURES

Figure 1 Genetic tools for functional manipulations in *Drosophila* 3
Figure 2 Chemical synapse: steps of synaptic transmission 8
Figure 3 Voltage-gated ion channels 9

Figure 4 The fly optic lobe 11
Figure 5 Synaptic sites distributed over T4 and T5 dendritic arbors 14
Figure 6 Models for motion detection 15
Figure 7 Distribution of the presynaptic partners, input synapses and receptors on the T4 and T5 dendrites 60
Figure 8 Lobula plate intrinsic neurons (LPis) 63
Figure 9 Tangential cells receive null direction responses from LPi neurons 64
Figure 10 Fly and mouse motion detection circuits 68

1 INTRODUCTION

1.1 *DROSOPHILA* AS A MODEL ORGANISM

Drosophila melanogaster is one of the most powerful model organisms available for the functional dissection of neural circuits. It allows for sophisticated *in vivo* neural manipulations that includes imaging, activation, and suppression of neural activity. The *Drosophila* research community has developed thousands of 'driver-lines' that can be used to express genes of interest in a neuron-specific manner (Pfeiffer *et al.* 2008). Additionally, *Drosophila* offers several practical advantages: fruit flies are small, have a short generation time of about 10 days, and are easy to grow in the lab.

The *Drosophila* brain is estimated to contain only about 200,000 neurons (Raji & Potter 2021) but produces behavior of rich complexity (Card & Dickinson 2008; Pavlou & Goodwin 2013; Ryu *et al.* 2022). In systems neuroscience, a common goal is to understand how the brain processes and extracts relevant information from the sensory inputs to produce behavior. *Drosophila* constitutes an ideal model organism to study the neural circuits and computations underlying behavior. Given some surprising parallels between how the fly and mammalian brains process information (Borst & Helmstaedter 2015), insights about the nervous system obtained in *Drosophila* often might be relevant for understanding the brain of other species (Bellen *et al.* 2010).

1.2 TOOLS FOR FUNCTIONAL DISSECTION OF *DROSOPHILA* NEURAL CIRCUITS

To have a detailed understanding of how a neural circuit functions, the role each individual neuron plays in that particular circuit needs to be known. To achieve this, the following three types of manipulations can be performed on the given neuron: (i) record neuronal activity, (ii) activate the neuron, and (iii) silence the neuron. Fortunately, decades of research in *Drosophila* have provided multiple tools that allow for these manipulations in the choice of the neuron. The most important tool that enables to do this in a neuron-specific manner is the Gal4-UAS system (figure 1).

1.2.1 Targeting cell types: Gal4-UAS

Following the discovery of transposable DNA sequences (P-elements) in the *Drosophila* genome (Rubin & Spradling 1982), the Gal4-UAS system was designed (Brand & Perrimon 1993). The Gal4-UAS system is a binary expression system consisting of two main components: the yeast transcriptional factor Gal4 expressed in a specific pattern, and a reporter gene under the control of a upstream activation sequence (UAS) promoter that is silent in the absence of Gal4. The Gal4-UAS system involves crossing two fly lines: one called the ’driver-line’, defines which neurons express the required effector gene; the other called ’reporter-line’, defines what gene is expressed in the neurons defined by the driver line (figure 1).

Another independent binary transcriptional system that can be used is the LexA-lexAop system. This method is based on the bacterial DNA-binding operator lexAop and controlled by the expression of LexA. The LexA binds to and activates the lexA operator (lexAop). The LexA-lexAop system can be used in combination with the Gal4-UAS system to simultaneously express two different genes in two different neuronal populations.

Initially, the Gal4 fly lines were created by injecting randomly integrating P-elements transposons into the Drosophila embryos. However, the lack of control over specific insertion sites often resulted in broader expression patterns, making them unsuitable for circuit manipulations. Currently, DNA fragments with presumed enhancer activity are directly cloned for increased efficacy, and intersectional strategies, such as the split-Gal4 are used for increased specificity (Jenett *et al.* 2012; Pfeiffer *et al.* 2008). In this method, the coding region of the Gal4 is split into two units: (i) the Gal4 activating domain (AD), and (ii) the Gal4 DNA binding domain (DBD). The expression of the Gal4-AD is under the control of one enhancer and the expression of the Gal4-DBD is under the control of another enhancer. The DBD and AD proteins alone are not able to promote gene expression; only cells where both enhancers are active produce functional Gal4 protein. Therefore, only in cells containing both subunits, the gene of interest is expressed (Luan *et al.* 2006). Thousands of fly lines have been generated as a result, and nearly every type of fly neuron can be targeted with high specificity (Pfeiffer *et al.* 2010).

1.2.2 Measuring neural activity

ELECTROPHYSIOLOGY Electrophysiological recordings are used to measure neural activity by recording voltage or current changes across the neuronal membrane at a high temporal resolution. Depending on where the electrode is placed in relation to the cell, electrophysiological recordings can be classified into three main types: (1) extracellular recordings; (2) intracellular recordings; and (3) patch-clamp recordings. The large membrane voltage changes during an action potential causes local, temporary differences in potential in the extracellular space near the membrane of an active neuron. In extracellular recordings, an electrode is placed in the vicinity of the neuron to record these extracellular voltage changes. In insects, however, neurons often do not fire action potentials, but rather use graded potentials (Haag & Borst 1998). In the blowfly *Calliphora erythrocephala*, intracellular recordings using a sharp electrode were used to characterize the large lobula plate tangential cells (Hausen 1976; Krapp *et al.* 1998).

The small size of *Drosophila* neurons makes sharp electrode recordings difficult. The third variant, the whole-cell patch-clamp recordings were found

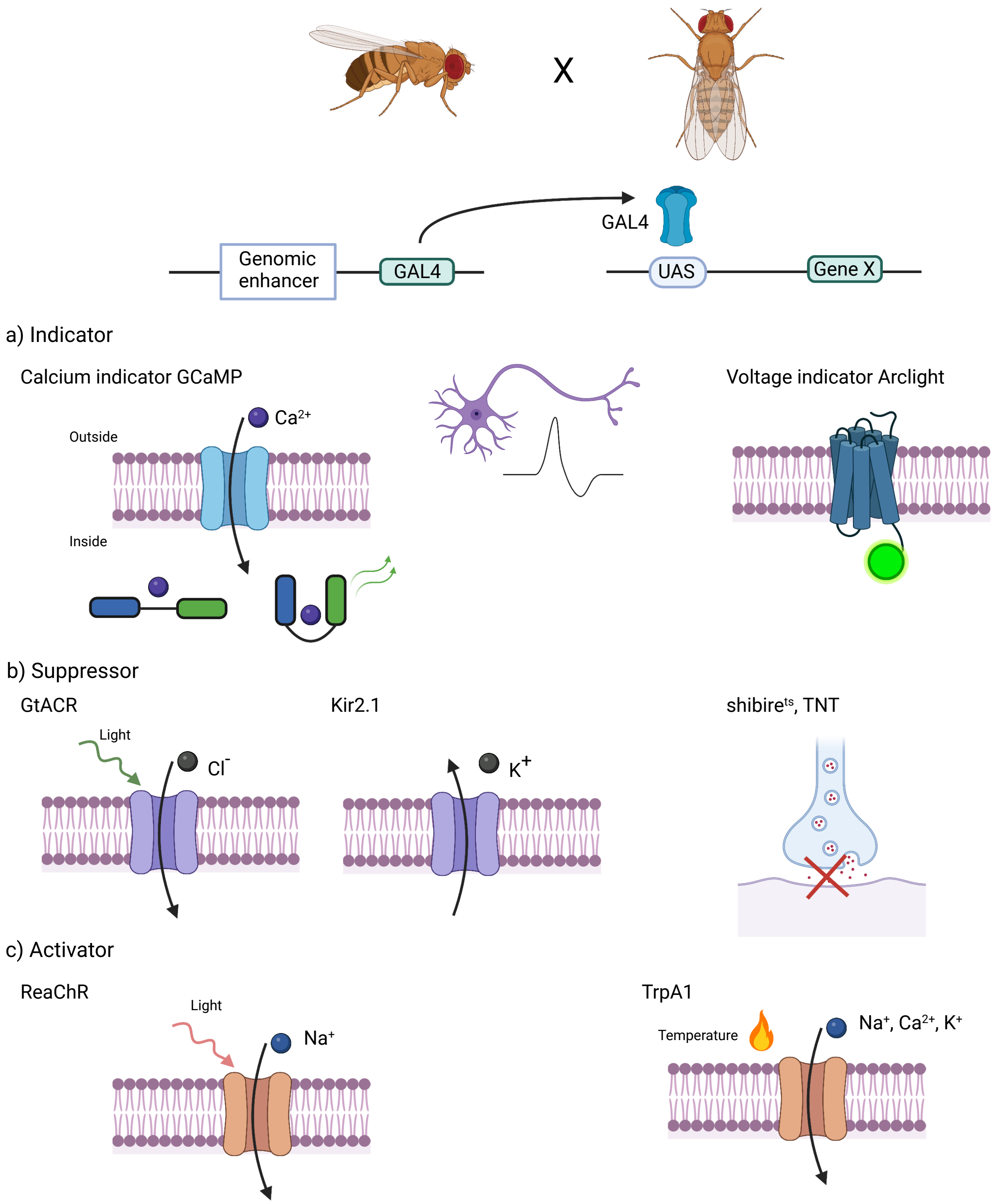
X
Genomic enhancer
GAL4
GAL4
UAS
Gene X
a) Indicator
Calcium indicator GCaMP
Outside
Inside
Ca2+
Voltage indicator Arclight
b) Suppressor
GtACR
Light
Cl-
Kir2.1
K+
shibirets, TNT
c) Activator
ReaChR
Light
Na+
TrpA1
Temperature
Na+, Ca2+, K+

Figure 1: The Gal4-UAS system is used to express a gene of interest in a specific subset of neurons. (a) The calcium indicator is used to record neural activity using intracellular calcium concentration. The voltage indicator is used to optically record membrane potential changes in the neuron. (b) Neural activity can be suppressed by expressing light-sensitive chloride channels, overexpression of potassium channels resulting in potassium efflux or by blocking synaptic transmission. (c) Neurons can be activated via the expression of light-sensitive or tempearture-sensitive cation channels. (modified from Borst 2009)

to be better suited (Hamill *et al.* 1981). The patch-clamp method involves making tight contact with a tiny patch of the neuronal membrane with a glass micropipette. By briefly applying strong suction to the pipette, the membrane patch within it can be disrupted and the interior of the pipette can be continuous with the cytoplasm. In this configuration, electrical potentials and currents are measured from the entire cell, thus the method is called whole-cell recording. Several brain areas, including the visual (Behnia *et al.* 2014; Groschner *et al.* 2022; Gruntman *et al.* 2018; Joesch *et al.* 2008) and olfactory systems (Wilson *et al.* 2004), have been recorded *in vivo* using patch-clamp techniques in *Drosophila*.

TWO-PHOTON MICROSCOPY Although electrophysiology is widely used to record action potentials and sub-threshold changes in membrane potential, it has significant disadvantages. Electrodes must be inserted into the neurons or the brain tissue. This can cause cell or tissue damage. Additionally, only a limited number of neurons can be recorded simultaneously. With the advent of silicon probe technology, which allows multiple probes to be inserted into the brain (each with hundreds of contact points), a greater number of neurons and brain regions can be sampled using electrophysiology. However, these recordings are more invasive, more expensive, and have the same limitations as single-neuron electrode recordings. Optical probing of neural activity, especially combining calcium or voltage imaging with two-photon microscopy has become popular as an alternative to electrophysiology.

The invention of two-photon microscopy (Denk *et al.* 1990) has been one of the major breakthroughs in neuroscience. It allows high-sensitivity and high-resolution fluorescence detection in brain tissue *in vivo*. In two-photon microscopy, two low-energy near-infrared or infrared photons (usually from the same laser) cooperate to produce an electronic transition in a fluorescent molecule from the ground to the excited state. In other words, a fluorescent molecule can achieve a higher energy state either by absorbing a single photon from 455 nm light or by absorbing two photons simultaneously from a light of wavelength 910 nm. Compared to one-photon techniques, two-photon excitation provides several advantages for microscopy in scattering specimens like the brain (Denk *et al.* 1994; Svoboda & Yasuda 2006). First, compared to the visible wavelengths used in one-photon microscopy, the near-infrared or infrared excitation wavelengths used in two-photon microscopy penetrate the tissue better. This happens due to the reduced scattering and reduced absorption by endogenous chromophores. Second, the bleaching of fluorophores is reduced in two-photon imaging compared to one-photon imaging. Fluorophores lose their brightness when exposed to high-energy light. Light of higher wavelength used in two-photon microscopy carries less energy and hence, causes reduced bleaching. Third, the light above 900nm in the infrared region is beyond the spectral sensitivity of a fly's eye. Hence, the laser light won't interfere with the light used to create visual stimuli. Combining two-photon microscopy with a precise genetic expression of genetically encoded calcium indicators (GECIs) (Chen *et al.* 2013) has been extensively used to measure neural activity in *Drosophila* neuroscience.

TWO-PHOTON CALCIUM IMAGING *In vivo* two-photon calcium imaging is based on the principle that when neurons are sufficiently depolarized, intracellular calcium rise, which can be detected using GECIs that bind to calcium (figure 1a). GECIs typically consist of a calcium-binding domain - calmodulin, calmodulin-binding peptide M13, and a reporter element which is based on either a single fluorescent protein or two fluorescent proteins (Broussard *et al.* 2014). In the case of a single fluorescent protein for example in GCaMPs, calmodulin (CaM) binds to the M13 peptide in the presence of calcium. This coupling results in conformational changes in the fluorescent protein, resulting in a change in fluorescence intensity (Nagai *et al.* 2001).

Two-photon calcium imaging provides several advantages over electrophysiology. First, two-photon calcium imaging is less invasive. Second, it can be combined with genetic tools (for example, Gal4-UAS, LexA-lexAop), to precisely target and record from a specific subset of neurons. Third, two-photon calcium imaging allows recording from several neuronal compartments including soma, dendrites, axons, or single spines and boutons (Grienberger *et al.* 2022). In this thesis, I used GCaMP6f (Chen *et al.* 2013) in combination with two-photon microscopy for recording neural activity.

TWO-PHOTON VOLTAGE IMAGING Despite the many advantages that two-photon calcium imaging offer, there are some disadvantages. Calcium imaging does not reveal inhibitory, hyperpolarizing signals. Also, calcium imaging is limited on the temporal scale. It is possible to overcome the limitations inherent in calcium imaging with optical voltage imaging. The genetically encoded voltage indicators (GEVIs) consist of a voltage-sensing domain fused together with a fluorescent protein. The coupling of voltage sensing with optical output is achieved either via Förster resonance energy transfer (FRET) between fluorescent proteins (FPs) or by sensitizing a single fluorescent protein by circular permutation.

The voltage indicators produce weak optical signals compared to calcium indicators GCaMPx, which is why few system neuroscience studies have been conducted on them. However, the potential of GEVIs is very high, and therefore a lot of effort is being put into improving the existing GEVIs and also developing new ones. Due to the low signal amplitude, experiments with optical voltage indicators such as ASAP2f have been challenging (Yang *et al.* 2016). In this thesis, I used a fluorescence protein voltage sensor called Arclight (Jin *et al.* 2012). Arclight is based on the fusion of the voltage sensing domain of *Ciona intestinalis* voltage-sensitive phosphatase (Murata *et al.* 2005) and the fluorescent protein super ecliptic pHluorin with an A227D mutation. Arclight's fluorescence decreases with membrane depolarization and increases with membrane hyperpolarization. Arclight has been shown to robustly report both subthreshold events and action potentials in genetically targeted neurons in the intact *Drosophila* brain (Cao *et al.* 2013). I used Arclight in combination with two-photon imaging to record changes in the neuronal membrane potential.

1.2.3 Manipulating neural activity

The above-mentioned tools are suitable for measuring the neural activity and characterizing a neuron. It is necessary, however, to also activate or silence a neuron in order to investigate its functional contribution to the neural circuit.

SILENCING NEURONS There are several genetic tools that allow for silencing neurons in *Drosophila* (figure 1b). First, the cell death genes such as *reaper (rpr)* or *head involution defective (hid)* can be expressed to induce apoptosis and kill the neurons (P. Chen *et al.* 1996; Grether *et al.* 1995). Second, the synaptic output of neurons can be permanently blocked. The *tetanus toxin light chain (TNT)* cleaves the synaptic vesicle protein synaptobrevin and inhibits neurotransmitter exocytosis at chemical synapses (Sweeney *et al.* 1995). Third, the expression of *Kir2.1* – an inwardly rectified potassium channel, can cause neurons to constantly hyperpolarize, resulting in suppressed excitability (Johns *et al.* 1999). While using the Gal4-UAS system to express these effector proteins provides effective control over the functionality of the targeted neurons, their expression cannot be reversed and the precise timing of silencing the neurons cannot be determined. To overcome these limitations, the conditional effector proteins like $\texttt{shibire}^{ts}$ and *GtACR*, which is activated by higher temperature and light respectively can be used.

The *Drosophila* gene *shibire* encodes the protein *dynamin*, which is involved in the process of endocytosis and is essential for vesicle recycling. The dominant-negative temperature-sensitive allele $\texttt{shibire}^{ts}$ is defective in synaptic vesicle recycling at the restrictive temperature (>29°C). The reuptake of vesicles from the synaptic cleft, mediated by the GTPase dynamin, is still functional at a permissive temperature (~25°C). Thus, a rapid and reversible inhibition of synaptic transmission can be achieved by controlling the temperature of the specimen (Kitamoto 2001). As an alternative to temperature, light can be used to control the timing of silencing the neuron. Light-gated anion channel, *Guillardia theta* anion channel rhodopsins (GtACR) can be expressed in the neurons of interest. The application of light causes these channels to open, allowing an influx of chloride ions, thus causing the neurons to hyperpolarize. This is an extremely sensitive, precisely timed, and reversible method for manipulating neural activity (Govorunova *et al.* 2015; Mauss *et al.* 2017; Mohammad *et al.* 2017).

ACTIVATING NEURONS A second or complementary approach to probing the functional role of a neuron in a neural circuit is by activating the neuron (figure 1c). Temperature-sensitive channels can be used for activating the neurons. Flies naturally express the transient receptor potential cation channel TrpA1 which is implicated in temperature detection (Hamada *et al.* 2008; Pulver *et al.* 2009). The expression of these channels in the neurons allows for temperature-mediated excitation. The light-gated optogenetic tools, however, allow for greater temporal control compared to the above-mentioned temperature-sensitive method. The light-gated cation channel *Channelrhodopsin (ChR)* was extracted from the green algae *Chlamydomonas reinhardtii* and expressed in *C. elegans* and mammalian hippocampal neurons (Boyden *et al.* 2005; Nagel *et al.* 2005). By expressing these light-gated cation channels in the neurons of interest, a precise, reversible, and reliable excitation of the neurons can be achieved.

1.3 NEURAL COMMUNICATION

Camillo Golgi's silver-stain method made it possible for the first time, to visualize single neurons in tissue samples under the light microscope (1873). Santiago Ramón y Cajal in 1888 described the nervous system as a network of individual cells. About a decade later, in 1897, the term 'synapse', derived from the Greek word 'synapsis' (meaning 'conjunction'), was used to describe the connections between two neurons. Neurons form networks where they communicate via synapses. Two types of synapses exist 1) electrical synapses and 2) chemical synapses.

1.3.1 Electrical synapses

In electrical synapses, two cells are directly connected by a cluster of intercellular channels called gap junctions (Bennett & Zukin 2004). The gap junctions provide a conductive pathway for electrical current to spread between cells. Consequently, electrical currents underlying action potentials or graded potentials directly propagate to postsynaptic neurons, without additional delay. Since electrical signals propagate bidirectionally, signalling events generated in the postsynaptic cells can also spread to presynaptic cells. In *Drosophila*, electrical synapses are widely distributed throughout the nervous system and are essential to neuronal function (Ammer *et al.* 2022; Liu *et al.* 2016; Stebbings *et al.* 2002).

1.3.2 Chemical synapses

Neurons communicate mostly via chemical synapses (figure 2). When the presynaptic membrane is sufficiently depolarized, voltage-gated calcium channels open and allow Ca^{2+} to enter the cell (Luo 2020). Calcium entry leads to the fusion of synaptic vesicles with the membrane and the release of neurotransmitter molecules into the synaptic cleft (Chapman 2002). As neurotransmitters diffuse across the synaptic cleft, they bind to receptors in the postsynaptic membrane, causing the postsynaptic neuron to depolarize or hyperpolarize, thereby passing the information from pre- to postsynaptic neurons (Di Maio 2008).

1.3.3 Voltage-gated ion channels

Voltage-gated ion channels are transmembrane proteins that allow certain inorganic ions to cross cell membranes (figure 3). Generally, these channels consist of two distinct but functionally coupled transmembrane domains: the voltage sensing domain and the pore domain. The voltage sensing domain changes the conformation of the pore domain in response to changes

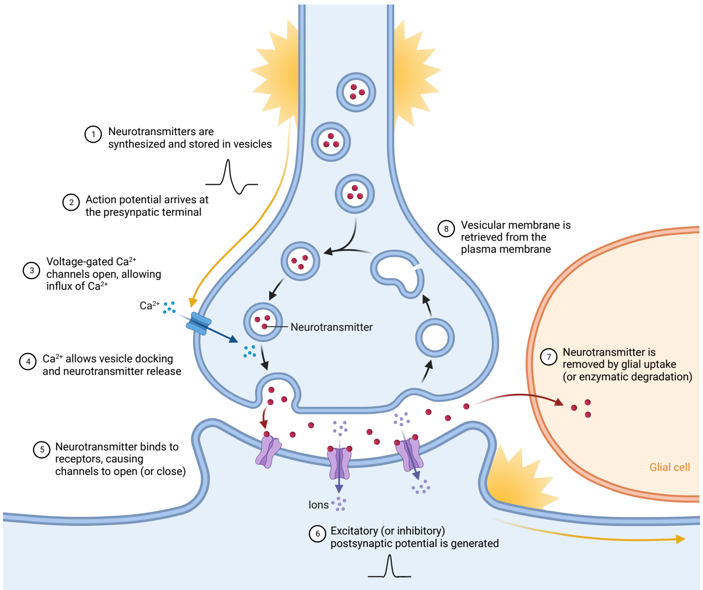
① Neurotransmitters are synthesized and stored in vesicles
② Action potential arrives at the presynpatic terminal
③ Voltage-gated Ca^{2+} channels open, allowing influx of Ca^{2+}
Ca^{2+}
④ Ca^{2+} allows vesicle docking and neurotransmitter release
Neurotransmitter
⑤ Neurotransmitter binds to receptors, causing channels to open (or close)
Ions
⑥ Excitatory (or inhibitory) postsynaptic potential is generated
⑦ Neurotransmitter is removed by glial uptake (or enzymatic degradation)
⑧ Vesicular membrane is retrieved from the plasma membrane
Glial cell

Figure 2: Chemical synapse: steps of synaptic transmission. (1) Synthesis and storage of neurotransmitters in the vesicles. (2) Depolarization in the presynaptic terminal causes (3) voltage-gated calcium channels to open and allow an influx of calcium ions. (4) High concentration of calcium ions triggers the fusion of neurotransmitters-filled vesicles with the presynaptic membrane and the release of neurotransmitters into the synaptic cleft. (5) Neurotransmitters released in the synaptic cleft bind to receptors in the postsynaptic membrane leading to (6) excitatory or inhibitory postsynaptic potential. (figure created with Biorender.com)

in transmembrane potential, allowing selected ions to flow down their electrochemical gradient.

VOLTAGE-GATED CALCIUM CHANNELS As mentioned above, voltage-gated calcium channels mediate depolarization-induced calcium influx that drives the release of neurotransmitters. The $\alpha 1$-subunit of the voltage-gated calcium channels forms the ion-conducting pore, which makes it distinct from other calcium channels. Three families of genes encode $\alpha 1$ subunits. *Drosophila* genome has one $\alpha 1$ subunit gene in each family: $\alpha 1D$ (Ca_v1), cac (Ca_v2), and $\alpha 1T$ (Ca_v3) (King 2007; Littleton & Ganetzky 2000). In *Drosophila* antennal lobe projection neurons, cac (Ca_v2) type and $\alpha 1T$ (Ca_v3) type voltage-gated calcium channels are involved in sustained and transient calcium currents, respectively (Gu *et al.* 2009; Iniguez *et al.* 2013).

VOLTAGE-GATED SODIUM CHANNELS In neurons, voltage-gated sodium channels play a crucial role in the initiation and propagation of action potentials (Hodgkin & Huxley 1952). Sodium channels are activated and deactivated within milliseconds when the membrane is depolarized by a few millivolts. There are at least ten genes in mammals that encode these large membrane proteins. In contrast, *paralytic (para)* is the only voltage-gated sodium channel gene described in *Drosophila* (Piggott *et al.* 2019).

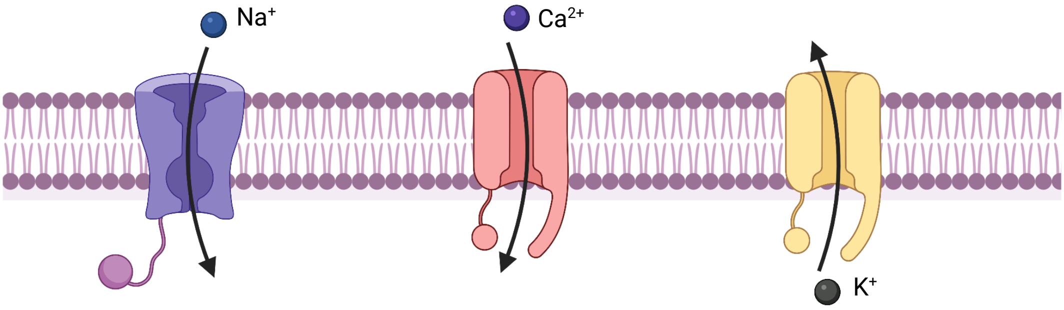

Figure 3: Voltage-gated ion channels: The sodium channels allow Na^+ ions to enter the cell. The calcium channels allow Ca^{2+} ions to enter the cell. The potassium channels allow efflux of the K^+ ions.

VOLTAGE-GATED POTASSIUM CHANNELS Voltage-gated potassium channels are transmembrane channels specific to potassium ions. They play a crucial role in repolarizing the depolarized cell to its resting membrane potential, after each action potential. Voltage-gated potassium channels are the most diverse family of voltage-gated ion channels in the human genome, with 40 members for α subunit grouped into 12 families (Gutman *et al.* 2005). The first voltage-gated potassium channel discovered in *Drosophila* was *Shaker* (Papazian *et al.* 1987). Afterwards, three additional *Shaker* like voltage-gated potassium genes were identified: *Shab*, *Shaw* and *Shal* (Covarrubias *et al.* 1991).

1.4 THE FLY VISUAL SYSTEM

As mentioned earlier, the *Drosophila melanogaster* nervous system consists of ~$200,000$ neurons (Raji & Potter 2021). Almost half of these neurons (~$100,000$ neurons) are dedicated to processing visual signals in the optic lobe of the fly brain. Unlike vertebrates, many invertebrate species have compound eyes, which are composed of multiple optical units called facets or ommatidia. Each compound eye contains around 750 ommatidia (Ready *et al.* 1976). The ommatidia are arranged in a regular lattice with a 5-degree inter-ommatidia angle (Land 1997). There are eight different photoreceptors in an ommatidium (R1-R8). A circular arrangement is formed by R1-R6 enclosing the central photoreceptors R7 and R8, which are stacked on top of one another. Due to this arrangement, the photoreceptors in an ommatidium sense incident light from slightly offset positions in space. With this configuration, six photoreceptors in six different adjacent ommatidia that possess identical optical axes project their axons to a single cartridge in the brain forming a so-called neuro-ommatidium (Strausfeld 1971). As a result of this neural superposition principle, the sensitivity increases without compromising the spatial resolution (Kirschfeld 1967).

PHOTOTRANSDUCTION The process of converting light enrgy into electrochemical signals is called phototransduction. This process occurs in rhabdomeres in the flies photoreceptors. In rhabdomeres, there are ~$30,000$ microvilli, each containing about 1000 photoactive molecules, called rhodopsin. The chromophore 3-hydroxy-11-cis-retinal is covalently bound to rhodopsin. Upon absorption of a photon by rhodopsin, the chromophore 3-hydroxy-11-cis-retinal is isomerized to all-trans-retinal, and the activated metarhodopsin state is formed. This activates a G-protein coupled cascade that results in the activation of phospholipase C (PLC). The PLC hydrolyzes phosphatidylinositol 4,5 bisphosphate (PIP2) to diacylglycerol (DAG), inositol 1,4,5 trisphosphate (InsP3), and a proton. Downstream to PLC, two light-sensitive channels (TRP and TRPL) are activated, allowing sodium and calcium to enter the cell and depolarize it. The photoreceptors upon activation release the inhibitory neurotransmitter histamine, thus inhibiting postsynaptic neurons (Hardie 1989; Hardie & Juusola 2015; Hardie & Raghu 2001).

1.4.1 The optic lobe

Following the photoreceptor layer in the retina, the fly's optic lobe consists of 4 layers of neuropils called the lamina, the medulla, the lobula, and the lobula plate. These neuropil layers are arranged in a columnar, retinotopic fashion with each column processing information from a small point in the visual space (figure 4a) (Fischbach & Dittrich 1989).

LAMINA The lamina is organized in an array of ~750 retinotopic columns (also called 'cartridges'). Each column corresponds to ~5° discrete sample of the visual world. The light-sensitive photoreceptors, R1-6 project their axons into each lamina column. Two other photoreceptors, R7 & R8 pass through the lamina and synapse in specific layers of the medulla. Along with photoreceptor axons, the lamina includes 5 lamina output neurons (L1-L5), six putative feedback neurons (T1, Lat, Law1, Law2, C2, C3), and one lamina intrinsic neuron (Lai). L1, L2, and L3 cells receive the majority of their input from photoreceptors R1-R6. L4 cells form reciprocal connections with L2 and receive only a small number of input from photoreceptor R6. L5 receives input from L2, L4, and lamina interneurons (Rivera-Alba *et al.* 2011). The lamina columnar monopolar neurons, L1-L5 send their axonal projections into specific layers of the medulla. (Fischbach & Dittrich 1989; Tuthill *et al.* 2013). Lamina output neurons L1 and L2 are the primary input cells for motion vision (Zhu 2013).

MEDULLA Lamina cells send input projections to the medulla, the second neuropil in the optic lobe. There are ten synaptic layers (M1 to M10) in the medulla consisting of over 60 types of cells. The medulla is composed of hexagonal columns, similar to the lamina. In this way, the mapping between the lamina and medulla remains retinotopic. The fibers connecting the lamina to the medulla form a chiasm, in which posterior medulla cartridges receive input from anterior lamina cartridges. Two main classes of columnar interneurons are found in the medulla: around 10 types of medulla intrinsic neurons (Mi) and around 30 types of transmedullary neurons (Tm). Mi neurons connect different layers of the medulla to each other. Dendrites of Mi cells are located in the distal medulla layers, while axons are located

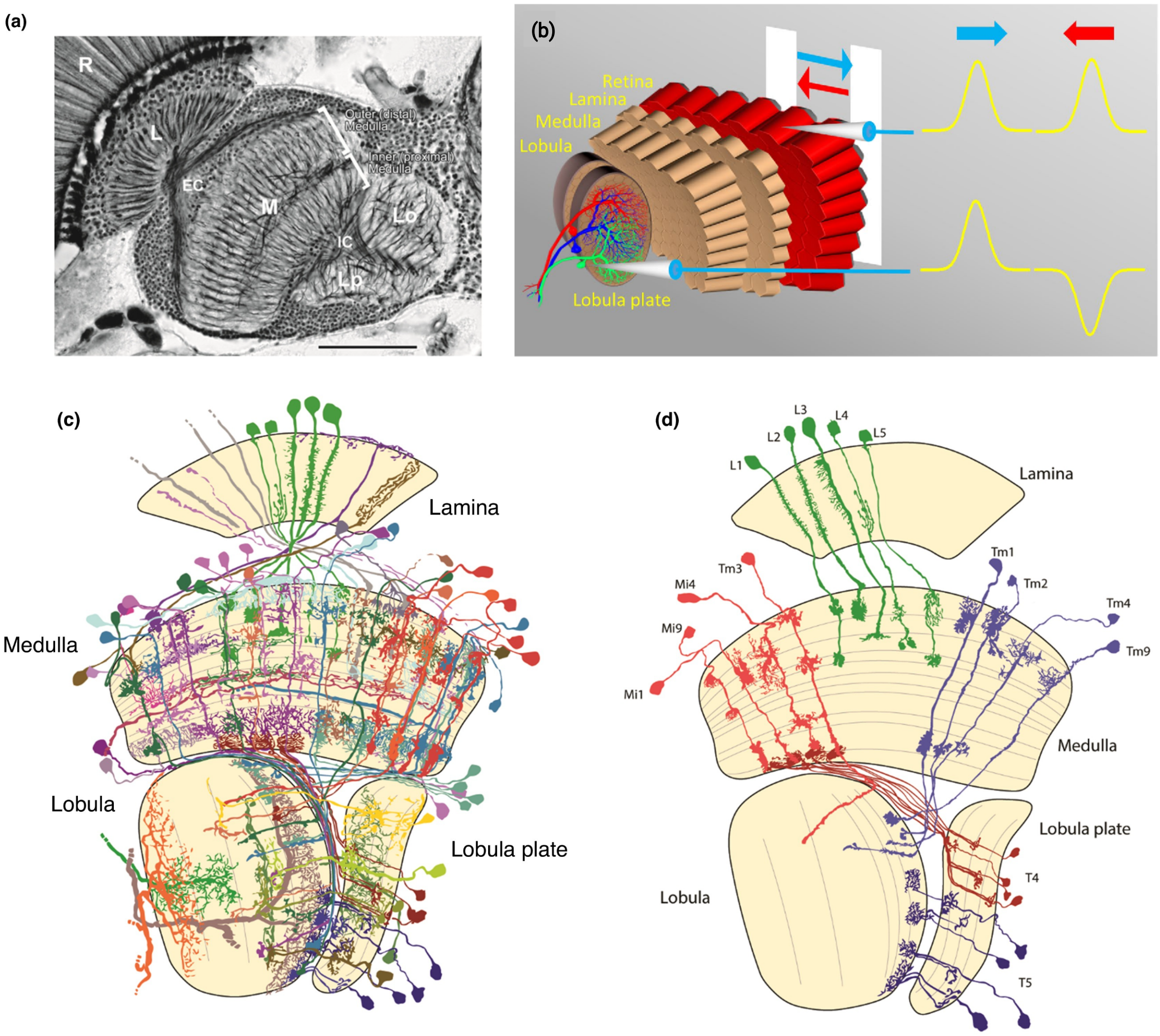
(a)
R
L
EC
M
Outer (distal) Medulla
Inner (proximal) Medulla
Lo
IC
Lp
(b)
Retina
Lamina
Medulla
Lobula
Lobula plate
(c)
Lamina
Medulla
Lobula
Lobula plate
(d)
L3
L4
L2
L5
L1
Lamina
Tm1
Tm3
Tm2
Mi4
Tm4
Mi9
Tm9
Mi1
Medulla
Lobula plate
T4
Lobula
T5

Figure 4: The fly optic lobe: (a) The horizontal cross-section of a reduced silver stain shows the columnar organization of the retina (R), lamina (L), external chiasm (EC), medulla (M), internal chiasm (IC), lobula (Lo), and lobula plate (Lp). Scale bar = 50 µm. Reproduced, with permission, from Takemura *et al.* 2008 (b) Schematic illustration of direction selectivity: moving a bar in front of a fly's eye leads to depolarization of photoreceptors every time, regardless of whether the bar moves to the right or left. It is a non-directional signal. A few synapses downstream, on the lobula plate tangential cells, signals are direction-selective: these cells depolarize during movement along one direction, i.e., their 'preferred' direction, and hyperpolarize during motion along the opposite direction, i.e., their 'null' direction. (c) An overview of all types of columnar cells in the *Drosophila* optic lobe. (Fischbach & Dittrich 1989) (d) Columnar cell types involved in the motion vision circuit. (Used with permission from Borst *et al.* 2020a,b)

in the proximal medulla layers. Tm neurons connect specific layers of the medulla to various layers in the lobula. Tm cells receive input in the distal medulla layers 1-5 from lamina monopolar cells and photoreceptors R7 and R8 and send their axonal projections to the lobula (Fischbach & Dittrich 1989; Takemura *et al.* 2011). In addition to these two types of neurons, the trans-medulla Y ('TmY') neurons connect specific layers of the medulla to various layers in the lobula and lobula plate.

LOBULA COMPLEX In the final stage of the visual processing in the optic lobe, the lobula complex consists of two neuropils: the lobula and the lobula plate. There are six layers in the lobula (Fischbach & Dittrich 1989). Lobula columnar (LC) neurons receive major inputs from the medulla and are the most prominent type of cell in the lobula. Multiple types of LC neurons span the entire visual field in a retinotopic manner (Otsuna & Ito 2006). In total, these neurons are divided into more than twenty distinct subtypes, each conveying information about a different visual feature (Wu *et al.* 2016). Lobula plates have four structurally distinct layers perpendicular to their columnar organization. A number of wide-field tangential cells are present in each layer (Strausfeld & Lee 1991). Dendritic trees of the tangential cells span large areas of the lobula plate, sometimes covering the entire layer. Thus, their receptive fields cover a large portion of the visual field. Two types of bushy T-cells T4 and T5 exist. Four subtypes of both T4 and T5 are found connecting the medulla and lobula respectively to the four layers of the lobula plate (Fischbach & Dittrich 1989).

1.4.2 Neural circuits underlying direction selectivity

Direction selectivity is the most important response characteristic of the lobula plate tangential cells. In response to a visual stimulus moving in their preferred direction, the cells depolarize. When the visual stimulus moves in the opposite direction (the null direction), the cells hyperpolarize. Two major types of lobula plate tangential cells have been described. The horizontal system (HS) cells respond preferentially to horizontal motion (Schnell *et al.* 2010), while vertical system (VS) cells respond preferentially to vertical motion (Joesch *et al.* 2008). Photoreceptor signals, in contrast, are not direction-selective, i.e. they display a similar response regardless of which direction the stimulus moves. Thus, a non-directional response at the photoreceptor level is transformed into a directional signal at the lobula plate tangential cell level (figure 4b). The lobula plate tangential cells, however, integrate signals over large parts of visual fields, i.e. they are not local motion detectors. Hence, the question arises: which cells are the local motion detectors?

Electrophysiological and two-photon calcium imaging experiments in the optic lobe over the years have revealed the following interesting results: (a) Visual processing in *Drosophila* occurs in two parallel processing pathways for luminance increment (ON) and luminance decrement (OFF) (Behnia *et al.* 2014; Eichner *et al.* 2011; Joesch *et al.* 2010, 2013; Shinomiya *et al.* 2014; Strother *et al.* 2014) (b) T4 and T5 are the first local motion detectors found in the *Drosophila* ON and OFF motion vision pathway respectively. Four subpopulation of T4a-d and T5a-d cells tuned to the four cardinal directions and projecting to the four layers in the lobula plate is found within each column (Maisak *et al.* 2013).

PARALLEL ON AND OFF PROCESSING PATHWAYS In striking similarity to the mammalian retina (Masland 2012), visual processing in *Drosophila* occurs in two parallel ON and OFF processing pathways (Borst & Helmstaedter 2015). The ON pathway transmits information about luminance increments, while the OFF pathway transmits information about luminance decrements. The split into the ON and OFF pathways occurs in the lamina. The L1 neurons provide inputs onto the ON pathway, while the L2 neurons provide inputs onto the OFF pathway. When the output of L1 neurons was genetically blocked, the downstream motion-sensitive lobula plate tangential cells no longer responded to ON motion. Blocking the output of L2 neurons abolished the responses of the tangential cells to OFF motion (Joesch *et al.* 2010). In behavioral experiments, walking flies were unable to follow either ON or OFF motion when either L1 or L2 was blocked respectively (Clark *et al.* 2011; Maisak *et al.* 2013). The flies became completely motion-blind when both L1 and L2 were permanently hyperpolarized (via *Kir2.1*) (Bahl *et al.* 2013; Tuthill *et al.* 2013). These experiments together showed that the L1 neurons specifically transmits information to the downstream ON motion detector, and the L2 neuron specifically transmits information to the downstream OFF motion detector.

T4 AND T5 CELLS Based on previous studies (Buchner *et al.* 1984; Fischbach & Dittrich 1989), T4 and T5 were long thought to be the prime candidates for local motion detectors in the ON and OFF pathways respectively. However, due to its small size, it was difficult to do electrophysiological recordings from T4 and T5 cells (Douglass & Strausfeld 1996). This problem was solved using a combination of two-photon imaging and a Gal4-UAS system to express GCaMP in T4, and T5 cells to record its neural activity in response to the ON and OFF stimuli. Stimulating the flies with visual motion in four cardinal directions (front-back, back-front, upwards, and downwards), direction-selective activity from T4/T5 cells were recorded (Maisak *et al.* 2013). Four sub-populations of T4a-d and T5a-d cells tuned to the four cardinal directions and projecting to the four layers in the lobula plate were found within each column. Further, the T4 cells were found to respond specifically to ON stimulus and the T5 cells were found to respond specifically to OFF stimulus. Blocking T4 and T5 cells led to a complete loss of motion response in the lobula plate tangential cells (Schnell *et al.* 2012), and of the optomotor response of tethered walking flies (Bahl *et al.* 2013). Specific blocking of T4 cells led to a reduction in tangential cells and optomotor responses to ON stimulus selectively, while specific blocking of T5 cells led to a reduction in tangential cells and optomotor responses to OFF stimulus selectively. These results together show T4 and T5 cells to be the elementary motion detector for the ON and OFF pathways respectively (Maisak *et al.* 2013).

Having identified T4 and T5 cells as elementary local motion detectors, the next question is which cells provide synaptic inputs to these cells. Elec-

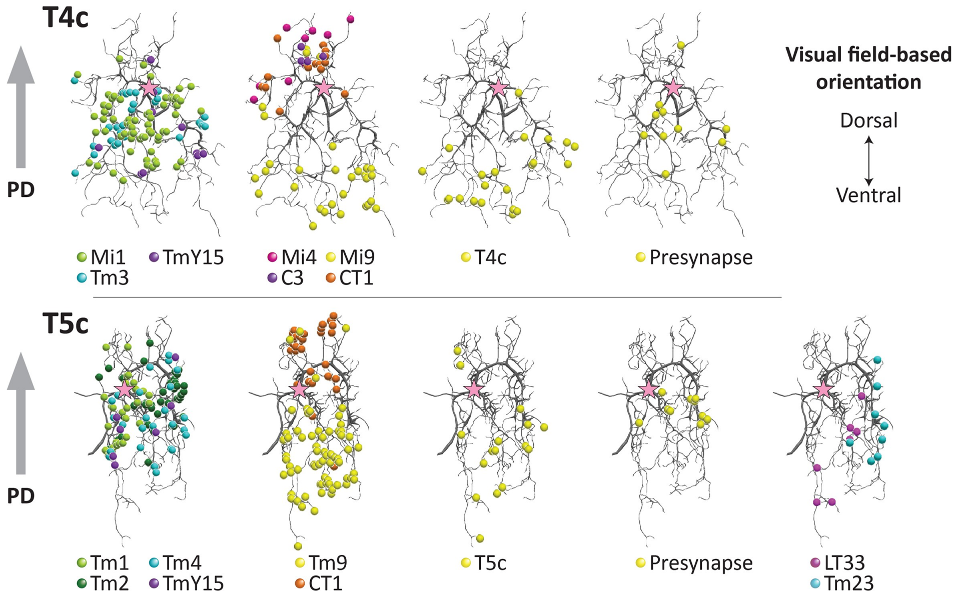

Figure 5: Synaptic sites distributed over T4 and T5 dendritic arbors: An arbor of a T4c (top panels) or T5c (bottom panels) cell is shown with synapse positions plotted on the dendritic arbors. Unless shown as 'Presynapse', puncta are postsynaptic sites (input to T4/T5 cells). T4c and T5c detect upward motion, and other subtypes of T4 and T5 cells show similar distribution patterns (not shown). An arbor's first branch point is indicated by pink stars. (Used with permission from Shinomiya *et al.* 2019)

tron Microscopy (EM) studies (Shinomiya *et al.* 2019; Takemura *et al.* 2017) provided the answer to this question. FIB-SEM (Focused Ion Beam Scanning Electron Microscopy) was used to record a volume of the optic lobe comprising seven columns of the medulla, lobula, and lobula plate (Shinomiya *et al.* 2019). All the different neuron types providing inputs to the T4 and T5 cells were identified. T4 cells receive input from Mi1, Tm3, Mi4, Mi9, C3, CT1, and TmY15. T5 cells receive input from Tm1, Tm2, Tm4, Tm9, CT1, TmY15, LT33, and Tm23. The T4 and T5 cells' dendrites span several columns along the preferred direction of the motion. The location where the different cell types synapse onto the dendrites of T4 and T5 was also found. For example, a T4c cell with the preferred direction of motion as upwards receives input from Mi1, Tm3, and TmY15 in the central part of its dendrite, from Mi9 and T4c on the ventral part, and from Mi4, C3, and CT1 on the dorsal part of its dendrite (figure 5 top). T4d cells with preferred direction as downwards receive input from Mi1, Tm3, and TmY15 in the central part, from Mi9 and T4d on the dorsal part, and from Mi4, C3, CT1 on the ventral part of its dendrite. In summary, all T4 subtypes receive inputs from Mi1, Tm3, and TmY15 in the central part, from Mi9 on the preferred side (i.e. the side from which a preferred direction stimulus approaches), and from Mi4, C3, and CT1 on the null side (i.e. the side from which a null direction stimulus approaches) of their dendrite. Similarly, all T5 subtypes receive inputs from Tm1, Tm2, and Tm4 on the central part, Tm9 on the preferred side, and CT1 on the null side of their dendrite (figure 5 bottom).

Most of these input elements have been characterised physiologically (Arenz *et al.* 2017; Behnia *et al.* 2014; Groschner *et al.* 2022; Meier & Borst 2019;

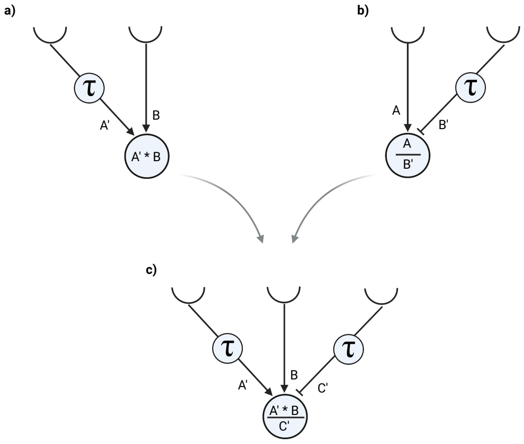

Figure 6: Models for motion detection: (a) The Hassenstein-Reichardt (HR) correlator (half-detector shown here) consists of two arms. Motion in the preferred direction (PD) causes two signals from neighboring photoreceptors to coincide due to a delay (τ) on the first arm. There is an enhancement in PD resulting from a multiplicative non-linearity. (b) The Barlow-Levick (BL) detector has the delay on the opposite arm, and the non-linearity is inhibitory, resulting in a null-direction (ND) suppression. (c) Hybrid detector consisting of one HR unit and one BL unit: Three points in space are sampled. There is a time delay (τ) on the outer two arms. The input signals from detector arms A and B are multiplied and divided by the signal from detector arm C in the following stage. Consequently, the signal in the preferred direction is enhanced and the signal in the null direction is suppressed.

Serbe *et al.* 2016; Strother *et al.* 2017). None of these cells were found to be direction-selective. Hence, the T4 and T5 cells are the elementary motion detector found in the ON and OFF pathway respectively, and thus represents an important processing stage where the direction is computed.

1.4.3 Neural algorithms underlying direction selectivity

Different models have been proposed to explain the neural computations involved in motion detection. In order to detect motion in a directionally selective manner, local motion detection mechanisms must meet certain minimum requirements (Borst & Egelhaaf 1989):

1. Spatial offset: Motion is a vector that needs two points to be represented, so at least two spatially separated inputs are required.
2. Temporal asymmetry: There must be at least one input that is delayed. If not, the input signals arrive in the subsequent stage simultaneously independent of the stimulus direction.
3. Non-linear interaction: It is necessary to integrate the input signals nonlinearly at a subsequent stage of the process. In the absence of this, the detector's output would be equal for both directions on average.

Classically two opposing models have been proposed for the implementation of direction selectivity. Both these models use two input lines, where one of the input lines has been asymmetrically delayed compared to the other, followed by a non-linear interaction. The Hassenstein-Reichardt (HR) model proposes a Preferred Direction (PD) enhancement: the signal on the preferred side is delayed and is subsequently amplified using multiplication of the signal from the other input line (figure 6a) (Hassenstein & Reichardt 1956). The Barlow-Levick (BL) detector, however, proposes a Null Direction (ND) suppression: the signal on the null side is delayed and divides the signal from the other input resulting in suppression (figure 6b) (Barlow & Levick 1965). Haag *et al.* 2016 used apparent motion stimuli to show that both the mechanisms i.e. PD enhancement on the preferred side and ND suppression on the null side are used by T4c and T5c cells to produce a direction-selective response (figure 6c). Is that special to upward-tuned T4c cells or is it general for all subtypes of T4 and T5 cells? In the first manuscript 2.1 (Haag *et al.* 2017), we showed that all four subtypes of T4 and T5 indeed use both PD enhancement and ND suppression to produce direction-selective responses. Therefore, we proposed a new model combining both PD enhancement on the preferred side and ND suppression on the null side. What are the neural correlates implementing these mechanisms?

The model requires a fast input at the center, slow input providing excitation on the preferred side, and slow input providing suppression on the null side. Interestingly, from the anatomical and functional characterization of the input data discussed earlier, the input neurons for T4 cells providing these three kinds of inputs can be predicted. Mi1 is a fast neuron providing input at the central part of the dendrite, thus a candidate for central fast input. Mi9 is a slow neuron providing input on the preferred side of the dendrite, hence a candidate for input on the preferred side. Mi4, C3, and CT1 are slow neurons providing input on the null side of the dendrite (Arenz *et al.* 2017).

In addition to the synaptic mechanisms on the dendrites of T4 cells described above, further processing in the T4 neurons– voltage to calcium transformation or calcium to neurotransmitter release, can enhance or decrease the direction selectivity of the output signals of T4 cells. Also, using two-photon voltage and calcium imaging in T5 neurons, Wienecke *et al.* 2018 showed that linear spatial summation is sufficient for the emergence of direction selectivity in T5 cells and that the preferred direction enhancement and null direction suppression in the calcium signal can arise from the non-linear voltage-to-calcium transformation. To better understand the voltage-to-calcium transformation, we compared voltage and calcium signals in T4 cells in the second manuscript 2.2, using two-photon voltage imaging and calcium imaging recordings. We found that the voltage to calcium transformation in T4c neurons enhances their direction selectivity across different stimuli conditions.

1.5 CONCLUDING REMARKS

In summary, the first manuscript in this thesis answers the following question: Is the preferred direction enhancement and the null direction suppression implemented in all 4 sub-types of T4 and T5 cells? In the second manuscript, the following questions are answered: (i) How does the voltage to calcium transformation affect the direction selectivity in T4 cells? (ii) Does the voltage to calcium transformation differ in direction-selective and non-direction-selective cells? (iii) Does the voltage to calcium transformation make the output of T4 cells more direction selective?

2 PUBLICATIONS

2.1 A COMMON DIRECTIONAL TUNING MECHANISM OF *DROSOPHILA* MOTION-SENSING NEURONS IN THE ON AND IN THE OFF PATHWAY

ABSTRACT In the fruit fly optic lobe, T4 and T5 cells represent the first direction-selective neurons, with T4 cells responding selectively to moving brightness increments (ON) and T5 cells to brightness decrements (OFF). Both T4 and T5 cells comprise four subtypes with directional tuning to one of the four cardinal directions. We had previously found that upward-sensitive T4 cells implement both preferred direction enhancement and null direction suppression (Haag et al., 2016). Here, we asked whether this mechanism generalizes to OFF-selective T5 cells and to all four subtypes of both cell classes. We found that all four subtypes of both T4 and T5 cells implement both mechanisms, that is preferred direction enhancement and null direction inhibition, on opposing sides of their receptive fields. This gives rise to the high degree of direction selectivity observed in both T4 and T5 cells within each subpopulation.

AUTHORS Juergen Haag, **Abhishek Mishra** and Alexander Borst

CONTRIBUTIONS Juergen Haag, Conceptualization, Data curation, Software, Investigation, Visualization, Writing, review and editing; Abhishek Mishra, Software, Investigation (collected and analysed data for figure 4), Visualization (figure 4); Alexander Borst, Conceptualization, Funding acquisition, Writing original draft, Project administration, Writing, review and editing

eLIFE
elifesciences.org

RESEARCH ADVANCE

A common directional tuning mechanism of *Drosophila* motion-sensing neurons in the ON and in the OFF pathway

Juergen Haag*, Abhishek Mishra, Alexander Borst

Max-Planck-Institute of Neurobiology, Martinsried, Germany

Abstract In the fruit fly optic lobe, T4 and T5 cells represent the first direction-selective neurons, with T4 cells responding selectively to moving brightness increments (ON) and T5 cells to brightness decrements (OFF). Both T4 and T5 cells comprise four subtypes with directional tuning to one of the four cardinal directions. We had previously found that upward-sensitive T4 cells implement both preferred direction enhancement and null direction suppression (Haag et al., 2016). Here, we asked whether this mechanism generalizes to OFF-selective T5 cells and to all four subtypes of both cell classes. We found that all four subtypes of both T4 and T5 cells implement both mechanisms, that is preferred direction enhancement and null direction inhibition, on opposing sides of their receptive fields. This gives rise to the high degree of direction selectivity observed in both T4 and T5 cells within each subpopulation.

DOI: https://doi.org/10.7554/eLife.29044.001

Introduction

The direction of visual motion is crucial for fundamental behaviors such as mate detection, prey capture, predator avoidance and visual navigation. This important visual cue, however, is not explicitly encoded at the output of a single photoreceptor but rather has to be computed by subsequent neural circuits. In order to extract local, directional information from moving images, mainly two competing algorithmic models of motion detectors have been proposed (***Figure 1a,b***). Both models implement a delay-and-compare mechanism where two input signals from neighboring image pixels interact in a nonlinear way after one of them has been delayed with respect to the other. This leads to an output that is larger for motion along one, the so-called 'preferred' direction than for the opposite, the so-called 'null' direction. Both models differ, however, by the type of non-linearity employed and the location of the delay. In the Hassenstein-Reichardt detector (***Figure 1a***), the delay is on the preferred side, that is where a preferred direction stimulus is entering the receptive field of the detector, and the non-linearity is excitatory. This leads to an enhancement of signals moving in the preferred direction (***Hassenstein and Reichardt, 1956***). In the Barlow-Levick detector (***Figure 1b***), the delay is on the null side, that is where a null direction stimulus is entering the receptive field of the detector, and the nonlinearity is inhibitory. This leads to a suppression of signals moving in the null direction (***Barlow and Levick, 1965***). While the predictions of both models concerning the responses to smooth grating motion are identical, apparent motion stimuli lend themselves well to discriminate between them (***Egelhaaf and Borst, 1992***; ***Eichner et al., 2011***). Instead of moving an object smoothly across the image plane, an apparent motion stimulus consists of a bright or dark bar or spot that is abruptly jumped from one location to an adjacent one. Comparing the responses of directional neurons to the sequence with the sum of the responses to each individual stimulus presentation ('linear expectation') allows one to calculate the nonlinear response component as the difference between the sequence response and the linear expectation. If this nonlinear response component is positive for sequences along the preferred direction, and zero for

***For correspondence:** haag@neuro.mpg.de

Competing interest: See page 13

Funding: See page 12

Received: 30 May 2017
Accepted: 21 August 2017
Published: 22 August 2017

Reviewing editor: Fred Rieke, Howard Hughes Medical Institute, University of Washington, United States

Copyright Haag et al. This article is distributed under the terms of the Creative Commons Attribution License, which permits unrestricted use and redistribution provided that the original author and source are credited.

sequences along the null direction, a preferred direction enhancement is at work, supporting the Hassenstein-Reichardt model (**Figure 1a**). If the nonlinear response component is zero for sequences along the preferred direction and negative for sequences along the null direction, a null direction suppression is at work, supporting the Barlow-Levick model (**Figure 1b**). In the following, we will apply this approach in order to investigate which of the two mechanisms is at work in primary motion-sensitive neurons of the fruit fly *Drosophila*.

In *Drosophila*, visual signals are processed in the optic lobe, a brain area comprised of the lamina, medulla, lobula, and lobula plate, each arranged in a columnar, retinotopic fashion (for review, see: **Borst, 2014**; **Behnia and Desplan, 2015**). In striking parallel to the vertebrate retina (**Borst and Helmstaedter, 2015**), the direction of visual motion is computed within the optic lobe separately in parallel ON and OFF motion pathways (**Joesch et al., 2010**; **Reiff et al., 2010**; **Eichner et al., 2011**; **Joesch et al., 2013**). Anatomically, these two pathways split at the level of the lamina (**Bausenwein et al., 1992**; **Rister et al., 2007**) and lead, via a set of various intrinsic medulla and transmedulla interneurons, onto the dendrites of T4 and T5 cells, respectively. First described by Golgi staining (**Cajal and Sanchez, 1915**; **Strausfeld, 1976**; **Strausfeld and Lee, 1991**; **Fischbach and Dittrich, 1989**), T4 cells extend their dendrites in the most proximal layer of the medulla, while the dendrites of T5 cells are located in the inner-most layer of the lobula. There exist generally four T4 and 4 T5 cells per column (**Mauss et al., 2014**). The four subtypes of T4 cells respond selectively to brightness increments moving along one of the four cardinal directions, the four subtypes of T5 cells selectively to brightness decrements moving along the same four cardinal directions as T4 cells (**Maisak et al., 2013**). According to their preferred direction, T4 and T5 cells project into one of the four lobula plate layers (layer 1, most frontal: front-to-back; layer 2: back-to-front; layer 3: upward; layer 4, most posterior: downward; **Maisak et al., 2013**). There, T4 and T5 cells provide direct excitatory cholinergic input onto the dendrites of wide-field, motion-sensitive tangential cells as well as onto glutamatergic lobula plate interneurons that inhibit wide-field tangential cells in the adjacent layer (**Mauss et al., 2014**; **Mauss et al., 2015**). Through this circuit arrangement, lobula plate tangential cells depolarize to motion in their preferred direction (PD) and hyperpolarize in response to motion in the opposite or null direction (ND) (**Joesch et al., 2008**; **Schnell et al., 2010**). With T4 and T5 cells blocked, tangential cells lose all their direction selectivity (**Schnell et al., 2012**) and flies become completely motion-blind (**Bahl et al., 2013**; **Schilling and Borst, 2015**). This suggests that T4 and T5 cells are the elementary motion detectors and carry all directional information in the fly brain. Electrophysiological (**Behnia et al., 2014**), optical voltage (**Yang et al., 2016**) and Calcium recordings (**Meier et al., 2014**; **Serbe et al., 2016**; **Arenz et al., 2017**; **Strother et al., 2014**; **Strother et al., 2017**) from presynaptic medulla neurons revealed that none of them is directionally selective. Therefore, T4 and T5 cells are the first neurons in the visual processing chain that respond to visual motion in a direction selective manner.

Previous studies analyzed the mechanism underlying direction selectivity in T4 and T5 cells, yet arrived at different conclusions. Using apparent motion stimuli, one study found preferred direction enhancement to account for directional responses in T4 cells (**Fisher et al., 2015**). For T5 cells, the authors reported both enhancement for preferred and suppression for null direction sequences, but attributed the latter to circuit adaptation and not to the mechanism generating direction selectivity. The authors concluded that the dominant interaction producing direction selective responses in both T4 and T5 cells is a nonlinear signal amplification (**Fisher et al., 2015**). This conflicts with another report where spatio-temporal receptive fields of T5 cells were measured using white noise stimulation and reverse correlation. Based on ON and OFF subfields tilted in the space-time plane, T5 cells were concluded to incorporate both preferred direction enhancement and null direction suppression (**Leong et al., 2016**). This interpretation, however, suffers from a possible confusion of ON and OFF receptive subfields of T5 input neurons with the mechanism generating direction selectivity within T5 cells themselves. Addressing the same question, we recently applied apparent motion stimuli to one class of T4 cells that have upward as their preferred direction and, thus, project to layer 3 of the lobula plate. Using a telescopic stimulation technique to place the stimulus precisely onto the hexagonal lattice of the fly's eye (**Kirschfeld, 1967**; **Braitenberg, 1967**; **Franceschini, 1975**; **Schuling et al., 1989**), layer 3 T4 cells turned out to implement both mechanisms within different

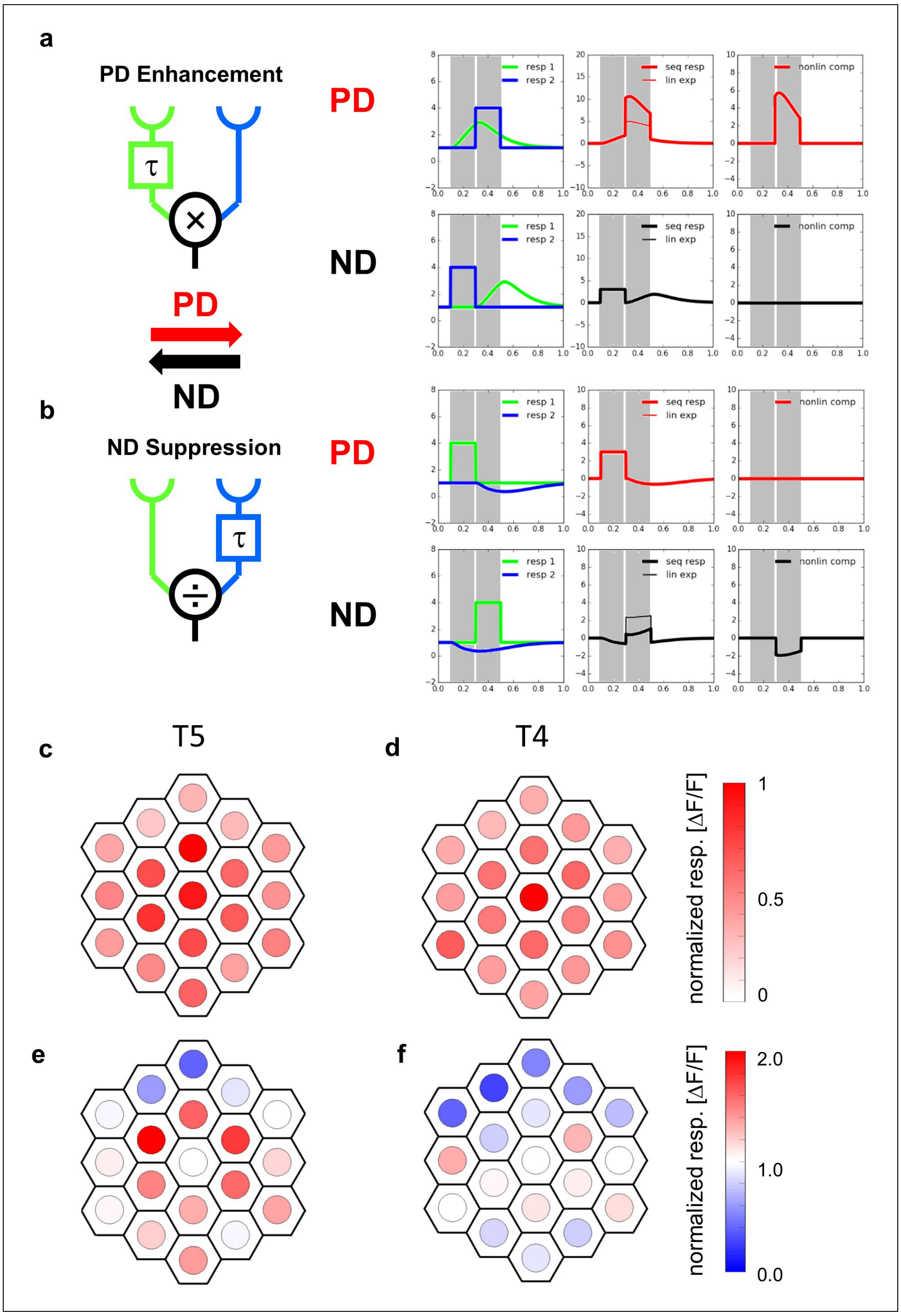

Figure 1. Receptive fields and responses to apparent motion stimuli of T5-cells. (**a**) The Hassenstein-Reichardt model incorporates PD enhancement only, realized by a multiplication. Left: Responses to individual light pulses ('Flicker') delivered at the two different positions. The responses are shifted according to the stimulus sequence used for the subsequent apparent motion stimuli. Middle: Responses of the model to apparent motion stimuli in preferred (upper row) and null direction (lower row, thick line = measured response, thin line = linear expectation, that is sum of responses to the single

Figure 1 continued on next page

Figure 1 continued

light pulses). Right: Nonlinear response component defined as the difference between measured response and linear expectation. (**b**) same as (**a**) but for a Barlow-Levick model. This model incorporates ND-suppression only, realized by a division. (**c**) Average responses of five T5 cells to flicker stimuli (stimulus size: 5 degree) delivered to different optical columns. In order to average the responses of different flies, the response patterns were aligned and normalized with respect to the maximum response (central column) and shown in a false color code. (**d**) Same as (**c**) but for T4-cells. Data represent the mean of 10 T4-cells from 10 flies (from ***Haag et al., 2016***). (**e**) Responses of T5 cells to stimuli presented to the central column and simultaneously to one of the columns of the two surrounding rings. As in c, the responses of different flies were aligned with respect to the column eliciting the maximum response when stimulated individually and normalized to it. Depending on the location, simultaneous stimulation of a second column led to either a suppressed (blue colors) or an enhanced (red colors) response compared to the exclusive stimulation of the central column. The suppression is stronger on the null side of the T5 cells. Data represent the mean of 6 T5 cells from 6 different flies. (**f**) Same as e) but for T4-cells. Data represent the mean of T4-cells from 8 flies (from ***Haag et al., 2016***).

DOI: https://doi.org/10.7554/eLife.29044.002

The following figure supplements are available for figure 1:

Figure supplement 1.

DOI: https://doi.org/10.7554/eLife.29044.003

Figure supplement 2. Responses of T4-cells and T5 cells to stimuli presented to the central column and simultaneously to one of the columns of the two surrounding rings.

DOI: https://doi.org/10.7554/eLife.29044.004

parts of their receptive field (***Haag et al., 2016***): While preferred direction enhancement was found to be dominant within the ventral part of the receptive field, a null direction suppression was significant in the dorsal part of their receptive field (***Haag et al., 2016***).

To resolve the conflicting evidences mentioned above and to test whether T5 cells are using the same or a different mechanism to compute the direction of motion as do T4 cells, we used the same strategy as in our previous account (***Haag et al., 2016***) and applied it to investigate the mechanism underlying direction selective responses of both T4 and T5 cells of all four directional tuning subtypes.

Results

In a first set of experiments, we used the same driver line as in our previous study (***Haag et al., 2016***) expressing the Calcium indicator GCaMP6m (***Chen et al., 2013***) in both T4 and T5 cells projecting to layer 3 of the lobula plate and, hence, having upward motion as their preferred direction. Since T5 cells are known to be OFF sensitive, we used dark spots on a bright background projected onto the raster of optical columns via a telescope to stimulate the cells and recorded the fluorescence changes in the lobula plate. We started by measuring the flicker responses of T5 cells to optical stimulation of 19 individual columns, forming two rings surrounding a central column. In ***Figure 1c***, the responses of five T5 cells were averaged and are shown in false color code overlaid on the columnar raster. T5 cells responded maximally to the stimulation of the central column, with about 50–100% amplitude to stimulation of the surrounding columns and about 20–50% to the next outer ring. An individual example trace and statistical evaluation of the responses are shown in ***Figure 1—figure supplement 1***. Compared to T4 cells (***Figure 1d***, data replotted from ***Haag et al., 2016***), the receptive field of T5 cells turned out to be broader with a somewhat stronger sensitivity within the surrounding columns. To explore spatial interactions within the receptive field of T5-cells, we stimulated the central column, simultaneously with one of surrounding columns. The results (***Figure 1e***) indicate a strong suppression of the response in the dorsal part of the receptive field compared to when the central column was stimulated alone, similar to what was found previously for T4 cells (***Figure 1f***, data replotted from ***Haag et al., 2016***).

Experiments performed on layer 3 T4 cells with apparent motion stimuli revealed different mechanisms of direction selectivity in different parts of the receptive field (***Haag et al., 2016***): Two-pulse apparent motion stimuli in the dorsal part of the receptive field led to a null direction suppression, apparent motion stimuli in the ventral part evoked preferred direction enhancement. We asked whether we could find this spatial arrangement of null direction suppression and preferred direction enhancement in T5 cells as well. In order to measure that, we presented OFF stimuli to four neighboring columns along the dorsal-ventral axis (***Figure 2a,b***). The columns were chosen in relation to

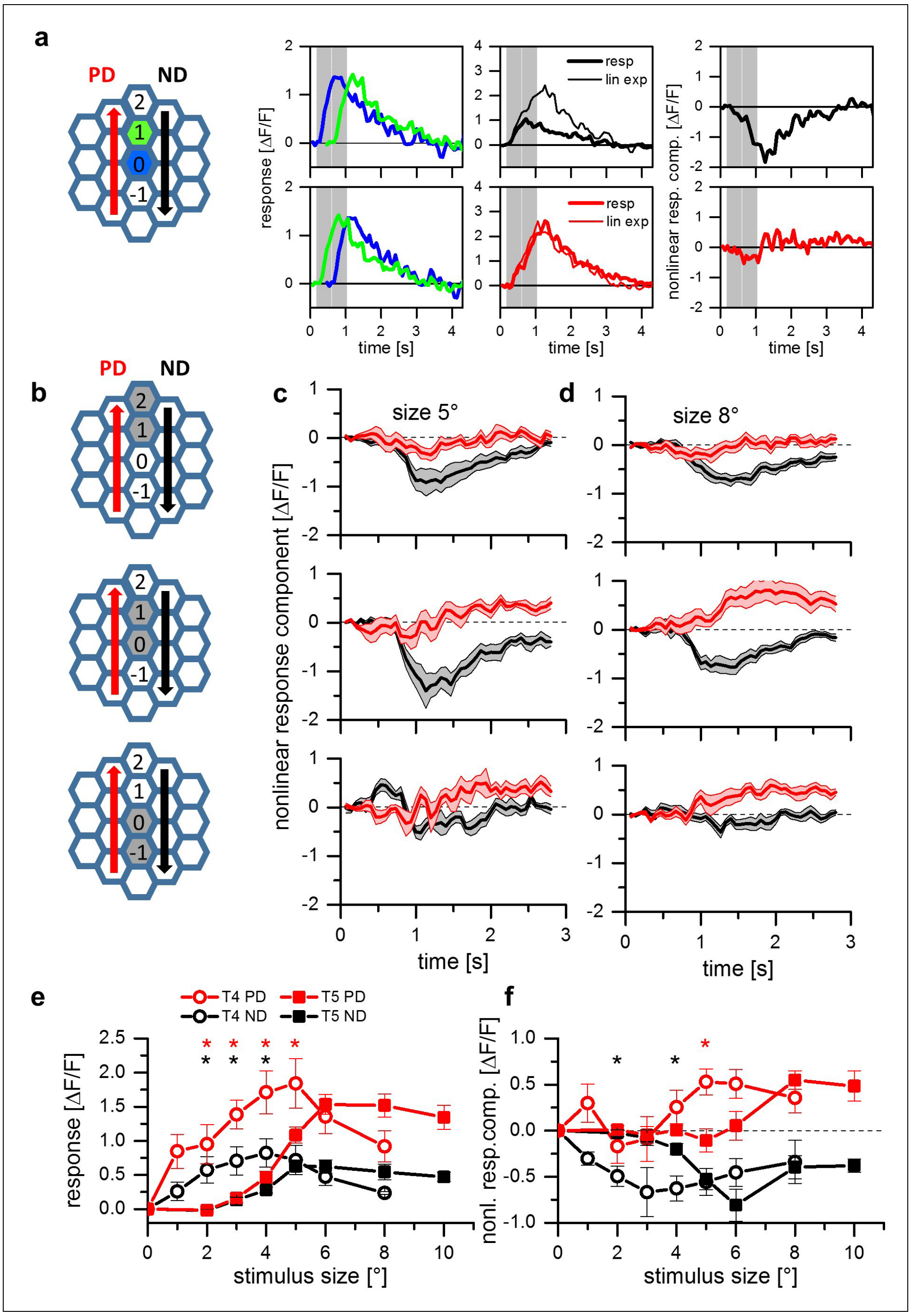

Figure 2. Apparent motion stimuli between adjacent cartridges. (**a**) Response of a single T5 cell recorded in a single sweep to two-step apparent motion stimuli. The schematic to the left shows the position of the two stimuli (blue and green shading). Left: Responses to individual light pulses ('Flicker') delivered at the two different positions. The responses are shifted in time according to the stimulus sequence used for the subsequent apparent motion stimuli.Middle: Responses of T5 to apparent motion stimuli in preferred and null direction (thick line = measured response, thin

Figure 2 continued on next page

Figure 2 continued

line = linear expectation, that is sum of responses to the single light pulses). Right: Nonlinear response component defined as the difference between measured sequence response and linear expectation. The responses are the mean obtained from n = 3 stimulus repetitions. (**b**) Two-step apparent motion stimuli were shown at three different position in the receptive field of T5 cells. The stimulus consisted of light off pulses positioned on one column for 472 ms, immediately followed by a light off pulse for 472 ms to the upper, neighboring cartridge. The same stimuli were repeated along the opposite direction. (**c**) Nonlinear response component, that is the difference between sequence response and the sum of the responses to the individual pulses, as a function of time for a stimulus size of 5 degree. Apparent motion stimuli delivered to the upper two cartridges resulted in a null direction suppression and no preferred direction enhancement. Apparent motion stimuli in the lower cartridges did not lead to a deviation from the linear expectation. For all three stimuli no preferred direction enhancement could be found. Data represent the mean ± SEM in 6 T5-cells measured in 6 different flies. (**d**) Same as d, but with a stimulus size of 8 degree. In contrast to the results for a smaller stimulus size, we found preferred direction enhancement for stimulation of the lower and the central pair of columns. Data shows the mean ± SEM in 10 T5-cells measured in 8 different flies. (**e**) Responses of T4 (open circles) and T5 cells (closed squares) to apparent motion stimuli in preferred (red colors) and null direction (black colors) between the two central columns 0 and 1. Compared to the responses of T4, T5 responses to two-pulse sequences along the preferred (PD) and the null (ND) direction are shifted to larger stimulus sizes. Data represent the mean values ± SEM of 10 T5 cells measured in 5 flies and of 7 T4 cells in 4 different flies, respectively. Black asterisks represent statistically significant (t-test, p-value<0.05) differences for null-direction responses of T4-cells and T5-cells, red asterisks for preferred direction responses. (**f**) Nonlinear response components of T4 and T5 cells. Same dataset as in ***Figure 1e***.

DOI: https://doi.org/10.7554/eLife.29044.005

the column that elicited the strongest response in each cell (central column 0). We then tested T5 cells with two consecutive light OFF pulses of 472 ms duration in immediate succession. Each light pulse was positioned on one of two neighboring columns resulting in three stimulus sequences (***Figure 2b***). To extract the nonlinear response component, we subtracted the sum of the responses to the individual stimuli from the response to the apparent motion sequence. Example traces from an individual experiment stimulating columns 0 and 1 are shown in ***Figure 2a***. Using the same spot diameter as in our previous account, that is 5 degree, we found null direction suppression for stimulation of the central (column 0 and 1) and the dorsal (column 1 and 2) pairs, and only a slight, if any, sign of preferred direction enhancement for stimulation of the ventral pair (column -1 and 0) (***Figure 2c***). This changed when we enlarged the spot size from 5 to 8 degree. Now, in addition to null direction suppression for the central and dorsal stimulus pairs, preferred direction enhancement for the ventral and central stimulus pairs was observed (***Figure 2d***). This result mirrors our previous finding for T4 cells where both null direction suppression and preferred direction enhancement was found to account for direction selectivity (***Haag et al., 2016***). In further agreement with T4 cells, these two mechanisms are spatially separated, with null direction suppression on the null and preferred direction enhancement on the preferred side of the receptive field (***Haag et al., 2016***).

The above experiments indicate a different dependence of null direction suppression and preferred direction enhancement on the diameter of the stimulus spot in T5 cells. To measure this dependence in a gradual way, we again used apparent motion stimuli and varied the size of the stimuli from 1 to 10 degree. Since stimuli centered on the central column pair (0 and 1) resulted in both types of nonlinearity (***Figure 2d***, middle graph), we presented apparent motion stimuli with different stimulus sizes to these central columns only. To compare the results of T5 cells with the ones of T4 cells, the stimulus set consisted of either bright pulses on a dark background (for T4 cells) or dark pulses on a bright background (for T5 cells). ***Figure 2e*** shows the responses of T4 (circle symbols) and T5 (square symbols) to apparent motion stimuli as a function of the stimulus size for preferred (PD, red traces) and null (ND, black traces) direction sequences. For both directions of motion, T4 cells respond to smaller stimuli than T5 cells. The strongest response in T4 can be found for stimulus sizes of 4 to 5 deg. For stimulus sizes beyond these values, the responses of T4 cells decline. In contrast, T5 cells only start responding at these stimulus sizes and plateau for larger values. When instead of the response the nonlinear response component is plotted as a function of the stimulus size (***Figure 2f***, same symbol and color code as in ***Figure 2e***), both preferred direction enhancement and null direction suppression become apparent, with both curves shifted to larger stimulus sizes for T5 cells. Furthermore, for both cell types, null direction suppression peaks at smaller stimulus sizes than preferred direction enhancement.

The results presented so far point towards a common mechanism for T4 and T5 cells underlying direction selectivity. However, the experiments on T4 and T5 cells were confined to those that terminate in layer 3 of the lobula plate. In order to investigate whether the properties described above generalize to T4 and T5 cells of all four tuning categories, we next used a fly line expressing GCaMP5 in T4 and T5 cells projecting to all four layers. Similar to the experiments shown in ***Figure 2c and d***, two-step apparent motion stimuli consisting of ON-ON pulses of 5 degree diameter for T4 cells as well of OFF-OFF pulses of 8 degree diameter for T5 cells were presented in three adjacent pairs of columns aligned to the column that elicited the strongest flicker response (***Figure 3a***). As before, the stimulus protocol consisted in the presentation of individual stimulus pulses for the calculation of the linear expectation as well as in the presentation of the two-pulse sequences, to measure the sequence response. From the latter, the linear expectation was subtracted to obtain the nonlinear response component. The time traces of these nonlinear response components are shown in ***Figure 3b and c***. For T4 (***Figure 3b***) and T5 (***Figure 3c***) cells projecting to all layers, we found both preferred direction and null direction suppression, with a spatial separation that follows the same pattern: on the preferred side of the receptive field, a clear preferred direction enhancement was observed without any null direction suppression (***Figure 3b and c***, left column). In the center of the receptive field, both preferred direction enhancement and null direction suppression prevailed (***Figure 3b and c***, center column). On the null side of the receptive field, only null direction suppression was detectable (***Figure 3b and c***, right column). To investigate possible differences between T4 and T5 cells and between cells with different directional tuning, we performed a 3-way ANOVA test. Choosing a significance level of p=0.05, no significant differences were found, neither between T4 and T5 cells, nor between the neurons projecting to the four different layers. In ***Figure 3d*** (T4 cells) and ***3e*** (T5 cells), the nonlinear response components are shown as averaged between 1 and 2 s of the time courses shown above, as well as averaged across the cells from all four layers. On these data, two-sided t-tests were performed between T4 and T5 cell responses for each individual stimulus condition. Choosing again a significance level of p=0.05, no differences were found between T4 and T5 cell responses for 5 out of 6 stimulus conditions. Only the response amplitude of T4 cells to null direction stimulus sequences from column 2 to 1 was found to be significantly smaller than the respective value of T5 cells.

The results from apparent motion experiments reported so far suggest a common directional tuning mechanism for T4 and T5 cells for all cardinal directions. One, thus, would expect identical high degrees of direction selectivity in response to moving gratings mechanism within the different layers of the lobula plate. To test this directly, we used the same fly line as above expressing in both T4 and T5 cells of all four layers and presented grating motion along all four cardinal directions on a screen. For each pixel, we first calculated the vector sum of the responses and represented the vector angle in false color. The resulting image from one example fly is shown in ***Figure 4a***. Clearly, the preferred direction is extremely homogeneous with little variation within each layer. We repeated such experiments in five different flies and determined the distribution of all preferred directions obtained from the whole data set. The histogram (***Figure 4b***) reveals exactly four sharp peaks separated by 90 degrees, corresponding to the preferred directions of T4 and T5 cells within each of the four layers. This transition from the hexagonal coordinates of the fly eye to Cartesian coordinates is likely to occur on the dendrites of T4 and T5 cells by their sampling from appropriately grouped columns (***Takemura et al., 2017***). From the same data set, we calculated a direction selectivity index for each pixel within each layer as the difference of the responses to preferred and null direction, divided by the sum of the responses. We then determined the mean direction selectivity for each layer from each fly and averaged the resulting values across the different experiments. The results reveal an extremely high degree of direction selectivity of about 0.8 that is almost identical within each layer (***Figure 4c***). To measure direction selectivity separately for T4 and T5 cells, we stimulated the flies with ON and OFF edges instead of gratings and obtained similar values of about 0.8 on average (***Figure 4d***).

Discussion

Having analyzed the mechanisms underlying direction selectivity of all fours subtypes of both T4 and T5 cells, we found a common scheme that pertains to all of these cells: regardless of the directional tuning and the contrast preference for ON or OFF stimuli, elementary motion-sensitive neurons in *Drosophila* implement a preferred direction enhancement on the preferred side and a null direction suppression of input signals on the null side of their receptive field.

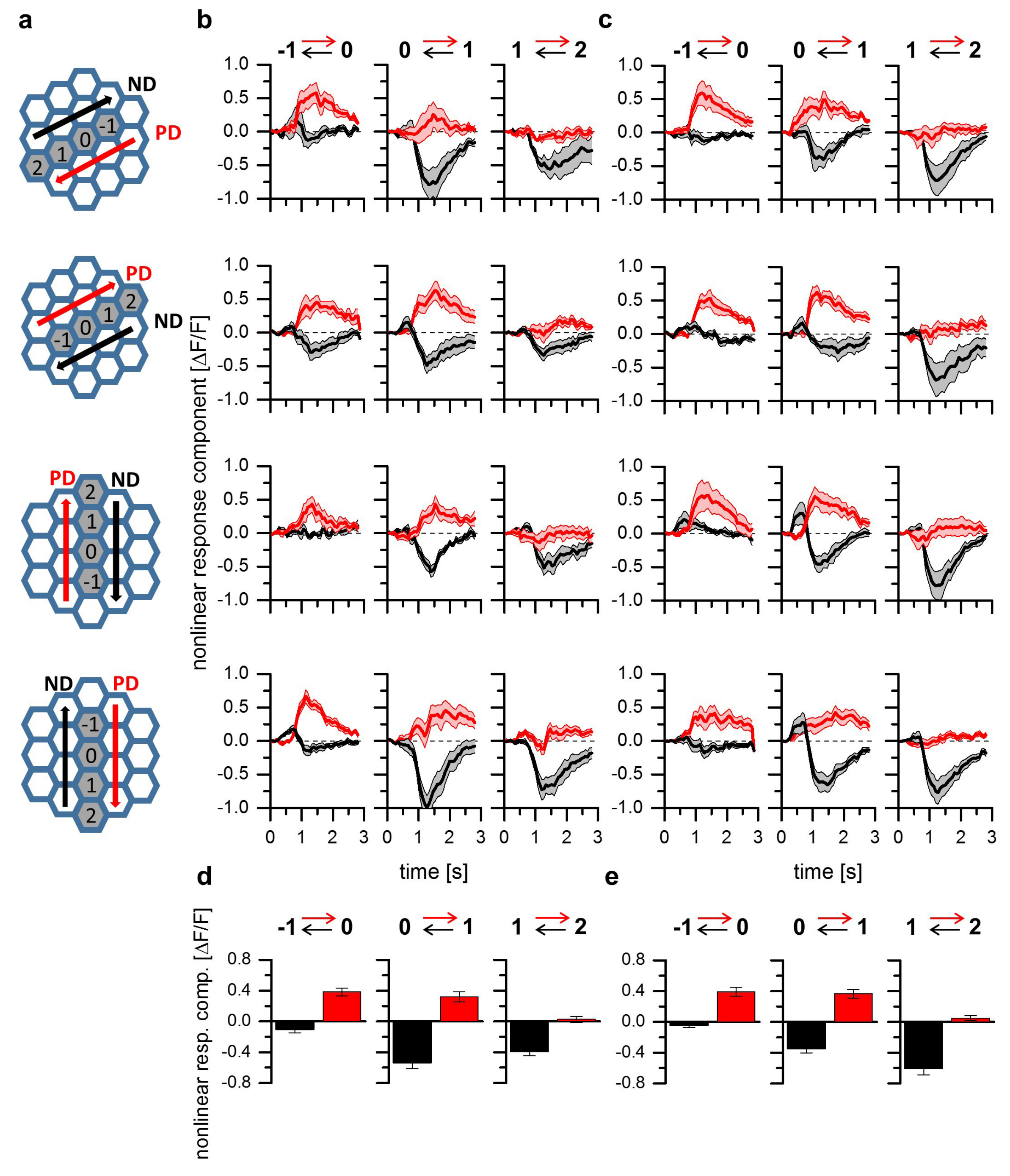

Figure 3. A common mechanism for direction selectivity in all four subtypes of T4 and T5 cells. (**a**) Pictograms indicating the stimulus positions and the preferred and null-direction of the respective layer. (**b**) Nonlinear response components of T4-cells to apparent motion stimuli in different layers of the lobula plate. For T4 cells projecting to all four layers, preferred direction enhancement and null direction suppression are found to be spatially distributed within the receptive field such that enhancement is found on the preferred side while suppression is predominant on the null side of the

Figure 3 continued on next page

Figure 3 continued

receptive field. Data represent the mean ± SEM of 6, 8, 7 and 9 T4 cells (from layer 1–4). (c) Nonlinear response components of T5 cells to apparent motion stimuli in different layers of the lobula plate. Data represent the mean ± SEM of 8, 5, 6 and 13 T5 cells (from layer 1–4).

DOI: https://doi.org/10.7554/eLife.29044.006

ON and OFF pathways seemed to have adapted to the asymmetry of luminance distributions found in the real world. Consequently, functional differences between ON and OFF pathways have been described in the mammalian retina and in flies as well (**Ratliff et al., 2010**; **Clark et al., 2014**; **Baden et al., 2016**; **Leonhardt et al., 2016**). In fly motion vision, our finding of a common mechanism for T4 and T5 cells suggests the above mentioned asymmetries to rely on quantitative instead of qualitative differences, such as different time-constants used by the ON and the OFF pathway (**Leonhardt et al., 2016**; **Arenz et al., 2017**). One difference between T4 and T5 cells found in this

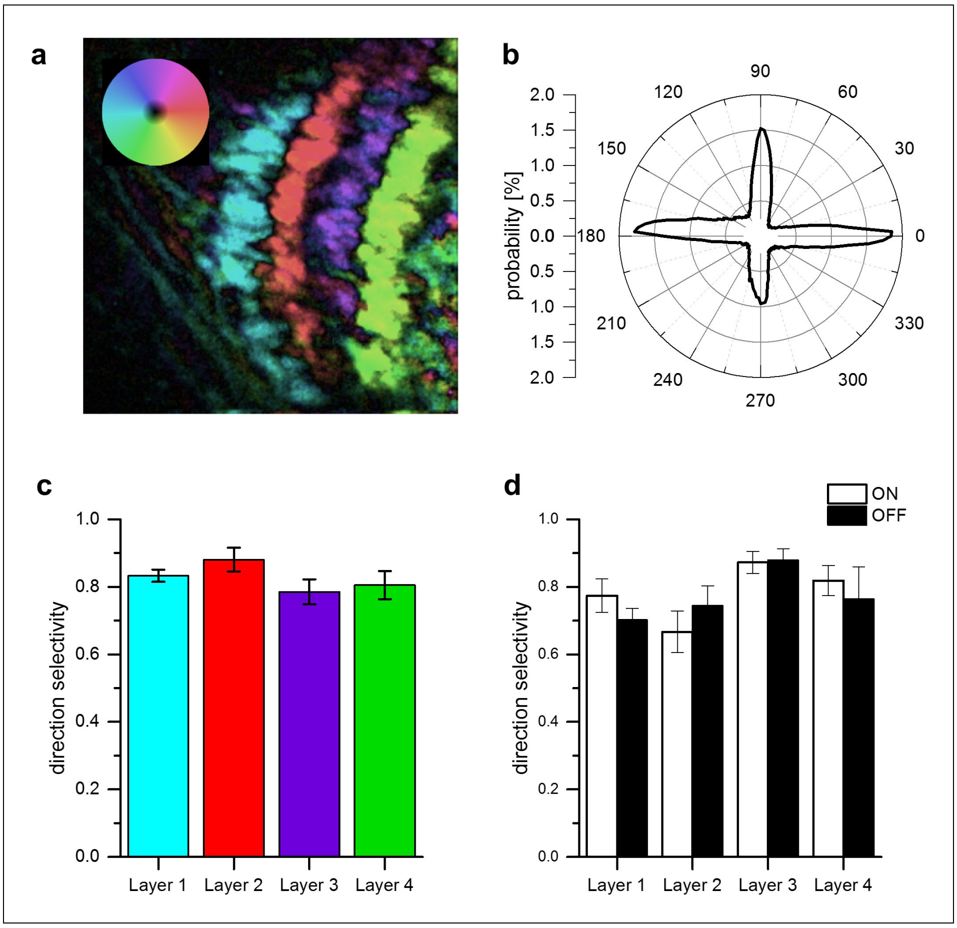

Figure 4. Directional tuning and selectivity of T4 and T5 cells. (a) Example of directional tuning to grating motion as determined by the vector sum of responses to grating motion along four cardinal directions. All neurons within each layer have almost identical preferred directions. (b) Histogram of preferred directions within all four layers. Clear peaks appear at the four cardinal directions. Data were obtained from 5 different flies. (c) Direction selectivity within each layer, as defined by the difference between the preferred and null direction responses, divided by the sum. Data represent the mean ± SEM obtained from 5 flies (same data set as in b). (d) Same as c, but flies were stimulated by ON and OFF edges, respectively. Data represent the mean ± SEM obtained from 3 flies.

DOI: https://doi.org/10.7554/eLife.29044.007

study relates to the dependence of the directional motion signal on the spot size in the apparent motion paradigm (**Figure 2e,f**). Given a half-width of the photoreceptor acceptance angle of approximately 5 degree in *Drosophila* (**Götz, 1965**), any stimulus is spatially low-pass filtered by a Gaussian with 5 degree full width at half maximum. Accordingly, enlarging the spot size will have two different effects: first, it will lead to an increasing peak intensity at the column where the stimulus spot is centered on, and second, it will lead to an increasing activation of neurons in neighboring columns. Which of these two effects is responsible for the higher threshold of T5 cells compared to T4 cells, and whether the sensitivity difference is in the input neurons or in T4/T5 cells themselves, cannot be decided by the present study.

In any case, our finding readily explains the high degree of direction selectivity found already at the processing stage where direction-selective signals first arise: neither a signal enhancement for preferred direction sequences nor a signal suppression for null direction sequences by itself would lead to such a strong direction selectivity as observed experimentally with large signals for preferred direction motion and zero responses for null direction motion (**Maisak et al., 2013**; **Fisher et al., 2015**). In analogy to the results presented for layer 3 T4 cells (Figure 5 in **Haag et al., 2016**), the responses of all T4 and T5 cells can be captured in algorithmic terms by a common mechanism, using a delayed, low-pass filtered input on the preferred side enhancing a fast, central input, with the result being suppressed by again a low-pass filtered input on the null side.

At the next processing stage, that is at the level of lobula plate tangential cells, the signals of oppositely tuned T4 and T5 cells become subtracted via inhibitory lobula plate interneurons (**Mauss et al., 2015**). This process, in a way, replicates the action of null direction suppression implemented on the dendrites of T4 and T5 cells. Since both mechanisms, that is the combination of preferred direction enhancement and null direction suppression on the dendrites of T4 and T5 cells as well as the subtraction of oppositely tuned T4 and T5 cells on the dendrites of tangential cells lead to high degree of direction selectivity at the output of the system, one might ask about the functional advantage of such a dual strategy. This question can be answered by either blocking null direction suppression on the T4/T5 cells dendrite or blocking the inhibitory lobula plate interneurons. The latter experiment has indeed been done, and the results revealed a loss of flow-field specificity of the tangential cells, due to the lack of inhibition caused by the non-matching part of the optic flow field (**Mauss et al., 2015**). For the converse situation, no experimental data exist so far and one has to rely on computer simulations (**Haag et al., 2016**, Figure 5). They suggest that a high direction selectivity is retained in tangential cells. This high degree of direction selectivity, however, rests on the relatively small differences between large, but poorly tuned signals and, thus, would be highly prone to noise. Improving the direction-tuning already at the level of T4 and T5 cells by the additional null-direction suppression should, therefore, increase the system's robustness to noise.

Our results open the door to the next level question about its neural implementation. Here, a recent connectomic study identified the major interneurons providing synaptic input to T4 cells as well as their placement on the dendrite (**Takemura et al., 2017**). Takemura and colleagues describe 4 columnar cell types, that is Mi1, Mi4, Mi9 and Tm3 as the major input elements to T4 cells, in addition to columnar cell types C3, TmY15, a wide-field neuron CT1 and other T4 cells with identical preferred direction. Columnar input neurons contact the T4 cell dendrite in a way that depends on the direction tuning subtype: while Mi9 synapses are clustered on the preferred side of the dendrite, Mi1 and Tm3 synapse on the central part and Mi4 are found predominantly on the null side. Most interestingly, the dynamic response properties of these different types of T4 input neurons match their position on the dendrite to suggest a specific function in the detector model discussed above: Mi9 and Mi4 indeed exhibit the temporal low-pass properties postulated for the inputs on the preferred and the null side, while Mi1 and Tm3 display fast band-pass properties needed for the central input (**Arenz et al., 2017**). This proposed correspondence needs to be tested by blocking individual input cell types and measuring the resulting effect on direction selectivity in T4 cells. Specifically, one would expect to abolish preferred direction enhancement when blocking Mi9, while blocking Mi4 should lead to a loss of null direction suppression. It is, however, important to stress that the effect of such blocking experiments is expected to be quite specific and directly observable only in directional responses of T4 cells: due to further network processing involving a subtraction of T4 cell signals with opposite directional tuning at the level of tangential cells (see previous paragraph, and **Mauss et al., 2015**), the effect might be far more subtle when downstream cells or behavior are used as a read-out (**Strother et al., 2017**). Nevertheless, blocking the central inputs Mi1 and Tm3 while recording from tangential cells revealed that Mi1 cells are absolutely essential for proper functioning of the ON pathway under all stimulus conditions tested, while blocking Tm3 only led to a loss of sensitivity for high edge velocities (**Ammer et al., 2015**). With respect to the polarity of the synapses of the various T4 input neurons, the correspondence outlined above predicts that Mi1 and Tm3 are excitatory while Mi4 should be inhibitory. In line with this, recent studies suggest a cholinergic phenotype in Mi1 and Tm3 (**Pankova and Borst, 2017**; **Takemura et al., 2017**) and a GABAergic one in Mi4 (**Takemura et al., 2017**). Seemingly in contrast to an enhancing action of Mi9 postulated above, this cell was found to be OFF sensitive (**Arenz et al., 2017**). However, Mi9 turned out to be immune-positive for the vesicular Glutamate reporter VGlut (**Takemura et al., 2017**). Together with the inhibitory action of Glutamate via the GluCl channel, well documented for other neurons of the Drosophila CNS (**Liu and Wilson, 2013**; **Mauss et al., 2014**; **Mauss et al., 2015**), this raises the possibility that Mi9 enhances the input from Mi1 and Tm3 onto T4 by a release from inhibition.

As for T4 cells, the major input neurons to T5 cells were identified by an EM study (**Shinomiya et al., 2014**). There, trans-medulla neurons Tm1, Tm2, Tm4, and Tm9 were found to make up for about 80% of all input synapses to T5 cell dendrites. However, the exact placement of the different inputs on the dendrite and, hence, the relative position of their receptive fields could not be determined by this report. As for their dynamic properties, only one of the cell types, Tm9, reveals low-pass characteristics, while all others (Tm1, Tm2 and Tm4) can be described as band-pass filters with different time-constants (**Meier et al., 2014**; **Serbe et al., 2016**; **Arenz et al., 2017**). In analogy of the arrangement of input neurons of T4 cells, **Arenz et al., 2017** found that placing the two slowest cells (Tm1 and Tm9) on the outer arms and the fast Tm2 cell on the central arm of the three-input detector gives rise to a motion detector that fits real T5 cells both with respect to their high degree of direction selectivity and their temporal tuning optimum. Since, in contrast to T4 cells, the position of these interneurons on the dendrite of T5 cells is less well known so far, no prediction can be made whether blocking of Tm1 should lead to a loss of preferred direction enhancement and blocking of Tm9 to a loss of null direction suppression, or the other way round. Therefore, as is the case with T4 cells, further experiments are needed to determine which cell is playing which role in the functional context of preferred direction enhancement and null direction inhibition determined by the present study.

In summary, thus, we have found a common, uniform mechanism of direction selectivity for T4 and T5 cells that consists of combination of preferred direction enhancement and null direction suppression in different location of their receptive field, precisely related to their directional tuning. Mapping the different input neurons to T4 and T5 cells to their specific function in this context represents the next step of the analysis. The major challenge for future experiments will then consist in understanding the biophysical mechanisms underlying enhancement and suppression. Here, different ideas have been discussed in the past (**Torre and Poggio, 1978**; **Koch and Poggio, 1992**; **Gabbiani et al., 2002**), and the different thresholds for preferred direction enhancement and null direction suppression described above might be an important result to decide between the various possibilities. These can now be tested at the molecular level using genome editing techniques available in *Drosophila* (**Venken et al., 2011**; **Zhang et al., 2014**; **Fisher et al., 2017**; **Pankova and Borst, 2017**).

Materials and methods

Flies

(*Drosophila melanogaster*) were raised at 25°C and 60% humidity on a 12 hr light/12 hr dark cycle on standard cornmeal agar medium. For calcium imaging of T5 cells, flies were used expressing the genetically-encoded calcium indicator GCaMP6m (**Chen et al., 2013**) in T4/T5 neurons with axon terminals predominantly in layer 3 of the lobula plate (w^{-}; Sp/cyo; VT50384-lexA, lexAop-GCaMP6m/TM6b). For the imaging experiments of T4 and T5 cells in the four layers of the lobula plate we used flies expressing the calcium indicator GCaMP5 in both T4 and T5 cells in all layers of the lobula plate (*w^{-}; +/+; UAS-GCaMP5, R42F06-GAL4/UAS-GCaMP5,R42F06-GAL4*).

Calcium imaging

Fly surgery was performed, and the neuronal activity was measured from the left optical lobe on a custom-built 2-photon microscope (**Denk et al., 1990**) as previously described (**Haag et al., 2016**). Images were acquired at a resolution of 64 × 64 pixels and at a frame rate of 15 Hz with the ScanImage software (**Pologruto et al., 2003**) in Matlab.

Optical stimulation

Stimulation with a telescopic stimulus device was similar to that used in our previous study (**Haag et al., 2016**). For the experiments shown in **Figure 4**, a regular stimulus display was used as described in (**Arenz et al., 2017**). The gratings had a spatial wavelength of 30 deg, a contrast of 100%, a mean luminance of 34 cd/m^2 and was moving along one of the four cardinal directions at 30 deg/sec.

Experimental protocol

In order to discriminate between T4 and T5 cells we stimulated single optical columns with bright pulses on a dark background. The cells were selected based on their response to light-on stimuli. While T4 cells respond to the onset of a light pulse, the T5 cells respond to the light-off. For the experiments the stimuli consisted either of dark pulses on a bright background (T5 cells) or bright pulses on a dark background (T4 cells). The pulses had a duration of 472 ms. At each position, three stimulus presentations were delivered. The resulting responses were averaged and the peak of the averaged response was taken. Apparent motion stimuli consisted of consecutive light stimuli to two neighboring cartridges. The second stimulus was presented right after the first turned off, resulting in a delay from onset to onset of 472 ms.

Data analysis

was performed offline using custom-written routines in Matlab. Regions of interests (ROIs) were selected by hand of the lobula plate. Time courses of relative fluorescence changes (ΔF/F) were calculated from the raw imaging sequence. Responses to the stimulus were baseline-subtracted, averaged across repetitions, and quantified as the peak responses over the stimulus epochs. Those responses were averaged across experiments. Where indicated, responses were normalized to the maximum average response before averaging. For the apparent motion experiments, non-linear response components were calculated as the differences of the time-courses of the responses to the apparent motion stimuli and the sum of the appropriately time-shifted responses to flicker stimuli at the corresponding positions.

Acknowledgements

We thank Georg Ammer, Alexander Arenz and Alex Mauss for critically reading the ms. This work was supported by the Max-Planck-Society and the Deutsche Forschungsgemeinschaft (SFB 870).

Additional information

Competing interests

Alexander Borst: Reviewing editor, *eLife*. The other authors declare that no competing interests exist.

Funding

Funder	Grant reference number	Author
Max-Planck-Gesellschaft		Juergen Haag Abhishek Mishra Alexander Borst
Deutsche Forschungsgemeinschaft	SFB 870	Juergen Haag Abhishek Mishra Alexander Borst

The funders had no role in study design, data collection and interpretation, or the decision to submit the work for publication.

Author contributions

Juergen Haag, Conceptualization, Data curation, Software, Investigation, Visualization, Writing—review and editing; Abhishek Mishra, Investigation; Alexander Borst, Conceptualization, Funding acquisition, Writing—original draft, Project administration, Writing—review and editing

Author ORCIDs

Juergen Haag https://orcid.org/0000-0002-6535-0103
Abhishek Mishra http://orcid.org/0000-0002-1933-1251
Alexander Borst http://orcid.org/0000-0001-5537-8973

Decision letter and Author response

Decision letter https://doi.org/10.7554/eLife.29044.010
Author response https://doi.org/10.7554/eLife.29044.011

Additional files

Supplementary files

- Transparent reporting form

DOI: https://doi.org/10.7554/eLife.29044.008

References

Ammer G, Leonhardt A, Bahl A, Dickson BJ, Borst A. 2015. Functional Specialization of Neural Input Elements to the Drosophila ON Motion Detector. *Current Biology* **25**:2247–2253. DOI: https://doi.org/10.1016/j.cub.2015.07.014, PMID: 26234212

Arenz A, Drews MS, Richter FG, Ammer G, Borst A. 2017. The Temporal Tuning of the Drosophila Motion Detectors Is Determined by the Dynamics of Their Input Elements. *Current Biology* **27**:929–944. DOI: https://doi.org/10.1016/j.cub.2017.01.051, PMID: 28343964

Baden T, Berens P, Franke K, Román Rosón M, Bethge M, Euler T. 2016. The functional diversity of retinal ganglion cells in the mouse. *Nature* **529**:345–350. DOI: https://doi.org/10.1038/nature16468, PMID: 26735013

Bahl A, Ammer G, Schilling T, Borst A. 2013. Object tracking in motion-blind flies. *Nature Neuroscience* **16**:730–738. DOI: https://doi.org/10.1038/nn.3386, PMID: 23624513

Barlow HB, Levick WR. 1965. The mechanism of directionally selective units in rabbit's retina. *The Journal of Physiology* **178**:477–504. DOI: https://doi.org/10.1113/jphysiol.1965.sp007638, PMID: 5827909

Bausenwein B, Dittrich AP, Fischbach KF. 1992. The optic lobe of Drosophila melanogaster. II. Sorting of retinotopic pathways in the medulla. *Cell and Tissue Research* **267**:17–28. PMID: 1735111

Behnia R, Clark DA, Carter AG, Clandinin TR, Desplan C. 2014. Processing properties of ON and OFF pathways for Drosophila motion detection. *Nature* **512**:427–430. DOI: https://doi.org/10.1038/nature13427, PMID: 25043016

Behnia R, Desplan C. 2015. Visual circuits in flies: beginning to see the whole picture. *Current Opinion in Neurobiology* **34**:125–132. DOI: https://doi.org/10.1016/j.conb.2015.03.010, PMID: 25881091

Borst A, Helmstaedter M. 2015. Common circuit design in fly and mammalian motion vision. *Nature Neuroscience* **18**:1067–1076. DOI: https://doi.org/10.1038/nn.4050, PMID: 26120965

Borst A. 2014. Fly visual course control: behaviour, algorithms and circuits. *Nature Reviews Neuroscience* **15**:590–599. DOI: https://doi.org/10.1038/nrn3799, PMID: 25116140

Braitenberg V. 1967. Patterns of projection in the visual system of the fly. I. Retina-lamina projections. *Experimental Brain Research* **3**:271–298. DOI: https://doi.org/10.1007/BF00235589, PMID: 6030825

Cajal SR, Sanchez D. 1915. *Contribucion Al Conocimiento De Los Centros Nerviosos De Los Insectos*. Madrid: Imprenta de Hijos de Nicholas Moja.

Chen TW, Wardill TJ, Sun Y, Pulver SR, Renninger SL, Baohan A, Schreiter ER, Kerr RA, Orger MB, Jayaraman V, Looger LL, Svoboda K, Kim DS. 2013. Ultrasensitive fluorescent proteins for imaging neuronal activity. *Nature* **499**:295–300. DOI: https://doi.org/10.1038/nature12354, PMID: 23868258

Clark DA, Fitzgerald JE, Ales JM, Gohl DM, Silies MA, Norcia AM, Clandinin TR. 2014. Flies and humans share a motion estimation strategy that exploits natural scene statistics. *Nature Neuroscience* **17**:296–303. DOI: https://doi.org/10.1038/nn.3600, PMID: 24390225

Denk W, Strickler JH, Webb WW. 1990. Two-photon laser scanning fluorescence microscopy. *Science* **248**:73–76. DOI: https://doi.org/10.1126/science.2321027, PMID: 2321027

Egelhaaf M, Borst A. 1992. Are there separate ON and OFF channels in fly motion vision? *Visual Neuroscience* **8**: 151–164. DOI: https://doi.org/10.1017/S0952523800009317, PMID: 1558827

Eichner H, Joesch M, Schnell B, Reiff DF, Borst A. 2011. Internal structure of the fly elementary motion detector. *Neuron* **70**:1155–1164. DOI: https://doi.org/10.1016/j.neuron.2011.03.028, PMID: 21689601

Fischbach K-F, Dittrich APM. 1989. The optic lobe of *Drosophila melanogaster*. I. A Golgi analysis of wild-type structure. *Cell and Tissue Research* **258**:441–475. DOI: https://doi.org/10.1007/BF00218858

Fisher YE, Silies M, Clandinin TR. 2015. Orientation Selectivity Sharpens Motion Detection in Drosophila. *Neuron* **88**:390–402. DOI: https://doi.org/10.1016/j.neuron.2015.09.033, PMID: 26456048

Fisher YE, Yang HH, Isaacman-Beck J, Xie M, Gohl DM, Clandinin TR. 2017. FlpStop, a tool for conditional gene control in Drosophila. *eLife* **6**:e22279. DOI: https://doi.org/10.7554/eLife.22279, PMID: 28211790

Franceschini N. 1975. Sampling of the visual environment by the compound eye of the fly: fundamentals and applications. In: Snyder (Ed). *Photoreceptor Optics*. p. 98–125.

Gabbiani F, Krapp HG, Koch C, Laurent G. 2002. Multiplicative computation in a visual neuron sensitive to looming. *Nature* **420**:320–324. DOI: https://doi.org/10.1038/nature01190, PMID: 12447440

Götz KG. 1965. Die optischen Übertragungseigenschaften der Komplexaugen von Drosophila. *Kybernetik* **2**:215–221. DOI: https://doi.org/10.1007/BF00306417

Haag J, Arenz A, Serbe E, Gabbiani F, Borst A. 2016. Complementary mechanisms create direction selectivity in the fly. *eLife* **5**:e17421. DOI: https://doi.org/10.7554/eLife.17421, PMID: 27502554

Hassenstein B, Reichardt W. 1956. Systemtheoretische analyse der zeit-, reihenfolgen- und vorzeichenauswertung bei der bewegungsperzeption des rüsselkäfers Chlorophanus. *Zeitschrift Für Naturforschung B* **11**:513–524.

Joesch M, Plett J, Borst A, Reiff DF. 2008. Response properties of motion-sensitive visual interneurons in the lobula plate of Drosophila melanogaster. *Current Biology* **18**:368–374. DOI: https://doi.org/10.1016/j.cub.2008.02.022, PMID: 18328703

Joesch M, Schnell B, Raghu SV, Reiff DF, Borst A. 2010. ON and OFF pathways in Drosophila motion vision. *Nature* **468**:300–304. DOI: https://doi.org/10.1038/nature09545, PMID: 21068841

Joesch M, Weber F, Eichner H, Borst A. 2013. Functional specialization of parallel motion detection circuits in the fly. *Journal of Neuroscience* **33**:902–905. DOI: https://doi.org/10.1523/JNEUROSCI.3374-12.2013, PMID: 23325229

Kirschfeld K. 1967. Die projektion der optischen umwelt auf das raster der rhabdomere im komplexauge von Musca. *Experimental Brain Research* **3**:248–270. DOI: https://doi.org/10.1007/BF00235588

Koch C, Poggio T. 1992. Multiplying with synapses and neurons. In: , McKenna T, Davis J, Zornetzer SF (Eds). *And Single Neuron Computation*. Boston, Sand Diego, new Ork, London, Sydney, Tokyo, Toronto: Academic Press. p. 315–345.

Leong JC, Esch JJ, Poole B, Ganguli S, Clandinin TR. 2016. Direction Selectivity in Drosophila Emerges from Preferred-Direction Enhancement and Null-Direction Suppression. *Journal of Neuroscience* **36**:8078–8092. DOI: https://doi.org/10.1523/JNEUROSCI.1272-16.2016, PMID: 27488629

Leonhardt A, Ammer G, Meier M, Serbe E, Bahl A, Borst A. 2016. Asymmetry of Drosophila ON and OFF motion detectors enhances real-world velocity estimation. *Nature Neuroscience* **19**:706–715. DOI: https://doi.org/10.1038/nn.4262, PMID: 26928063

Liu WW, Wilson RI. 2013. Glutamate is an inhibitory neurotransmitter in the Drosophila olfactory system. *PNAS* **110**:10294–10299. DOI: https://doi.org/10.1073/pnas.1220560110, PMID: 23729809

Maisak MS, Haag J, Ammer G, Serbe E, Meier M, Leonhardt A, Schilling T, Bahl A, Rubin GM, Nern A, Dickson BJ, Reiff DF, Hopp E, Borst A. 2013. A directional tuning map of Drosophila elementary motion detectors. *Nature* **500**:212–216. DOI: https://doi.org/10.1038/nature12320, PMID: 23925246

Mauss AS, Meier M, Serbe E, Borst A. 2014. Optogenetic and pharmacologic dissection of feedforward inhibition in Drosophila motion vision. *Journal of Neuroscience* **34**:2254–2263. DOI: https://doi.org/10.1523/JNEUROSCI.3938-13.2014, PMID: 24501364

Mauss AS, Pankova K, Arenz A, Nern A, Rubin GM, Borst A. 2015. Neural circuit to integrate opposing motions in the visual field. *Cell* **162**:351–362. DOI: https://doi.org/10.1016/j.cell.2015.06.035, PMID: 26186189

Meier M, Serbe E, Maisak MS, Haag J, Dickson BJ, Borst A. 2014. Neural circuit components of the Drosophila OFF motion vision pathway. *Current Biology* **24**:385–392. DOI: https://doi.org/10.1016/j.cub.2014.01.006, PMID: 24508173

Pankova K, Borst A. 2017. Transgenic line for the identification of cholinergic release sites in Drosophila melanogaster. *The Journal of Experimental Biology* **220**:1405–1410. DOI: https://doi.org/10.1242/jeb.149369, PMID: 28167805

Pologruto TA, Sabatini BL, Svoboda K. 2003. ScanImage: flexible software for operating laser scanning microscopes. *Biomedical Engineering Online* **2**:13. DOI: https://doi.org/10.1186/1475-925X-2-13, PMID: 12801419

Ratliff CP, Borghuis BG, Kao YH, Sterling P, Balasubramanian V. 2010. Retina is structured to process an excess of darkness in natural scenes. *PNAS* **107**:17368–17373. DOI: https://doi.org/10.1073/pnas.1005846107, PMID: 20855627

Reiff DF, Plett J, Mank M, Griesbeck O, Borst A. 2010. Visualizing retinotopic half-wave rectified input to the motion detection circuitry of Drosophila. *Nature Neuroscience* **13**:973–978. DOI: https://doi.org/10.1038/nn.2595, PMID: 20622873

Rister J, Pauls D, Schnell B, Ting CY, Lee CH, Sinakevitch I, Morante J, Strausfeld NJ, Ito K, Heisenberg M. 2007. Dissection of the peripheral motion channel in the visual system of Drosophila melanogaster. *Neuron* **56**:155–170. DOI: https://doi.org/10.1016/j.neuron.2007.09.014, PMID: 17920022

Schilling T, Borst A. 2015. Local motion detectors are required for the computation of expansion flow-fields. *Biology Open* **4**:1105–1108. DOI: https://doi.org/10.1242/bio.012690, PMID: 26231626

Schnell B, Joesch M, Forstner F, Raghu SV, Otsuna H, Ito K, Borst A, Reiff DF. 2010. Processing of horizontal optic flow in three visual interneurons of the Drosophila brain. *Journal of Neurophysiology* **103**:1646–1657. DOI: https://doi.org/10.1152/jn.00950.2009, PMID: 20089816

Schnell B, Raghu SV, Nern A, Borst A. 2012. Columnar cells necessary for motion responses of wide-field visual interneurons in Drosophila. *Journal of Comparative Physiology A* **198**:389–395. DOI: https://doi.org/10.1007/s00359-012-0716-3, PMID: 22411431

Schuling FH, Mastebroek HAK, Bult R, Lenting BPM. 1989. Properties of elementary movement detectors in the fly Calliphora erythrocephala. *Journal of Comparative Physiology A* **165**:179–192. DOI: https://doi.org/10.1007/BF00619192

Serbe E, Meier M, Leonhardt A, Borst A. 2016. Comprehensive characterization of the major presynaptic elements to the Drosophila OFF motion detector. *Neuron* **89**:829–841. DOI: https://doi.org/10.1016/j.neuron.2016.01.006, PMID: 26853306

Shinomiya K, Karuppudurai T, Lin TY, Lu Z, Lee CH, Meinertzhagen IA. 2014. Candidate neural substrates for off-edge motion detection in Drosophila. *Current Biology* **24**:1062–1070. DOI: https://doi.org/10.1016/j.cub.2014.03.051, PMID: 24768048

Strausfeld N. 1976. *Atlas of an Insect Brain*. Heidelberg, New York, Berlin: Springer Verlag.

Strausfeld NJ, Lee JK. 1991. Neuronal basis for parallel visual processing in the fly. *Visual Neuroscience* **7**:13–33. DOI: https://doi.org/10.1017/S0952523800010919, PMID: 1931797

Strother JA, Nern A, Reiser MB. 2014. Direct observation of ON and OFF pathways in the Drosophila visual system. *Current Biology* **24**:976–983. DOI: https://doi.org/10.1016/j.cub.2014.03.017, PMID: 24704075

Strother JA, Wu ST, Wong AM, Nern A, Rogers EM, Le JQ, Rubin GM, Reiser MB. 2017. The Emergence of Directional Selectivity in the Visual Motion Pathway of Drosophila. *Neuron* **94**:168–182. DOI: https://doi.org/10.1016/j.neuron.2017.03.010, PMID: 28384470

Takemura SY, Nern A, Chklovskii DB, Scheffer LK, Rubin GM, Meinertzhagen IA. 2017. The comprehensive connectome of a neural substrate for 'ON' motion detection in Drosophila. *eLife* **6**:e24394. DOI: https://doi.org/10.7554/eLife.24394, PMID: 28432786

Torre V, Poggio T. 1978. A synaptic mechanism possibly underlying directional selectivity to motion. *Proceedings of the Royal Society B: Biological Sciences* **202**:409–416. DOI: https://doi.org/10.1098/rspb.1978.0075

Venken KJ, Schulze KL, Haelterman NA, Pan H, He Y, Evans-Holm M, Carlson JW, Levis RW, Spradling AC, Hoskins RA, Bellen HJ. 2011. MiMIC: a highly versatile transposon insertion resource for engineering Drosophila melanogaster genes. *Nature Methods* **8**:737–743. DOI: https://doi.org/10.1038/nmeth.1662, PMID: 21985007

Yang HH, St-Pierre F, Sun X, Ding X, Lin MZ, Clandinin TR. 2016. Subcellular imaging of voltage and calcium signals reveals neural processing in vivo. *Cell* **166**:245–257. DOI: https://doi.org/10.1016/j.cell.2016.05.031, PMID: 27264607

Zhang X, Koolhaas WH, Schnorrer F. 2014. A Versatile Two-Step CRISPR- and RMCE-Based Strategy for Efficient Genome Engineering in *Drosophila* . *G3: Genes|Genomes|Genetics* **4**:2409–2418 . DOI: https://doi.org/10.1534/g3.114.013979

2.2 VOLTAGE TO CALCIUM TRANSFORMATION ENHANCES DIRECTION SELECTIVITY IN *DROSOPHILA* T4 NEURONS

ABSTRACT An important step in neural information processing is the transformation of membrane voltage into calcium signals leading to transmitter release. However, the effect of voltage to calcium transformation on neural responses to different sensory stimuli is not well understood. Here, we use in vivo two-photon imaging of genetically encoded voltage and calcium indicators, ArcLight and GCaMP6f, respectively, to measure responses in direction-selective T4 neurons of female *Drosophila*. Comparison between ArcLight and GCaMP6f signals reveals calcium signals to have a significantly higher direction selectivity compared with voltage signals. Using these recordings, we build a model which transforms T4 voltage responses into calcium responses. Using a cascade of thresholding, temporal filtering and a stationary nonlinearity, the model reproduces experimentally measured calcium responses across different visual stimuli. These findings provide a mechanistic underpinning of the voltage to calcium transformation and show how this processing step, in addition to synaptic mechanisms on the dendrites of T4 cells, enhances direction selectivity in the output signal of T4 neurons. Measuring the directional tuning of postsynaptic vertical system (VS)-cells with inputs from other cells blocked, we found that, indeed, it matches the one of the calcium signal in presynaptic T4 cells.

AUTHORS **Abhishek Mishra**, Alexander Borst, and Juergen Haag

CONTRIBUTIONS Abhishek Mishra, Conceptualization, Investigation, Data curation, Software, Visualization, Writing original draft, review and editing; Juergen Haag, Conceptualization, Data curation, Software, Investigation, review and editing; Alexander Borst, Conceptualization, Funding acquisition, Project administration, Review and editing

The Journal of Neuroscience, April 5, 2023 • 43(14):2497–2514 • **2497**

Systems/Circuits

Voltage to Calcium Transformation Enhances Direction Selectivity in *Drosophila* T4 Neurons

Abhishek Mishra,[1,2] **Etienne Serbe-Kamp,**[1] **Alexander Borst,**[1,2] **and Juergen Haag**[1]
[1]Max Planck Institute for Biological Intelligence, 82152 Martinsried, Germany and [2]Graduate School of Systemic Neurosciences, Ludwig Maximilian University of Munich, 82152 Martinsried, Germany

An important step in neural information processing is the transformation of membrane voltage into calcium signals leading to transmitter release. However, the effect of voltage to calcium transformation on neural responses to different sensory stimuli is not well understood. Here, we use in vivo two-photon imaging of genetically encoded voltage and calcium indicators, ArcLight and GCaMP6f, respectively, to measure responses in direction-selective T4 neurons of female *Drosophila*. Comparison between ArcLight and GCaMP6f signals reveals calcium signals to have a significantly higher direction selectivity compared with voltage signals. Using these recordings, we build a model which transforms T4 voltage responses into calcium responses. Using a cascade of thresholding, temporal filtering and a stationary nonlinearity, the model reproduces experimentally measured calcium responses across different visual stimuli. These findings provide a mechanistic underpinning of the voltage to calcium transformation and show how this processing step, in addition to synaptic mechanisms on the dendrites of T4 cells, enhances direction selectivity in the output signal of T4 neurons. Measuring the directional tuning of postsynaptic vertical system (VS)-cells with inputs from other cells blocked, we found that, indeed, it matches the one of the calcium signal in presynaptic T4 cells.

Key words: **direction selectivity; *Drosophila*; imaging; nonlinear model; voltage to calcium transformation**

Significance Statement

The transformation of voltage to calcium influx is an important step in the signaling cascade within a nerve cell. While this process has been intensely studied in the context of transmitter release mechanism, its consequences for information transmission and neural computation are unclear. Here, we measured both membrane voltage and cytosolic calcium levels in direction-selective cells of *Drosophila* in response to a large set of visual stimuli. We found direction selectivity in the calcium signal to be significantly enhanced compared with membrane voltage through a nonlinear transformation of voltage to calcium. Our findings highlight the importance of an additional step in the signaling cascade for information processing within single nerve cells.

Introduction

Neurons encode information via graded changes in membrane potential or action potential frequency. Mostly, they communicate via chemical synapses which require the release of neurotransmitters. When the presynaptic membrane is sufficiently depolarized, voltage-gated calcium channels open and allow calcium to enter the cell (Luo, 2020). Calcium entry leads to the fusion of synaptic vesicles with the membrane and the release of neurotransmitter molecules into the synaptic cleft (Chapman, 2002). As neurotransmitters diffuse across the synaptic cleft, they bind to receptors in the postsynaptic membrane, causing the postsynaptic neurons to depolarize or hyperpolarize. This way, information is passed from presynaptic to postsynaptic neurons (Di Maio, 2008). Voltage to calcium transformation, therefore, represents a crucial step in neural information processing and neural computation.

A classic example of neural computation is how *Drosophila* neurons compute the direction of visual motion (Borst and Helmstaedter, 2015; Yang and Clandinin, 2018; Borst et al., 2019, 2020). In *Drosophila*, visual information is processed in parallel ON (contrast increments) and OFF (contrast decrements) pathways (Joesch et al., 2010; Eichner et al., 2011; Strother et al., 2014). Three synapses downstream of photoreceptors, direction selectivity emerges in T4 cells of the ON pathway and in T5 cells of the OFF pathway (Maisak et al., 2013). There exist four subtypes of T4 and T5 cells (Fischbach and Dittrich, 1989; Takemura et al., 2017;

Received Dec. 16, 2022; revised Feb. 3, 2023; accepted Feb. 8, 2023.

Author contributions: A.M., A.B., and J.H. designed research; A.M., E.S.-K., and J.H. performed research; A.M., E.S.-K., and J.H. analyzed data; A.M. wrote the first draft of the paper; E.S.-K., A.B., and J.H. edited the paper; J.H. wrote the paper.

This work was supported by the Max Planck Society. We thank Christian Theile and Romina Kutlesa for fly work and Georg Ammer for critically reading the manuscript.

The authors declare no competing financial interests.

Correspondence should be addressed to Juergen Haag at juergen.haag@bi.mpg.de.

https://doi.org/10.1523/JNEUROSCI.2297-22.2023

Copyright © 2023 the authors

Shinomiya et al., 2019), each responding selectively to one of the four cardinal directions (Maisak et al., 2013; Haag et al., 2017; Wienecke et al., 2018). The presynaptic inputs to T4 and T5 cells have been described in great detail (Behnia et al., 2014; Ammer et al., 2015; Serbe et al., 2016; Yang et al., 2016; Arenz et al., 2017; Takemura et al., 2017; Kohn et al., 2021; Gonzalez-Suarez et al., 2022; Groschner et al., 2022). Different studies provided evidence that T4 and T5 cells become selective for the direction of motion by preferred direction (PD) enhancement (Fisher et al., 2015; Salazar-Gatzimas et al., 2016; Groschner et al., 2022), by null direction (ND) suppression (Gruntman et al., 2018, 2019), and by a combination of both mechanisms (Haag et al., 2016, 2017; Leong et al., 2016).

Amazingly, right at the first stage where direction selectivity emerges, T4 and T5 cells exhibit a high degree of direction selectivity, with strong responses to preferred direction stimuli and weak or no responses to null direction stimuli. This statement is, however, based on calcium recordings (Maisak et al., 2013; Fisher et al., 2015; Haag et al., 2017; Wienecke et al., 2018). Voltage recordings show a somewhat different picture: while preferred direction stimuli also lead to large membrane depolarizations, edges or gratings moving along the null direction elicit smaller but significant depolarizing membrane responses as well (Gruntman et al., 2018, 2019; Wienecke et al., 2018; Groschner et al., 2022). This discrepancy between calcium and voltage signals hints at an additional processing step where voltage signals are transformed into calcium signals that increase the direction selectivity of the cells. In order to study this step systematically, we recorded both voltage and calcium fluorescence signals in response to a large stimulus set that includes gratings and edges moving along various directions at different speeds and contrasts. Since the calcium and voltage signals might be different in the dendrites and the axon terminals of T4-cells, we compared the directional tuning between the different compartments. Using these data, we built a model that captures the transformation from voltage to calcium by a combination of linear and nonlinear processing steps. Measuring the directional tuning in postsynaptic vertical system (VS)-cells while blocking input from other cells, we found it to match the narrow tuning of the calcium signal in presynaptic T4 cells. Therefore, we conclude that the output of T4 cells reflects the tuning of its calcium signal.

Materials and Methods

Flies

Flies (*Drosophila melanogaster*) were raised at 25°C and 60% humidity on a 12/12 h light/dark cycle on a standard cornmeal agar medium. Female flies 1–7 d after eclosion were used for the experiments. For calcium imaging experiments, genetically-encoded calcium indicator GCaMP6f (Chen et al., 2013) was expressed in T4c neurons with axon terminals predominantly in layer three of the lobula plate. Similarly, for voltage imaging experiments, the genetically-encoded voltage indicator (GEVI) ArcLight (Cao et al., 2013) was expressed in T4c neurons. The flies' genotypes were as follows:

1. T4c>GCaMP6f: w+; VT15785-Gal4AD/UAS-GCaMP6f; VT50384-Gal4DBD/UAS-GCaMP6f
2. T4c>ArcLight: w+; VT15785-Gal4AD/UAS-ArcLight; VT50384-Gal4DBD/+

For Mi1 and Tm3 experiments, the flies' genotypes were as follows:

1. Mi1>GCaMP6f: w+; R19F01-Gal4AD/UAS-GCaMP6f; R71D01-Gal4DBD/UAS-GCaMP6f
2. Mi1>ArcLight: w+; R19F01-Gal4AD/UAS-ArcLight; R71D01-Gal4DBD/+
3. Tm3>GCaMP6f: w+; R13E12-Gal4AD/UAS-GCaMP6f; R59C10-Gal4DBD/UAS-GCaMP6f
4. Tm3>ArcLight: w+; R13E12-Gal4AD/UAS-ArcLight; R59C10-Gal4DBD/+

For VS recordings, the flies' genotypes were as follows:
T4c/T5c>TNT: w-/w+; VT50384-lexA/13xlexAop-IVS-TNT:HA

For the whole-brain image (Fig. 1*A*), brains were dissected in PBS and then fixed in 4% paraformaldehyde (PFA; in PBS with 0.1% Triton X-100). Afterwards, brains were washed three times in PBT (PBS + 0.3% Triton X-100), blocked in 10% normal goat serum (NGS; in PBT) and then incubated with the primary antibody (antibody in 5% NGS in PBT) for 2 d. Next, brains were washed in PBT overnight and then incubated with the secondary antibody for 2–3 d. Brains were then washed in PBT overnight, briefly rinsed with PBS and mounted in Vectashield (VectorLabs). Primary antibodies were used at dilutions of 1:25 (anti-nc82) or 1:1000 (anti-GFP). All secondary antibodies were used at a dilution of 1:500. Confocal images were acquired with a Leica SP8 confocal microscope at a resolution of 1024 × 1024 pixels. We used 488 nm and 633 nm lasers and HyD detectors and a Leica 63× glycerol objective. Image processing was performed with ImageJ/Fiji.

Calcium and voltage imaging

For imaging experiments, fly surgeries were performed as previously described (Maisak et al., 2013). Briefly, flies were anesthetized with CO_2 or on ice, fixed with their backs, legs and wings to a Plexiglas holder with the back of the head exposed to a recording chamber filled with a fly external solution. The cuticula at the back of the head on one side of the brain was cut away with a fine hypodermic needle and removed together with air sacks covering the underlying optic lobe. The neuronal activity was then measured from the optic lobe with a custom-built two-photon microscope as previously described (Maisak et al., 2013). Images were acquired at 64 × 64 pixels resolution and frame rate of 13 Hz with the Scanimage software in MATLAB (Pologruto et al., 2003).

Electrophysiology

Patch-clamp recordings from vertical system (VS) tangential cells were performed as previously described in Ammer et al., 2015. Briefly, the brain of the fly was visualized with an upright microscope (Axiotech Vario 100, Zeiss) equipped with a 40× water-immersion objective (LumPlanFL, NA 0.8, Olympus), a Hg-light source (HXP-120, Visitron Systems) and polarization filters for contrast enhancement. A glass electrode filled with collagenase (Collagenase IV, Invitrogen, 0.5 mg ml in extracellular saline) was used to expose the somata of LPTCs. Somata of VS-cells were patched with a glass electrode (5– 9 MΩ) filled with internal solution (140 mM potassium aspartate, 10 mM HEPES, 4 mM MgATP, 0.5 mM Na-GTP, 1 mM EGTA, 1 mM KCl, and 0.03 mM Alexa 568–hydrazide sodium, pH 7.26, 265 mOsm). Recordings were performed with an NPI BA-1S amplifier (NPI Electronics) in current-clamp bridge mode, low-pass filtered with a cutoff frequency at 3 kHz and digitized at 10 kHz.

Visual stimulation

For the study of visual responses of T4c cells, visual stimuli were presented on a custom-built projector-based arena as described in Arenz et al., 2017. Two micro-projectors (TI DLP Lightcrafter 3000) were used to project stimuli onto the back of an opaque cylindrical screen covering 180° in azimuth and 105° in elevation of the fly's visual field. To increase the refresh rate from 60 to 180 Hz (at eight-bit color depth), projectors were programmed to use only green LED (OSRAM L CG H9RN) which emits light between 500- and 600-nm wavelength. Two long-pass filters (Thorlabs FEL0550 and FGL550) were placed in front of each projector to restrict the stimulus light to wavelengths above 550 nm. This prevents overlap between fluorescence signal and arena light spectra. To allow only the fluorescence emission spectrum to be detected, a bandpass filter (Brightline 520/35) was placed in front of the photomultiplier. Stimuli were rendered using custom-written software in Python 2.7.

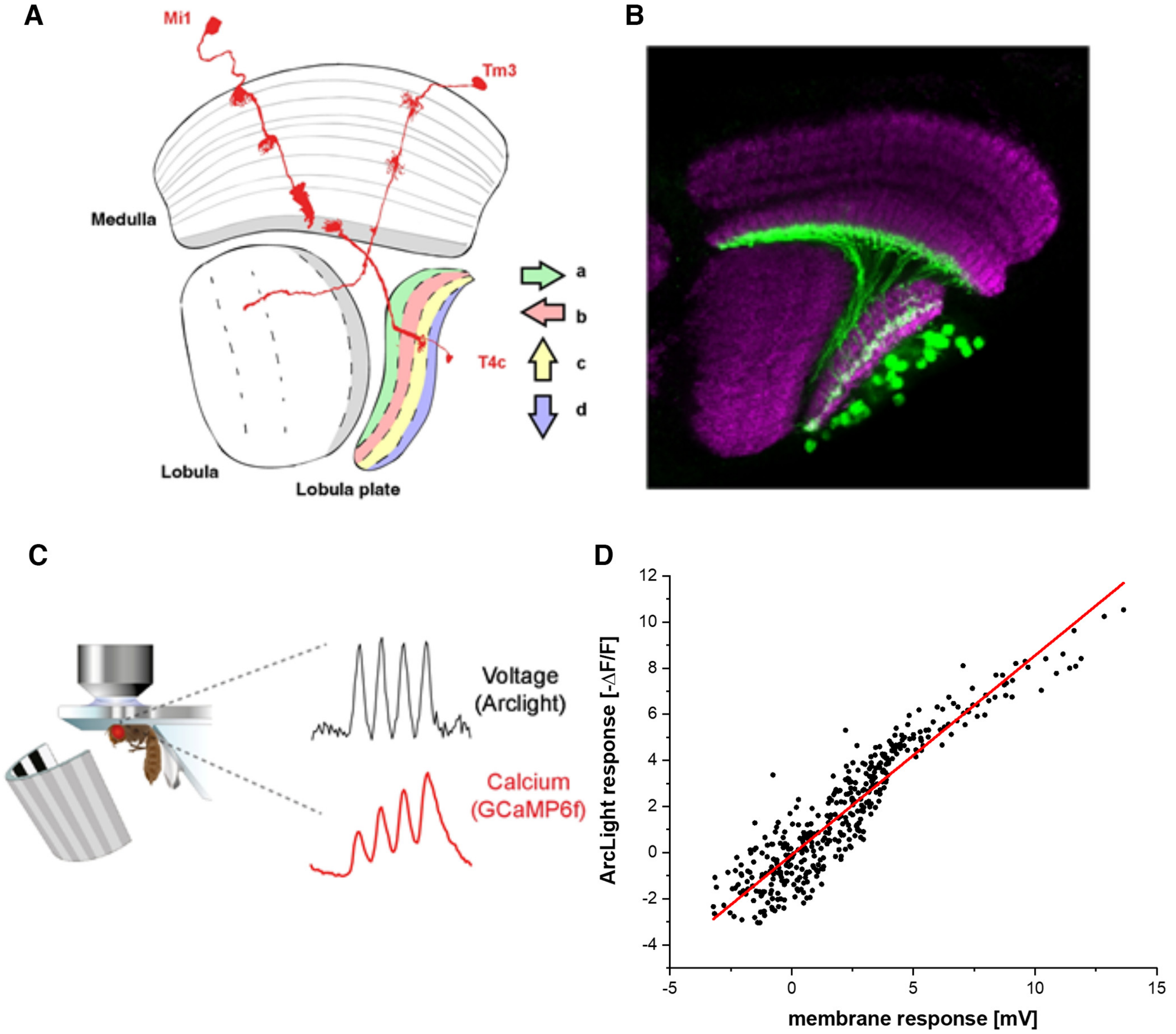

Figure 1. Schematic setup. ***A***, Schematic illustration of the optic lobe, together with the reconstruction of the three neuron types Mi1, Tm3, and T4c investigated. ***B***, Optic lobe with T4c neurons labeled with GCaMP6f (green) and nc82 (magenta). ***C***, Experimental setup: fly tethered to a plastic holder under the two-photon microscope looking onto the stimulus arena. ***D***, Comparison of the optically recorded ArcLight fluorescence change in T4 cells with the membrane potential as recorded by whole-cell patch from T4 cells (Groschner et al., 2022) elicited by identical visual stimuli.

Stimuli

Stimuli were presented with three to five repetitions per experiment randomly. To measure the directional and speed tuning, square-wave gratings with a spatial wavelength of 30° spanning the full extent of the stimulus arena were used. The gratings were moved along 12 different directions from 0° to 360° at four different speeds (15°/s, 30°/s, 60°/s,120°/s). Similarly, to measure direction and contrast tuning, square-wave gratings with a spatial wavelength of 30° spanning the full extent of the stimulus arena were used. The gratings moved at a speed of 30°/s in 12 different directions at four different contrasts (10%, 20%, 50%, 100%). For different contrasts, the brightness of the bright bar was decreased and the brightness of the dark bar was increased. Edge responses were measured using ON edges, i.e., bright edges moving on a dark background with full contrast. The ON edge moved along the preferred direction (upward) or null direction (downward) at four different speeds (15°/s, 30°/s, 60°/s, 120°/s). Similarly to gratings, edges moved at a speed of 30°/s in preferred direction (upward) or null direction at four different contrasts (10%, 20%, 50%, 100%).

Data analysis

Data analysis was performed using custom-written routines in MATLAB and Python 2.7, 3.7. Images were automatically registered using horizontal and vertical translations to correct the movement of the brain. Fluorescence changes ΔF/F were then calculated using a standard baseline algorithm (Jia et al., 2011). Regions of interest (ROIs) were drawn on the average raw image manually in the medulla layer M10 for signals from T4 dendrites. Averaging the fluorescence change over this ROI in space resulted in a ΔF/F time course. Voltage imaging with ArcLight and calcium imaging with GCaMP6f were performed and analyzed using the same settings.

As the ArcLight and GCaMP6f responses were recorded from cells in different flies with different receptive fields and therefore different phase relations, the responses had to be aligned before averaging in the time domain. To do so, we calculated the cross-correlation between the responses of different flies and shifted the responses accordingly.

The direction selectivity was evaluated using a direction selectivity index (DSI) calculated as the difference between the peak responses to preferred and null directions, divided by the sum of the absolute values of the peak responses:

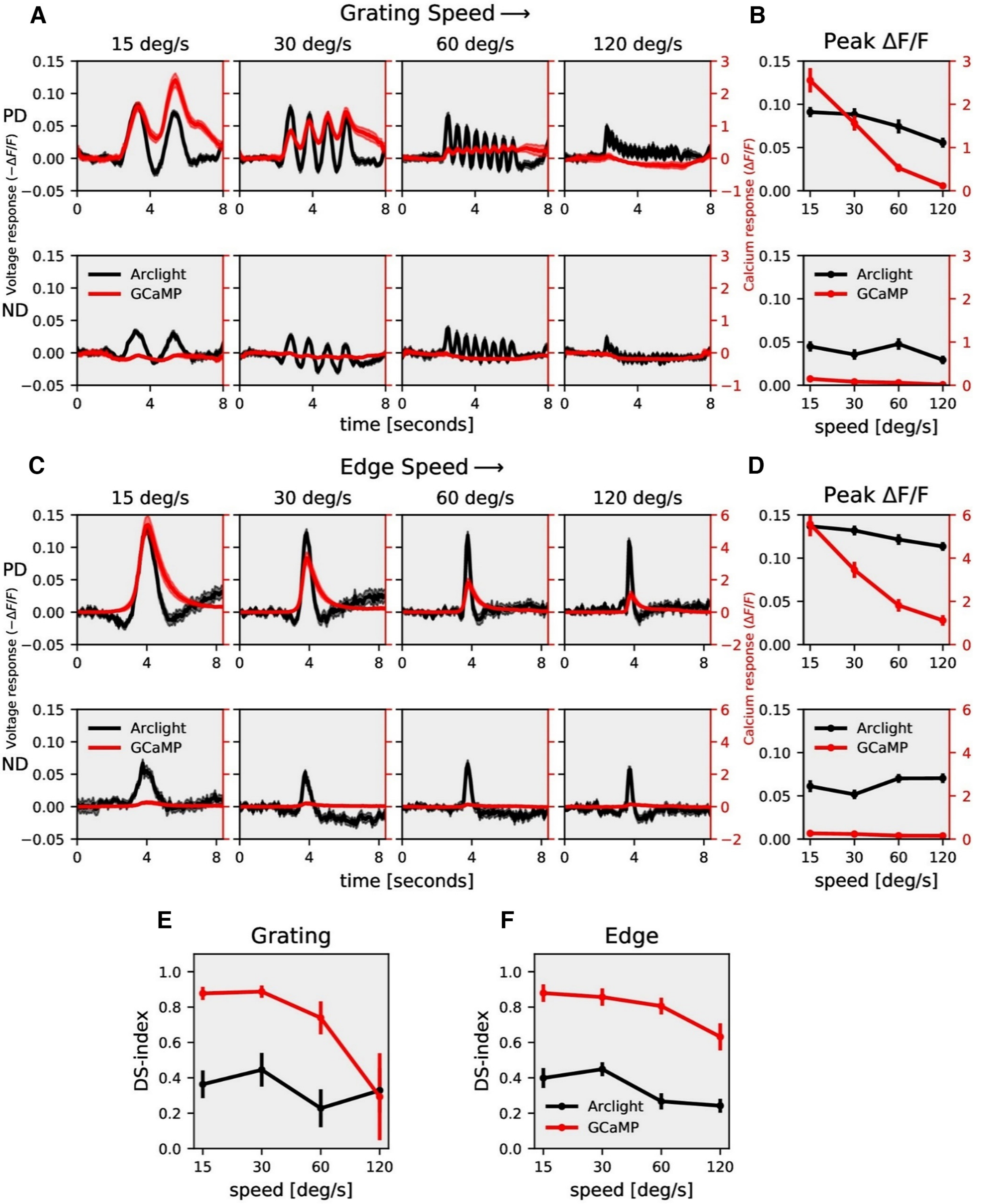

Figure 2. T4c speed dependence. ***A***, T4c ArcLight (black) and GCaMP6f (red) responses to grating moving in PD (top row) and ND (bottom row) at four different speeds. The plots have a twin *y*-axis. The left *y*-axis of the plot represents voltage responses, i.e., changes in ArcLight fluorescence (−ΔF/F) and the right *y*-axis of the plot represents calcium responses, i.e., changes in GCaMP6f fluorescence (ΔF/F). ***B***, T4c peak responses to grating moving in PD (top) and ND (bottom) at four different speeds ($n = 22$ ROIs from $N = 9$ flies for ArcLight, $n = 12$, $N = 8$ for GCaMP6f). ***C***, T4c ArcLight (black) and GCaMP6f (red) responses to ON-edge moving in PD (top row) and ND (bottom row) at four different speeds. ***D***, T4c peak responses to ON-edge moving in PD and ND at four different speeds ($n = 21$, $N = 9$ for ArcLight, $n = 12$, $N = 4$ for GCaMP6f). ***E***, Direction selectivity index (DS-index) calculated as the difference of peak responses in PD and ND divided by the sum of peak responses for grating. ***F***, Direction selectivity index (DSI) for ON-edge. All data show the mean ± SEM PD: preferred direction, ND: null direction.

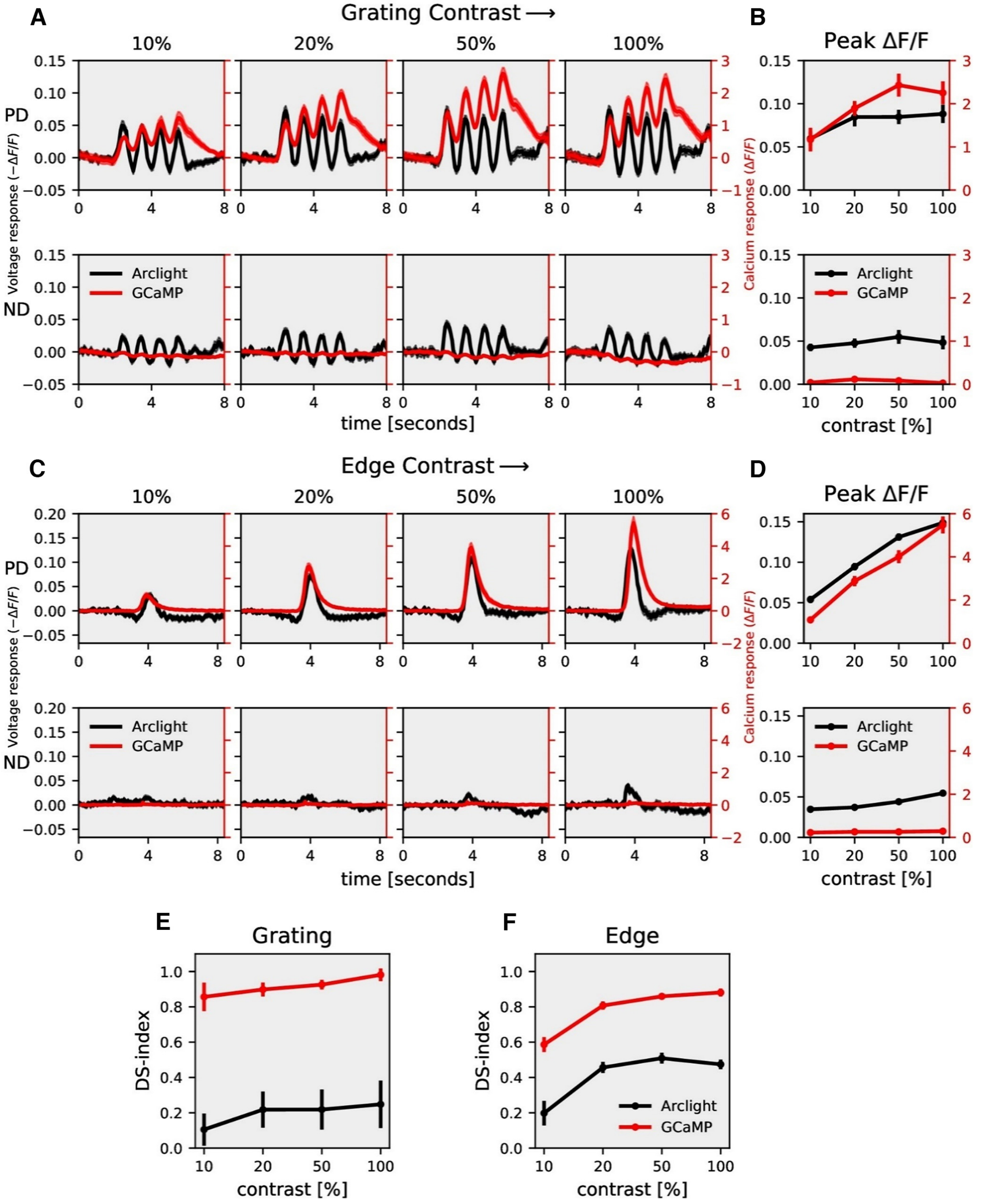

Figure 3. T4c contrast dependence. ***A***, T4c ArcLight (black) and GCaMP6f (red) responses to grating moving in PD (top row) and ND (bottom row) at four different contrasts. The left *y*-axis of the plot represents voltage responses, i.e., changes in ArcLight fluorescence (−ΔF/F) and the right *y*-axis of the plot represents calcium responses, i.e., changes in GCaMP6f fluorescence (ΔF/F). ***B***, T4c peak responses to grating moving in PD (top) and ND (bottom) at four different contrasts ($n = 17$ ROIs from $N = 10$ flies for ArcLight, $n = 15$, $N = 7$ for GCaMP6f). ***C***, T4c ArcLight (black) and GCaMP6f (red) responses to ON-edge moving in PD (top row) and ND (bottom row) at four different contrasts. ***D***, T4c peak responses to ON-edge moving in PD and ND at four different contrasts ($n = 36$, $N = 5$ for ArcLight, $n = 29$, $N = 5$ for GCaMP6f). ***E***, Direction selectivity index (DSI) calculated as the difference of peak responses in PD and ND divided by the sum of peak responses for grating. ***F***, Direction selectivity index (DSI) for ON-edge. All data show the mean ± SEM.

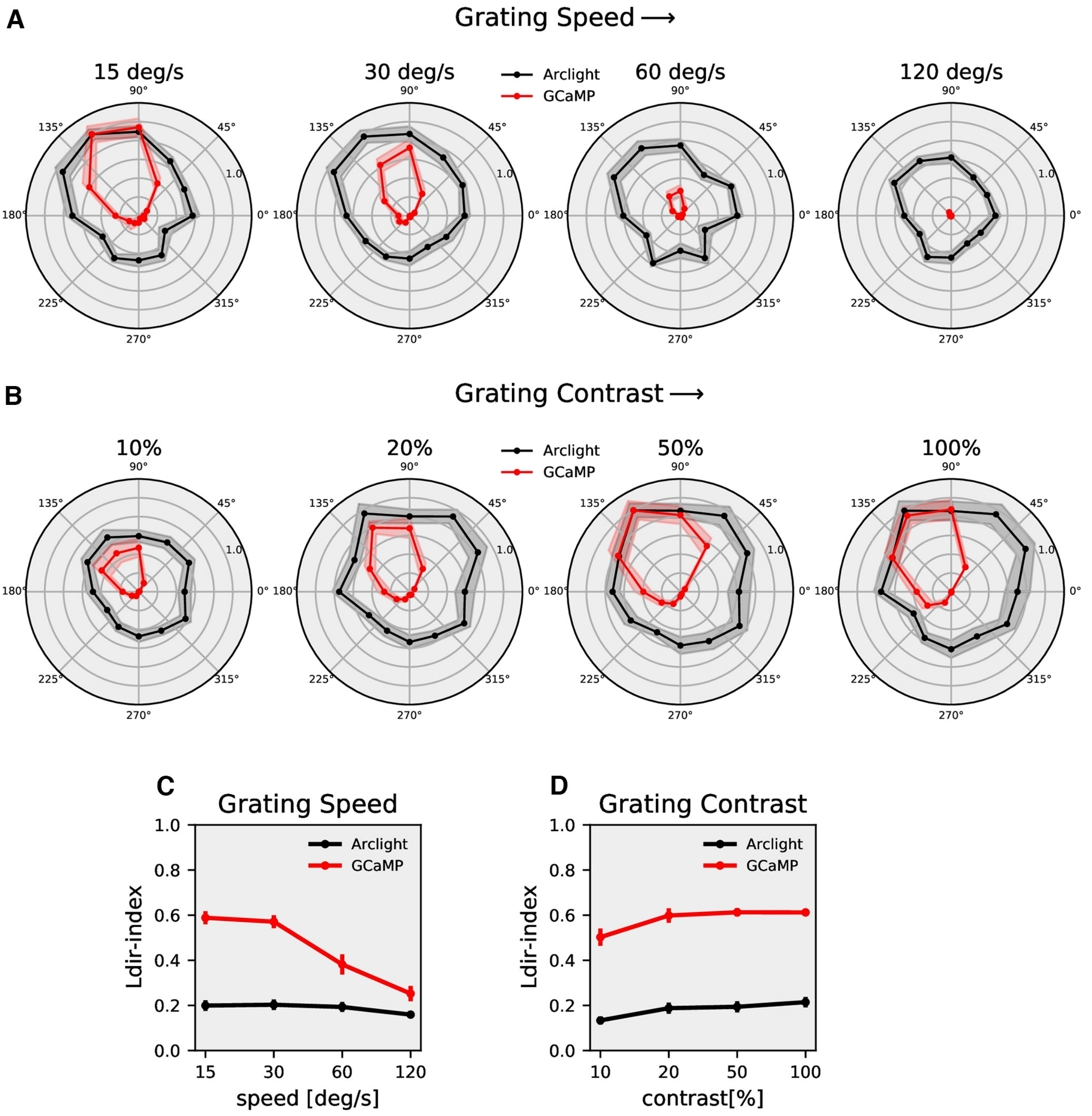

Figure 4. T4c directional tuning. ***A***, T4c ArcLight (black) and GCaMP6f (red) normalized peak responses to grating moving in 12 directions at four different speeds ($n = 22$ ROIs from $N = 9$ flies for ArcLight, $n = 26$, $N = 8$ for GCaMP6f). ***B***, T4c ArcLight (black) and GCaMP6f (red) normalized peak responses to grating moving in 12 directions at four different contrasts ($n = 17$, $N = 10$ for ArcLight, $n = 15$, $N = 7$ for GCaMP6f). ***C***, The directional tuning index L_{dir} for grating moving at four different speeds. The directional tuning index is calculated as the vector sum of the peak responses divided by the sum of all individual vector magnitudes. ***D***, The directional tuning index for grating at four different contrasts. All data show the mean ± SEM.

$$DSI = \frac{PDpeak - NDpeak}{|PDpeak| + |NDpeak|}. \qquad (1)$$

In the above measurement, only the difference in response between the two opposing directions of motion is quantified. To take into account all 12 directions of motion, we calculated the directional tuning index:

$$L_{dir} = \left| \frac{\sum_{\phi} \overrightarrow{v(\phi)}}{\sum_{\phi} |\overrightarrow{v(\phi)}|} \right|, \qquad (2)$$

where $\overrightarrow{v(\phi)}$ is a vector proportionally scaled with the peak response and points in the direction corresponding to the direction of motion given by the rotation angle ϕ of the stimulus (Mazurek et al., 2014). For two angles separated by 180°, the L_{dir} is equivalent to the DSI.

The calculation of the circular variance was done with the circular statistics toolbox for MATLAB (Berens, 2009).

Note, all calculations (Peak ΔF/F, DSI, L_{Dir}) were performed on the signals from individual ROIs and then averaged.

Model simulations

Custom-written Python3.7 scripts were used to simulate the models (Fig. 5). To calculate the optimal parameter values, we first defined an error function. For each stimulus condition (s_i), the error was calculated as

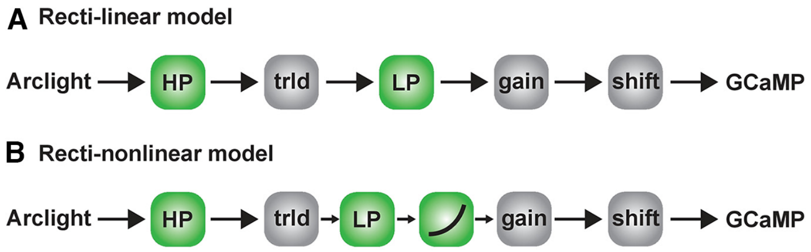

Figure 5. Models for voltage to calcium transformation. ***A***, Rectilinear model consisting of High-Pass filter (HP), threshold (trld), Low-Pass filter (LP), gain, and shift. ***B***, Recti-nonlinear model. The recti-nonlinear model consists of the same components than the rectilinear model with an additional power nonlinearity.

Table 1. Parameter for the models

Cell	Threshold (%)	τ HP (s)	τ-LP (s)	Exponent	Gain	Error (%)
Mi1						
Rectilinear model	−0.68	1.96	0.39		32.09	8.99
Recti-nonlinear model	−0.22	2.26	0.41	1.28	20.27	8.65
Tm3						
Rectilinear model	−0.60	0.67	0.79		77.17	6.79
Recti-nonlinear model	−0.34	0.56	1.03	1.48	58.57	4.92
T4c complete						
Rectilinear model	−1.15	0.33	3.91		347.30	39.48
Recti-nonlinear model	−0.34	0.45	2.41	2.53	297.67	21.59

$$\mathit{error}(s_i) = \sum_{t=0}^{t=N} \left(\mathit{model}(s_i t) - \mathit{data}(s_i t)\right)^2. \tag{3}$$

The model took as input the time averaged ArcLight data across all 112 different stimuli conditions. Next, we summed the error for all stimuli conditions:

$$\mathit{total\ error} = \sum_{i=1}^{i=112} \mathit{error}(s_i). \tag{4}$$

The model parameters were initialized with random values within the defined parameter bounds. The Python SciPy minimize function then used the L-BFGS-B (Limited Broyden Fletcher Goldfarb Shanno) algorithm to find the parameter values corresponding to the minimum total error. A total of 300 runs were performed, and the parameter values corresponding to the run with the lowest error were used to produce the final output signals. To compare the model performances with the time averaged GCaMP data, we calculated the model error as:

$$\mathit{model\ error}\,[\%\ \mathit{of\ data\ power}] = \frac{\mathit{total\ error}}{\sum_{i=1}^{i=112} \left(\mathit{data}(s_i)\right)^2} * 100. \tag{5}$$

Results

We expressed the genetically encoded calcium indicator GCaMP6f (Chen et al., 2013) in T4c cells projecting to layer three of the lobula plate (Fig. 1*A*,*B*). These cells have upward motion as their preferred direction (PD) and downward motion as their null direction (ND). We also expressed the genetically encoded voltage indicator ArcLight (Jin et al., 2012) using the same driver line. ArcLight's fluorescence decreases with membrane depolarization and increases with membrane hyperpolarization (Cao et al., 2013). To compare voltage and calcium signals, we recorded the activity in T4c cells dendrites in medulla layer 10 in response to the same set of stimuli using two-photon microscopy (Fig. 1*C*; Denk et al., 1990). The complete stimuli set included square-wave gratings of 30° spatial wavelength moving along 12 different directions, and ON edges moving in PD and ND, at four different speeds (15°/s, 30°/s, 60°/s, 120°/s) and four different contrasts (10%, 20%, 50%, 100%). In order to test how well ArcLight reflects the membrane potential, we compared the measured fluorescence changes in T4c cells to gratings moving at 30°/s in 8 different directions to membrane potential recordings (Fig. 1*D*; electrophysiology data from Groschner et al., 2022) to the same set of stimuli. The fluorescence change of ArcLight is shown (black dots) for every time point as a function of the membrane response. The fluorescence change depends in an almost linear way (red line) on the membrane potential change (slope 0.86, Pearson's $R = 0.93$).

In the first set of experiments, we measured voltage and calcium signals in response to gratings moving in PD and ND at four different speeds (Fig. 2*A*). As the grating stimuli consist of alternate bright and dark bars moving in a certain direction, there was a modulation at the same frequency as the contrast frequency of the grating (Egelhaaf and Borst, 1989; Single and Borst, 1998; Haag et al., 2004; Wienecke et al., 2018) in the ArcLight (black traces) and GCaMP6f (red traces) signals. GCaMP6f responses showed modulations only for slower speeds, while ArcLight responses revealed modulations also at higher speeds. In addition, the response amplitudes were much higher for GCaMP6f (≈2.0 ΔF/F) compared with ArcLight (≈−0.06 ΔF/F). The peak responses (maximum ΔF/F) decreased with increasing stimulus speed both for GCaMP6f and ArcLight signals (Fig. 2*B*). To understand how the voltage to calcium transformation affects direction selectivity in T4 cells, we compared the responses to gratings moving in PD and ND. GCaMP6f responses in ND were negligible compared with its responses in PD, while for ArcLight responses in ND were relatively high (Fig. 2*A*, *C*). We quantified the direction selectivity of the calcium and voltage responses by a direction selectivity index (DS-index) calculated as the difference between the peak responses to preferred and null directions, divided by the sum of the absolute values of the peak responses (Materials and Methods, Eq. 1). The results revealed a high degree of direction selectivity of ≈0.8 for GCaMP6f at slower velocities, compared with a direction selectivity of ≈0.4 for ArcLight (Fig. 2*E*). For both GCaMP6f and ArcLight signals, direction selectivity decreased with increasing velocity.

Next, instead of gratings, we used moving bright edges with all other stimulus parameters remaining the same (Fig. 2*C*). As the edge moves upward on the screen, it crosses the receptive field of T4c neurons only once. Hence, there was only a single peak in the response. The peak response decreased with increasing stimulus speed for GCaMP6f, while the peak response remained almost constant for ArcLight throughout all speeds (Fig. 2*D*). When comparing responses to edges moving along preferred and null directions, GCaMP6f showed negligible responses to the null direction while ArcLight revealed considerable responses to null direction stimuli. The direction selectivity index was again much higher for GCaMP6f compared with ArcLight (Fig. 2*F*). Together, these results show that GCaMP6f signals have a high level of direction selectivity compared with ArcLight signals, both for grating and edge stimuli.

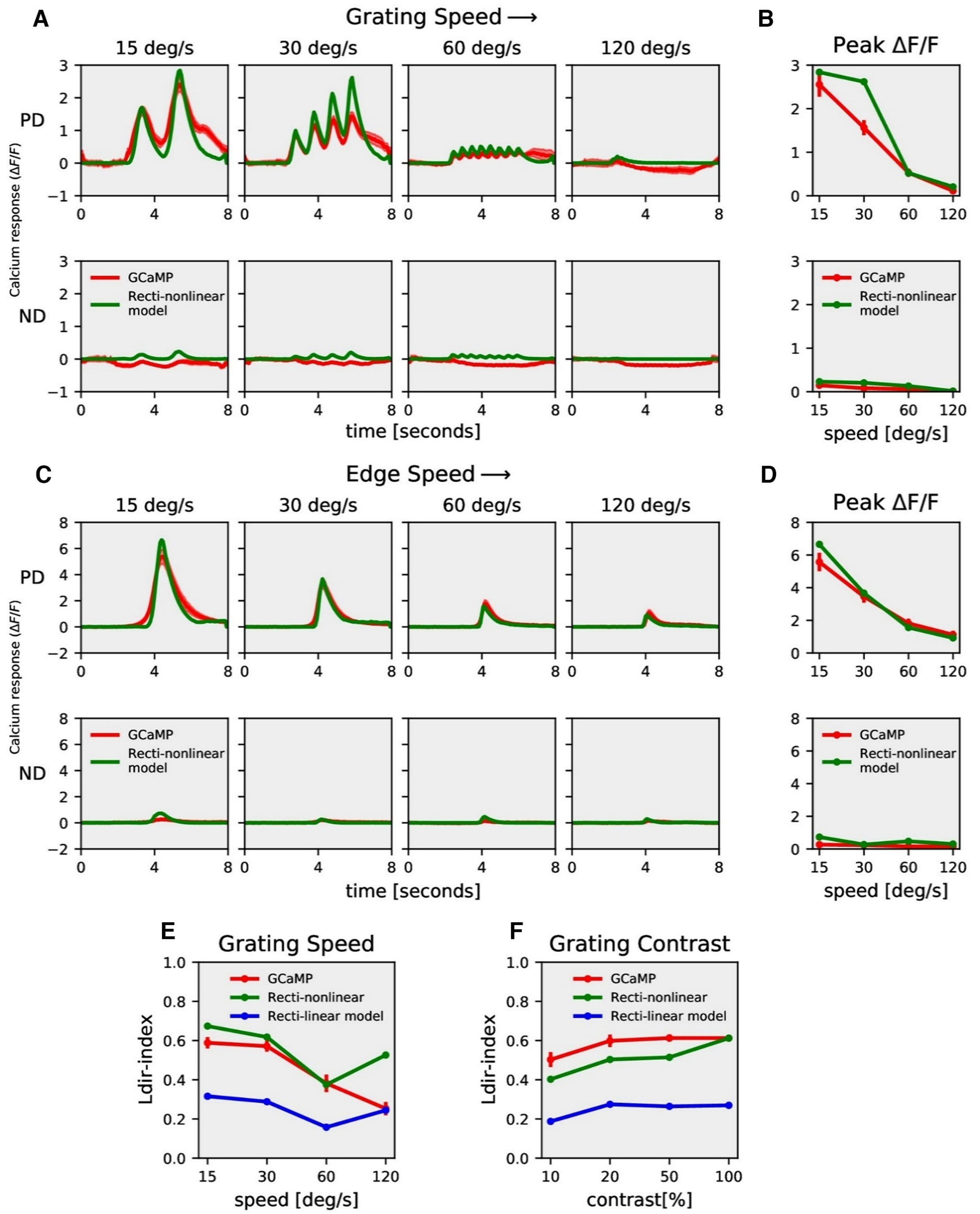

Figure 6. Model responses. ***A***, T4c GCaMP6f (red) and recti-nonlinear model (green) responses to grating moving in PD (top row) and ND (bottom row) at four different speeds. ***B***, T4c GCaMP6f and model peak responses to grating moving in PD (top) and ND (bottom) at four different speeds. ***C***, T4c GCaMP6f (red) and recti-nonlinear model (green) responses to ON-edge moving in PD (top row) and ND (bottom row) at four different speeds. ***D***, T4c GCaMP6f and model peak responses to ON-edge moving in PD (top) and ND (bottom) at four different speeds. ***E***, ***F***, The directional tuning index L_{dir} for GCaMP6f (red), recti-nonlinear (green), and rectilinear (blue) model for grating moving in 12 directions at four different speeds and at four different contrasts, respectively.

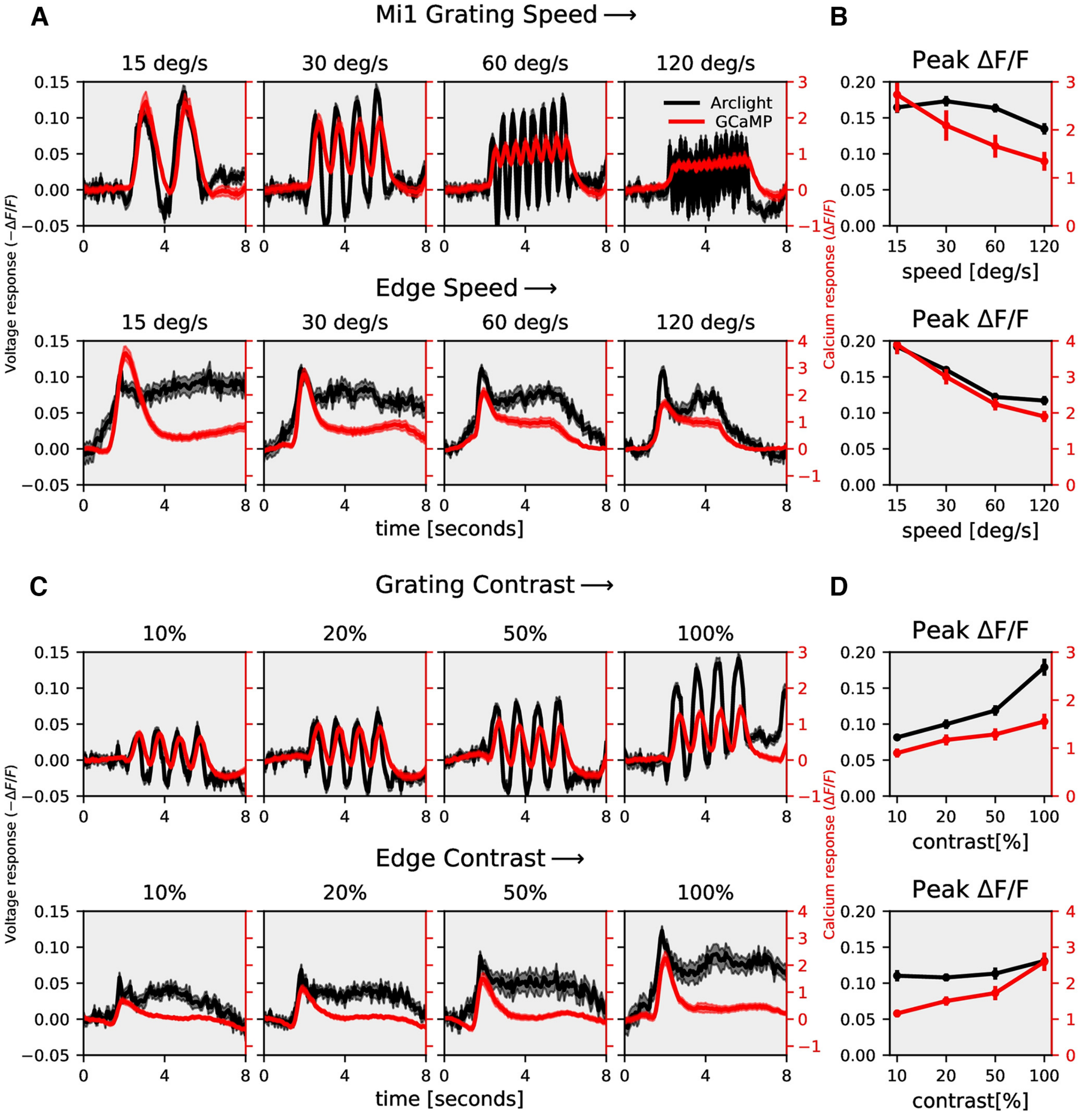

Figure 7. Mi1 speed and contrast dependence. ***A***, Mi1 ArcLight (black) and GCaMP6f (red) responses to grating (top row) and edges (bottom row) moving at four different speeds (gratings: $n = 24$ ROIs from $N = 5$ flies for ArcLight, $n = 19$, $N = 5$ for GCaMP; edge: $n = 27$, $N = 4$ for ArcLight, $n = 35$, $N = 5$ for GCaMP). ***B***, Mi1 peak responses to gratings (top) and edges (bottom) moving at four different speeds (top). ***C***, Mi1 ArcLight (black) and GCaMP6f (red) responses to grating (top row) and edges (bottom row) moving at four different contrasts (gratings: $n = 24$ ROIs from $N = 5$ flies for ArcLight, $n = 22$, $N = 5$ for GCaMP; edge: $n = 18$, $N = 4$ for ArcLight, $n = 24$, $N = 5$ for GCaMP). The left y-axis of the plot represents voltage responses, i.e., changes in ArcLight fluorescence (−ΔF/F) and the right y-axis of the plot represents calcium responses, i.e., changes in GCaMP6f fluorescence (ΔF/F). ***D***, Mi1 peak responses to gratings (top) and edges (bottom) moving at four different contrasts. All data show the mean ± SEM.

The stimulus strength was further varied by changing the contrast between bright and dark bars for gratings and between moving edges and background for edge stimuli. We measured ArcLight and GCaMP6f responses to gratings moving at 30°/s at four different contrasts (Fig. 3*A*). Increasing contrast resulted in an increase in response for both ArcLight and GCaMP6f. GCaMP6f signals were modulated at the temporal frequency of the grating but showed an additional rise over time. This slow increase was not observed in ArcLight signals. We also measured ArcLight and GCaMP6f responses to ON edges, all moving at the same speed of 30°/s but having different contrasts (Fig. 3*C*). The peak response (maximum ΔF/F) increased with increasing contrast (Fig. 3*D*). Similar to previous experiments, the direction selectivity index was much higher for GCaMP6f (≈0.9) compared with that for ArcLight (≈0.4; Fig. 3*E*,*F*).

In the results presented so far, we compared responses for two directions only, i.e., along the preferred (upward) and along the null direction (downward). Since the direction selectivity

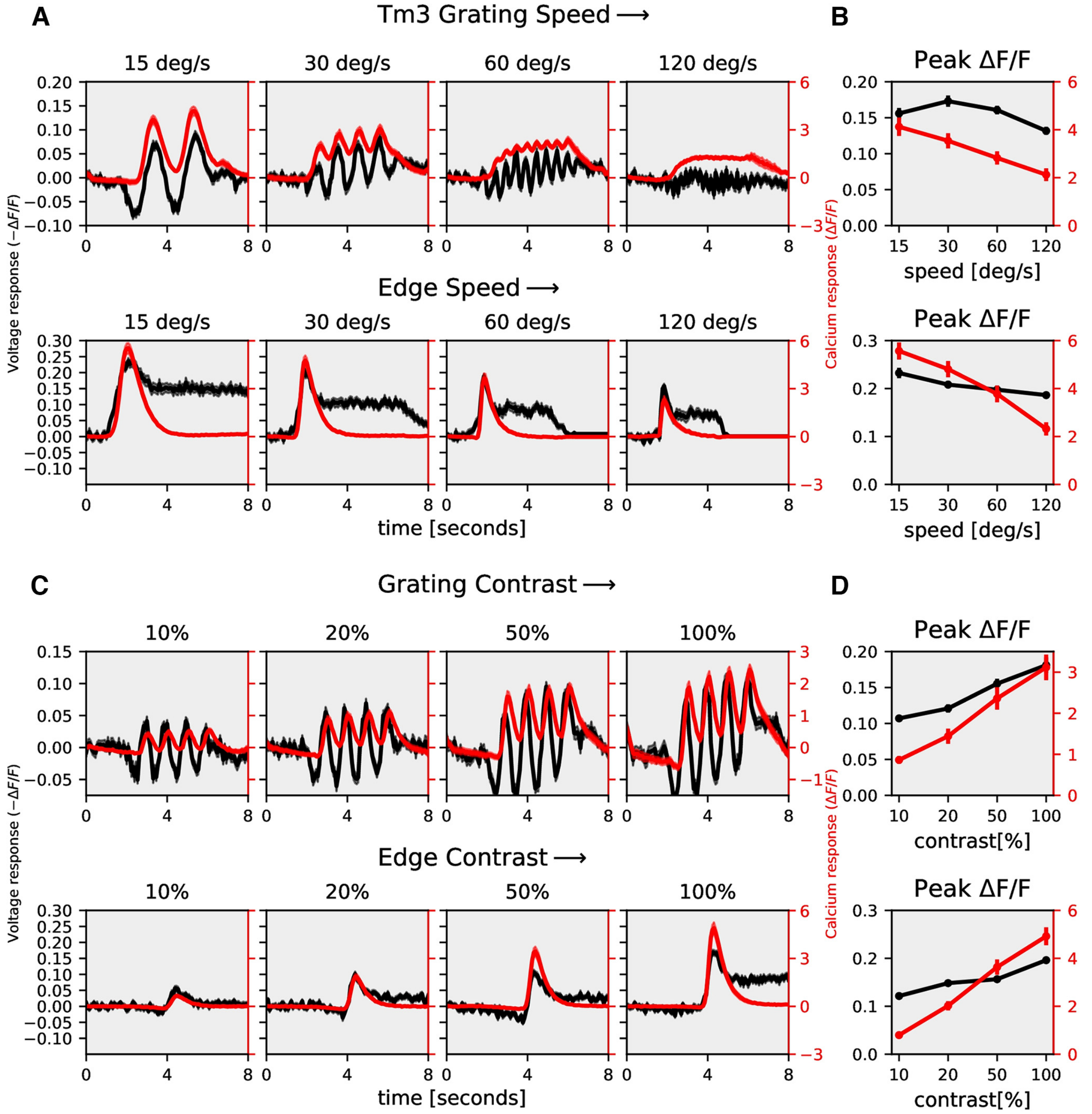

Figure 8. Tm3 speed and contrast dependence: Same as Figure 7, but for Tm3. ***A***, Gratings: $n = 52$ ROIs from $N = 5$ flies for ArcLight, $n = 26$, $N = 3$ for GCaMP; edge: $n = 28$, $N = 4$ for ArcLight, $n = 42$, $N = 4$ for GCaMP. ***B***, Tm3 peak responses to gratings (top) and edges (bottom) moving at four different speeds. ***C***, Gratings: $n = 35$ ROIs from $N = 5$ flies for ArcLight, $n = 36$, $N = 4$ for GCaMP; edge: $n = 29$, $N = 4$ for ArcLight, $n = 39$, $N = 4$ for GCaMP. ***D***, Tm3 peak responses to gratings (top) and edges (bottom) moving at four different contrasts. All data show the mean ± SEM.

index becomes rather unselective when PD and ND responses are close to zero, we next extended the comparison to motion along 12 directions, from 0° to 360° in steps of 30°. For this comparison, we determined the normalized peak responses of ArcLight and GCaMP6f signals to gratings moving at four different speeds and four different contrasts, respectively (Fig. 4*A*,*B*). The directional tuning was much sharper for GCaMP6f compared with ArcLight. To quantify this, we calculated the directional tuning index L_{dir} (Mazurek et al., 2014) for each speed and each contrast as the magnitude of the vector sum of the peak responses divided by the sum of all individual vector magnitudes (Materials and Methods, Eq. 2). In general, the directional tuning indices again were much higher for GCaMP6f (≃0.6) compared with that of ArcLight (≃0.2; Fig. 4*C*,*D*). Together, these results show that calcium signals have a higher degree of directional tuning across different speeds and contrasts than voltage responses, arguing for a nonlinear transformation from voltage to calcium.

How does the voltage to calcium transformation lead to calcium signals with significantly higher directional tuning compared with voltage signals? To address this question, we constructed an algorithmic model (Fig. 5), which takes ArcLight signals as inputs and outputs GCaMP signals. In order to find the optimal parameter values, we first defined an error function. For each stimulus condition, the error was calculated as the sum of the squared

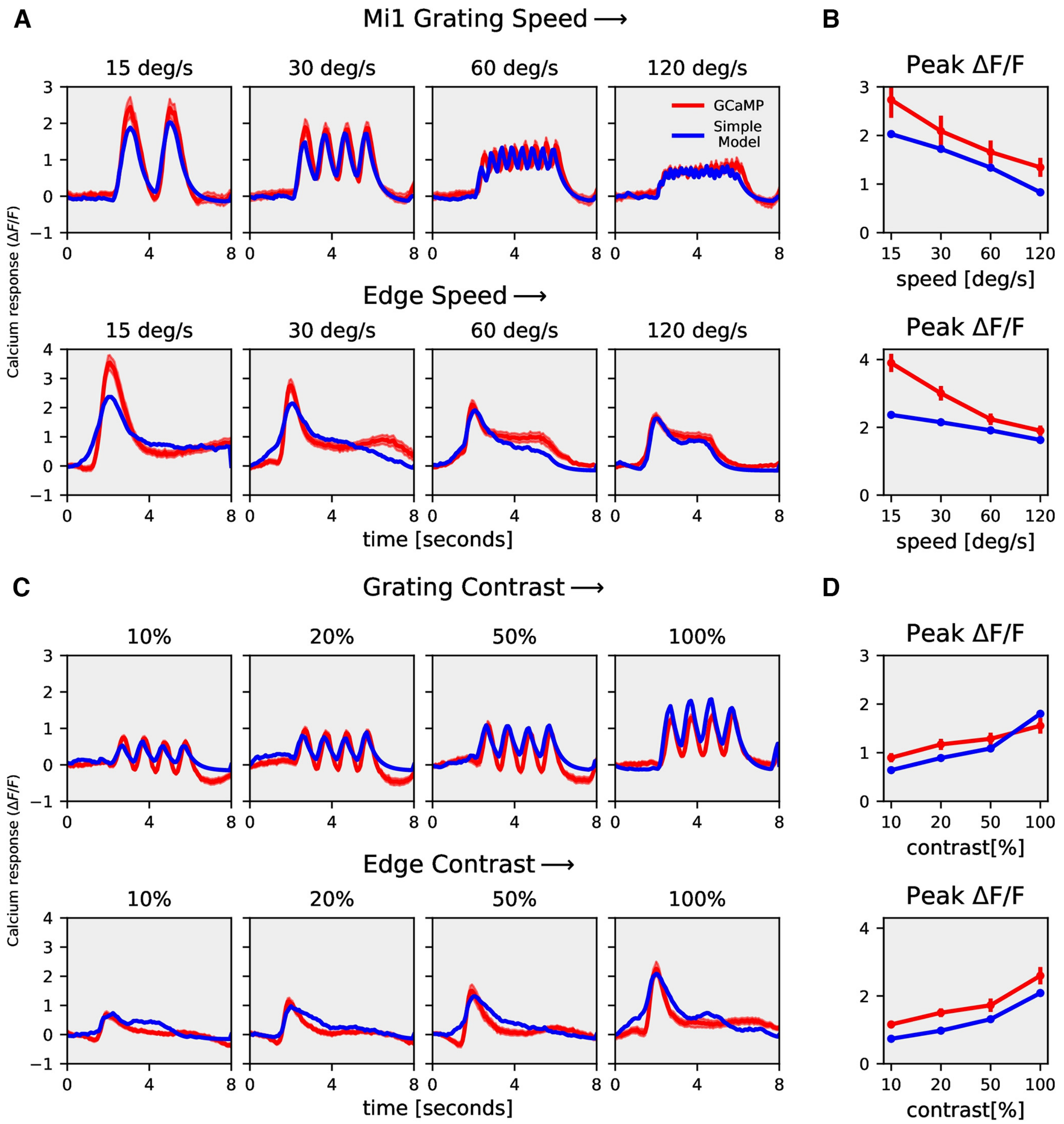

Figure 9. Mi1 rectilinear model responses. ***A***, Mi1 GCaMP6f (red) and rectilinear model (blue) responses to gratings moving at four different speeds (top row) and to gratings moving at four different contrasts (bottom row). ***B***, Mi1 GCaMP6f and model peak responses to gratings moving at four different speeds (top) and four different contrasts (bottom). ***C***, Tm3 GCaMP6f (red) and rectilinear model (blue) responses to gratings moving at four different speeds (top row) and to gratings moving at four different contrasts (bottom row). ***D***, Tm3 GCaMP6f and model peak responses to gratings moving at four different speeds (top) and four different contrasts (bottom).

difference between the model and the experimental data at each time point (Materials and Methods, Eq. 3). There was a total of 112 stimulus conditions: grating speed (four speeds, 12 directions), grating contrast (four contrasts, 12 directions), edge speed (four speeds, PD and ND), and edge contrast (four contrasts, PD and ND). The total error amounted to the sum of all errors across all stimulus conditions (Materials and Methods, Eq. 4). We defined the model error as the total error divided by the power of the data (Materials and Methods, Eq. 5). We then found the optimal parameter values of the model that correspond to the minimum total error using the Python SciPy minimize function (Virtanen et al., 2020). To avoid the risk of being trapped in a local minimum, we ran the parameter search 300 times with random starting parameters and chose the parameter set which resulted in the smallest error.

We started with a rectilinear model (Fig. 5*A*). The model first passes the ArcLight signal through a high-pass filter which removes slow fluctuations. This is followed by a threshold,

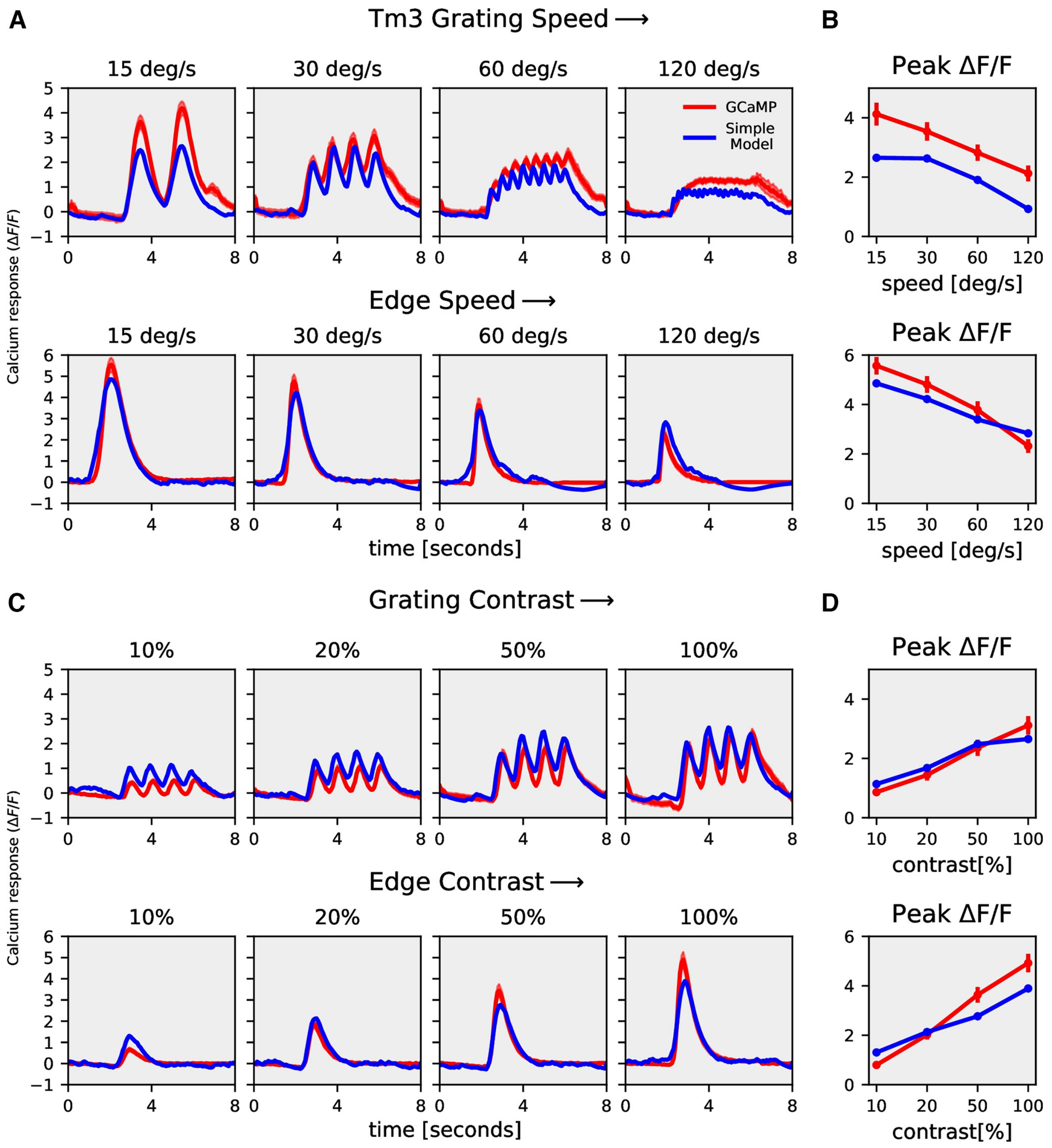

Figure 10. Tm3 rectilinear model responses. ***A***, Mi1 GCaMP6f (red) and rectilinear model (blue) responses to gratings moving at four different speeds (top row) and to gratings moving at four different contrasts (bottom row). ***B***, Mi1 GCaMP6f and model peak responses to gratings moving at four different speeds (top) and four different contrasts (bottom). ***C***, Tm3 GCaMP6f (red) and rectilinear model (blue) responses to gratings moving at four different speeds (top row) and to gratings moving at four different contrasts (bottom row). ***D***, Tm3 GCaMP6f and model peak responses to gratings moving at four different speeds (top) and four different contrasts (bottom).

assuming that the voltage changes below a certain threshold do not affect the calcium level in the cell (Yang et al., 2016). In addition, we further considered a few experimental observations for constructing the model. First, the GCaMP6f response to gratings showed modulations only for slower speeds, whereas the ArcLight response had modulations even at faster speeds (Fig. 2*A*). This suggests that the GCaMP6f signal is a low-pass filtered version of the ArcLight signal. In the rectilinear model, we used a single low-pass filter followed by a gain and time shift. Multiplication with a gain factor was required since GCaMP6f signals have a much higher magnitude compared with ArcLight. Since ArcLight and GCaMP6f responses were recorded from cells in different flies with different receptive fields, the responses had different phases. Therefore, a time shift was necessary to align the signals. However, the rectilinear model with a single low-pass filter could not reproduce responses across all stimuli. The model

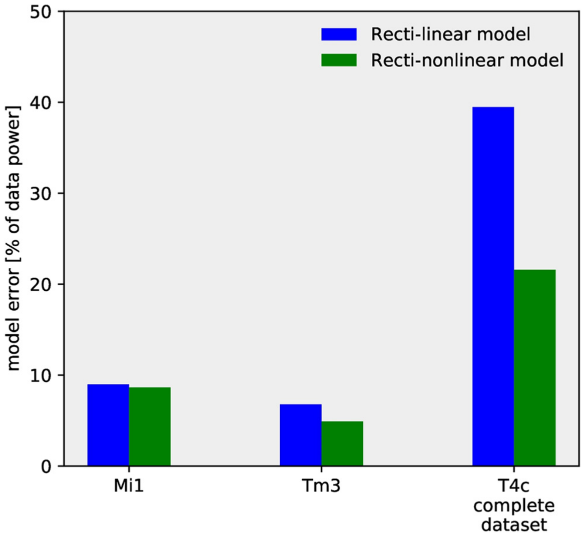

Figure 11. Model error for the rectilinear and recti-nonlinear model. The model error for the rectilinear model (blue) and recti-nonlinear model (green). Mi1 and Tm3 dataset consists of gratings at four different speeds and contrast moving in a single direction. T4c complete dataset consists of gratings moving in 12 different directions, and ON edge moving in PD, ND at four different speeds and contrasts, i.e., a total of 112 stimuli conditions.

error for the complete data set for the rectilinear model was around 39% (see Table 1 for list of parameters). Specifically, the rectilinear model failed to suppress the ND responses and to reproduce the edge responses. The directional tuning index L_{dir} was much smaller for the rectilinear model compared with the experimental data (Fig. 6*E*,*F*, blue lines). Second, the GCaMP6f responses in addition to modulation also had a steady rise over time whereas the ArcLight signal only had modulations (Figs. 2*A*, 3*A*). To quantify this rise, we calculated the modulation ratio of the peak amplitude of the last modulation divided by the peak amplitude of the first modulation for gratings moving at 15°/s. For the ArcLight signal the modulation ratio was 0.86 ± 0.04, for the GCaMP signal the modulation ratio was 1.69 ± 0.21. In order to reproduce the edge responses and modulation in grating responses, the model needed a low-pass filter with a small time constant. However, to simulate the steady rise in the grating signal, a low-pass filter with a large time constant was necessary. Hence, we combined the output of two low-pass filters. Summing up the low-pass filter outputs did not lead to much improvement. However, multiplying the outputs of the low-pass filters led to a significant decrease in the error. The model error dropped from 39% for the rectilinear model to 23% for the multiplicative model. Counterintuitively, optimizing parameters reliably found the time constant of the two low-pass filters to be identical. We therefore changed our model to a single low pass filter followed by a power nonlinearity (Fig. 5*B*).

This recti-nonlinear model thus has in total six parameters: high-pass filter time constant, threshold, the low-pass filter time constant, exponent, gain and shift. The recti-nonlinear model was able to reproduce calcium signals across different visual stimuli (Fig. 6). In contrast to the rectilinear model where we found a modulation ratio of 1.1, the recti-nonlinear model could reproduce both the modulation as well as the slow rise in the GCaMP6f signal in response to gratings (Fig. 6*A*; modulation ratio 1.60, parameter in Table 1). The recti-nonlinear model could also reproduce the ON edge speed tuning responses across different speeds (Fig. 6*C*,*D*). Consequently, the directional tuning index L_{dir} was similar for the recti-nonlinear model and experimental data across slower speeds and all contrasts (Fig. 6*E*,*F*).

To investigate whether the voltage to calcium transformation as described for T4-cells by a recti-nonlinear model also applies to nondirectional cells, or whether, in these cells, the simpler rectilinear model is sufficient, we expressed ArcLight and GCaMP6f in medulla neurons Mi1 and Tm3 cells, which are both nondirection-selective. Mi1 and Tm3 are presynaptic to T4 cells (Takemura et al., 2017) and have an ON-center receptive field (Behnia et al., 2014; Arenz et al., 2017; Strother et al., 2017; Groschner et al., 2022). We measured ArcLight (black), and GCaMP6f (red) responses of Mi1 and Tm3 cells to gratings and edges moving at four different speeds and to gratings moving at four different contrasts (Figs. 7, 8). The gratings and edges moved along only one direction since the direction does not affect nondirection-selective cells' responses. Contrary to T4, Mi1 GCaMP6f responses showed only modulation without a slow increase over time (modulation ratio: 1.0; Fig. 7*A*; 15°/s, modulation ratio 1.2) For gratings moving at 30°/s and 60°/s, there was an increase in Tm3 GCaMP6f response over time, but the ArcLight response already had a slow increment over time (Fig. 8*A*). Similar to T4, the peak response for Mi1 and Tm3 decreased with increasing stimulus speed and increased with increasing stimulus contrast (Figs. 7, 8). However, the decrease in amplitude for increasing speeds turned out to be much stronger for T4c than for Mi1 and Tm3 (compare Figs. 2*B*,*D* to 7*B*,*D* and 8*B*,*D*). This hints to a shorter time-constant of the low-pass filter for Mi1 and Tm3.

Next, we used the models described in Figure 5 to reproduce Mi1 and Tm3 calcium responses using their ArcLight responses. As discussed earlier, the rectilinear model (Fig. 5*A*) with a single low-pass filter was not able to reproduce T4 calcium responses across all stimuli. However, for Mi1 and Tm3, the rectilinear model accurately replicated the speed and contrast tuning (Figs. 9, 10; see Table 1 for parameter). We further compared the model error for the rectilinear and recti-nonlinear models for Mi1, Tm3, and T4c data (Fig. 11). The model error for Mi1 and Tm3 for the rectilinear model was ≈9% and ≅7%, respectively, compared with ≈9% and ≅5% for the recti-nonlinear model with exponents close to 1 (Mi1 exponent: 1.3; Tm3 exponent: 1.5). Thus, the rectilinear model already performed well for the Mi1 and Tm3 datasets, and changing to the recti-nonlinear model only slightly improved the performance. For the T4c dataset, the model error was ≈39% and ≈22% for the rectilinear and recti-nonlinear models (exponent: 2.5), respectively. Hence, the recti-nonlinear model performed better for the T4c dataset whereas for Mi1 and Tm3 the rectilinear model was sufficient to reproduce the calcium responses. This suggests that voltage to calcium transformation is different for the direction-selective cell T4 than for the nondirection-selective cells Mi1 and Tm3.

So far, all optical recordings have been made from dendritic compartments of T4 cells located in layer 10 of the medulla. As was shown for Mi1 cells, even in tiny neurons of *Drosophila*, calcium signals can be compartmentalized (Yang et al., 2016). In order to compare calcium responses in different compartments of T4c, we recorded the activity in axon terminals in the lobula plate (layer c). Figure 12 shows the directional tuning for different speeds (Fig. 12*A*) and different contrasts (Fig. 12*B*) for GCaMP6f responses in the medulla (red lines) and in the lobula plate (gray lines). We found that the directional tuning in the two compartments is very similar with a slightly narrower tuning in the lobula plate. To test for statistical significance, we

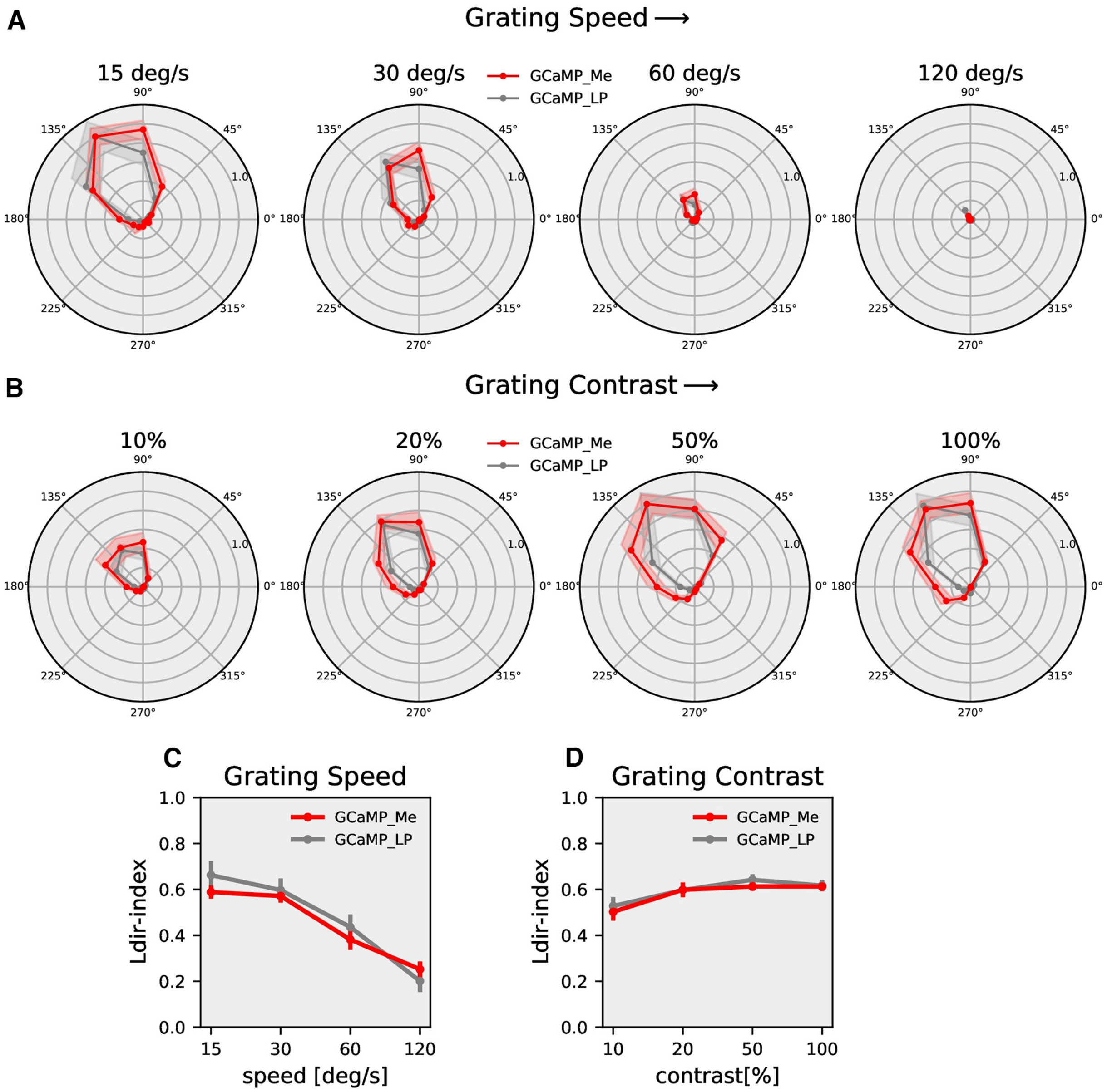

Figure 12. T4c directional tuning in the dendrite and the axon terminal. ***A***, T4c GCaMP6f (red) recorded in the medulla and T4c GCaMP6f (gray) recorded in the lobula plate. Shown are the normalized peak responses to grating moving in 12 directions at four different speeds (medulla: $n = 12$ ROIs from $N = 8$ flies; lobula plate: $n = 9$, $N = 6$). ***B***, Same as ***A*** but for four different contrasts (medulla: $n = 15$ ROIs from $N = 7$ flies; lobula plate: $n = 19$, $N = 8$). ***C***, The directional tuning index L_{dir} for grating moving at four different speeds. The directional tuning index is calculated as the vector sum of the peak responses divided by the sum of all individual vector magnitudes. ***D***, The directional tuning index for grating at four different contrasts. All data show the mean ± SEM.

calculated the circular variance (Berens, 2009) for each experiment and tested the values for differences in the two distributions with a two-sample *t* test. At the 5% significance level, the two distributions were not different ($p = 0.51$).

To further test whether calcium signals might be different in dendrites and axon terminals, we compared the calcium responses in the dendrite and axon terminal of individual T4 cells using the SPARC technique (Isaacman-Beck et al., 2020). This toolkit allows to express effectors in a sparse subset of cells of the same cell type. Figure 13*A* shows the anatomy of such a single T4c cell. The calcium responses to gratings moving at different speeds is shown in Figure 13*B*. There is no difference in the directional tuning between GCaMP signals measured in the axon terminal (gray line) and in the dendrite (red line), indicating that there is no compartmentalization for calcium signals (two sample *t* test for differences in the circular variances: $p = 0.81$).

In order to see whether cells postsynaptic to T4c cells follow their voltage or their calcium signals, we performed patch-clamp recordings from VS-cells. VS-cells integrate the excitatory output of downward tuned T4d/T5d cells on their dendrite. In addition, they are inhibited via LPi neurons which in turn are excited by upward tuned T4c/T5c cells (Fig. 14*B*; Mauss et al., 2015). In order to isolate the excitatory input from T4d/T5d cells, we

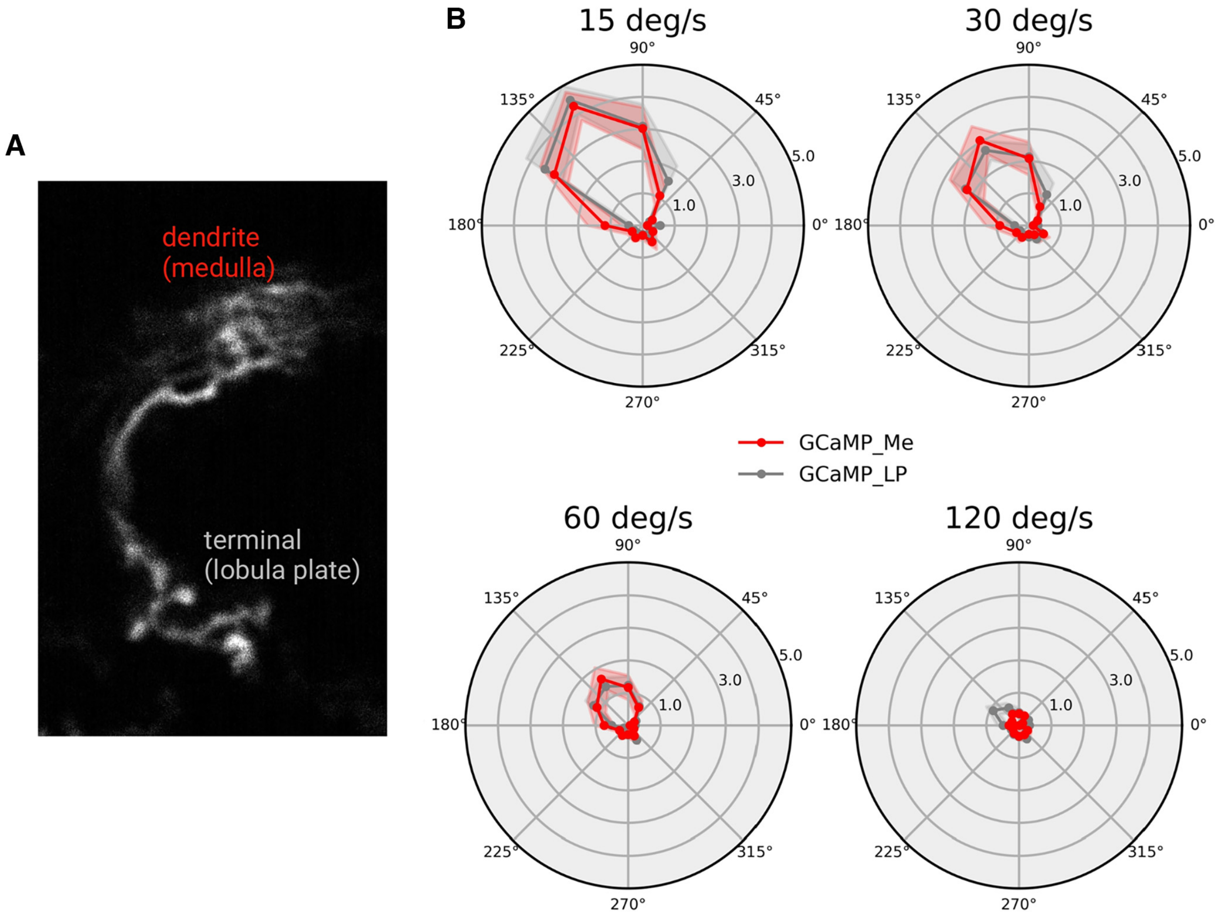

Figure 13. Directional tuning in the dendrite and axon terminal of single T4c cells. ***A***, Anatomy of a single T4c cell. ***B***, Directional tuning of single T4c cells to grating moving in 12 directions at four different speeds (dendrite red line: $n = 13$ ROIs from $N = 5$ flies; axon terminal gray line: $n = 13$, $N = 4$). Shown are the normalized peak responses (mean ± SEM) measured with GCaMP6f.

blocked synaptic transmission from T4c/T5c neurons by expressing tetanus toxin (TNT) while measuring voltage responses in VS-cells to grating stimuli moving at 30°/s in preferred and null direction (Fig. 14*C*,*D*, magenta line). As expected (Mauss et al., 2015), silencing synaptic output from T4c/T5c cells completely abolished null-direction hyperpolarization in VS-cells (Fig. 14*D*), while leaving the preferred direction response mediated by T4d/T5d unchanged (Fig. 14*C*). The only input that VS-cells receive after blocking of T4c/T5c is the direct excitatory input from T4d/T5d. Under the assumption that the voltage to calcium transformation in T4d/T5d is identical to the one measured in T4c/T5c, the directional tuning of VS-cells should reflect the one in the output signals of T4/T5 cells. The directional tuning in VS-cells (with T4c/T5c blocked) is similar to the tuning of T4c GCaMP signal (Fig. 14*E*, gray line). From this, we conclude that the output of T4 cells reflects the narrow tuning of its calcium signal.

Discussion

A neuron processes the input signals it receives from its presynaptic neurons and transforms them into a final transmitter output signal it provides to postsynaptic neurons. This signal flow comprises the following stages: (1) dendritic integration and processing of voltage signals; (2) transformation of voltage signals into calcium influx; and (3) transformation of calcium signals into transmitter release. Information processing can occur at different stages of this signaling cascade. In this study, we explored the transformation of voltage into calcium signals in T4 cells, the first direction-selective neurons in the *Drosophila* ON motion pathway. We showed that the voltage to calcium transformation enhances direction selectivity of voltage signals computed in the dendrites. By recording from postsynaptic cells, we also demonstrated that this enhanced direction selectivity of the calcium signal is indeed reflected in an enhanced direction selectivity of the transmitter output signal of T4 cells.

Electrophysiology has been the most frequently used method to measure the membrane potential changes in neurons. However, because of the small size of neurons in the optic lobe, single-cell electrophysiological recordings of these neurons have been difficult (but see Gruntman et al., 2018, 2019; Groschner et al., 2022). Genetically encoded voltage indicators (GEVIs) have evolved as powerful tools for recording changes in neuronal membrane potentials (Yang et al., 2016; Wienecke et al., 2018; Aimon et al., 2019). Optical methods of monitoring brain activity are appealing because they allow simultaneous, noninvasive monitoring of activity in many individual neurons. We used a fluorescence protein voltage sensor called ArcLight (Jin et al., 2012). ArcLight is based on the

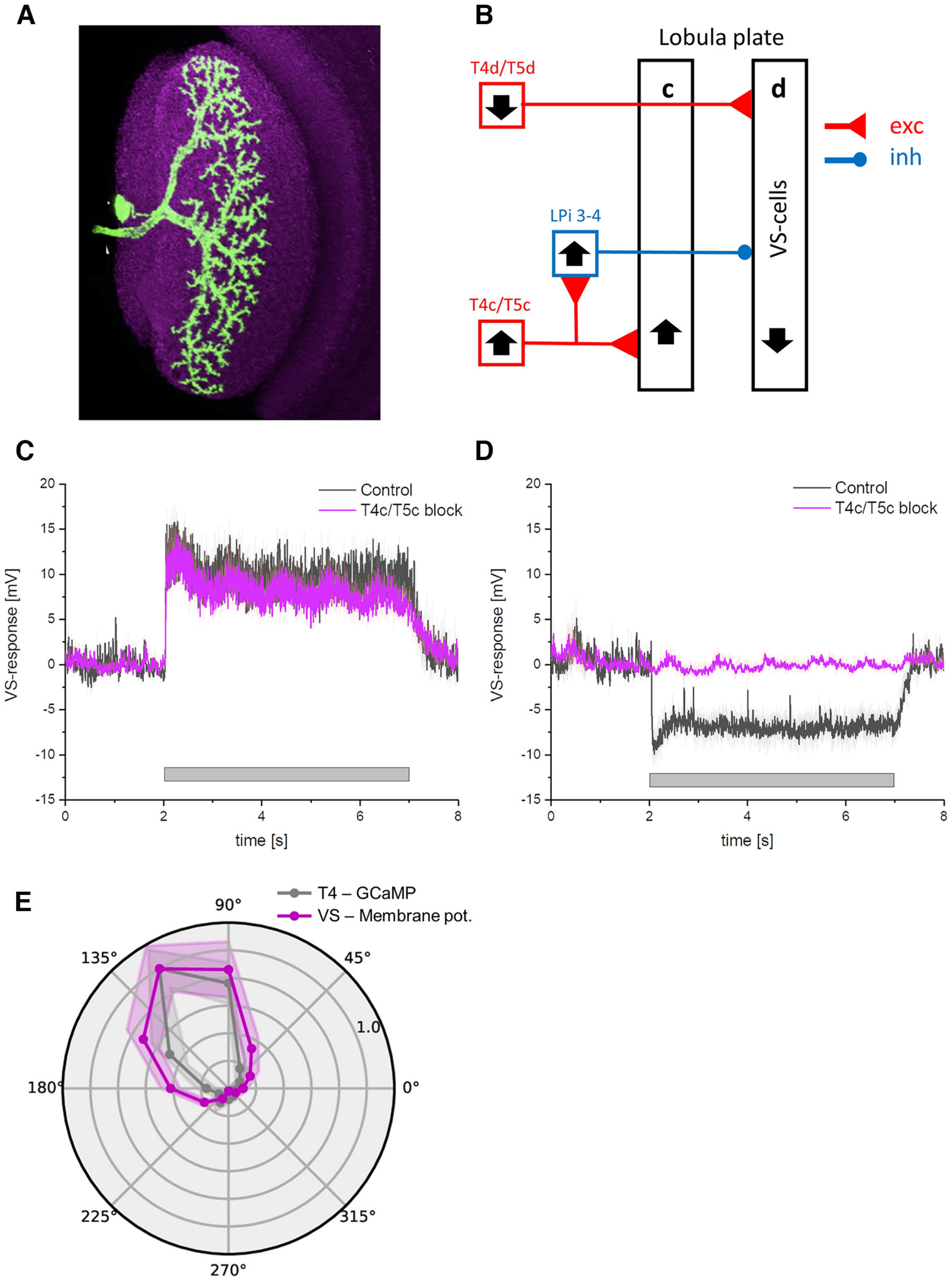

Figure 14. Comparison of T4 and VS-cell tuning. ***A***, Anatomy of a single VS-cell (from Mauss et al., 2015). ***B***, Schematic wiring diagram of VS-cells. VS-cells receive excitatory input from T4d/T5d cells and inhibitory input from LPi3-4 cells. LPi3-4 cells in turn receive excitatory input from T4c/T5c cells. Black arrows indicate the preferred direction. ***C***, VS-cells response to grating moving in preferred direction. The black trace shows the response in control flies, the magenta trace when T4c/T5c cells are blocked with TNT. The blocking did not change the PD response. ***D***, same as ***C*** but with grating moving in the null direction of VS-cells. Blocking of T4c/T5c led to a complete loss of the null direction response in VS-cells. ***E***, Normalized calcium responses of T4c cells (gray) and voltage responses of VS-cells (with T4c/T5c blocked, magenta) to gratings moving along 12 directions at four different speeds ($n = 9$ ROIs from $N = 6$ flies for GCaMP6f, $n = 8$ cells from $N = 6$ flies for VS-cells). Note, to compare the tuning curves of T4c GCaMP6f and VS-cell voltage responses, we shifted the orientation tuning of downward selective (270°) VS-cells to the tuning peak of T4c cells.

fusion of the voltage-sensing domain of *Ciona intestinalis* voltage-sensitive phosphatase (Murata et al., 2005) and the fluorescent protein super ecliptic pHluorin with an A227D mutation. ArcLight has been shown to robustly report both subthreshold events and action potentials in genetically targeted neurons in the intact *Drosophila* brain (Cao et al., 2013).

We built a model to capture voltage to calcium transformation in T4c, Mi1, and Tm3 cells. A rectilinear model with a single low-pass filter was able to reproduce calcium responses in nondirection-selective Mi1 and Tm3 cells (Figs. 9, 10), whereas a recti-nonlinear model with a supralinear function for mapping voltage onto calcium was required to reproduce T4c calcium responses (Fig. 6). The direction selectivity for the rectilinear model signals for T4c was lower compared with the recti-nonlinear model. This suggests that voltage to calcium transformation in Mi1 and Tm3 cells is different from those in T4c cells.

Differential expression of voltage-gated calcium channels in different cells could explain the different voltage to calcium transformations. Voltage-gated calcium channels mediate depolarization-induced calcium influx that drives the release of neurotransmitters. The α1-subunit of the voltage-gated calcium channels forms the ion-conducting pore, which makes it distinct from other calcium channels. Three families of genes encode α1 subunits. The *Drosophila* genome has one α1 subunit gene in each family: α1D (Ca_v1), cac (Ca_v2), and α1T (Ca_v3; Littleton and Ganetzky, 2000; King, 2007). In *Drosophila* antennal lobe projection neurons, cac (Ca_v2) type and α1T (Ca_v3) type voltage-gated calcium channels are involved in sustained and transient calcium currents, respectively (Gu et al., 2009; Iniguez et al., 2013). According to an RNA-sequencing study (Davis et al., 2020), α1T (Ca_v3) mRNA has a higher expression level in Mi1 compared with T4 and Tm3, while cac (Ca_v2) mRNA has a higher expression level in T4 compared with Mi1 and Tm3. Recent experiments with expressing RNAi against cac led to a significantly faster response in Mi1 and Tm3 cells (Gonzalez-Suarez et al., 2022). The differential expressions of voltage-gated calcium channels could cause different voltage to calcium transformations in nondirection selective and direction-selective cells.

We found that the voltage to calcium transformation in T4c neurons enhances their direction selectivity: calcium signals in T4c cells have a significantly higher direction selectivity and directional tuning index compared with membrane voltage across a large set of stimuli, including different speeds, different contrasts, different directions and different spatial structures (Figs. 2-4). Using a smaller stimulus set, a previous study on T5 cells also found the calcium signal to be more directionally selective than the voltage signal (Wienecke et al., 2018). Based on their experiments, the authors made a qualitative proposal for an adaptive supralinearity to account for the voltage to calcium transformation. In contrast, we demonstrate that a static supralinearity is sufficient to quantitatively match the experimental data derived from a comprehensive stimulus set covering a large range of speeds and contrasts.

As calcium is required for neurotransmitter release (Katz and Miledi, 1967), the voltage to calcium transformation is expected to increase the direction selectivity of T4/T5 cells' output signals. In the lobula plate, T4/T5 cells provide input to large lobula plate tangential cells that are depolarized during preferred and hyperpolarized during null direction motion (Mauss et al., 2015). For example, vertical system (VS)-cells with dendrites in layer four receive direct excitatory inputs from downward-tuned T4d/T5d neurons causing depolarization during motion in the downward preferred direction. These VS cells also receive indirect inhibitory inputs from upward-tuned T4c/T5c neurons via glutamatergic LPi3-4 neurons projecting from layer three to layer four causing hyperpolarization in VS-cells during motion in the upward null direction. Upon silencing LPi3-4 neurons' synaptic output via tetanus toxin, VS neurons depolarization response in the preferred direction did not change, but the inhibition for null direction was absent (Mauss et al., 2015). Furthermore, there was no depolarizing response to stimuli moving in null direction. This suggests that T4/T5 do not release any transmitter in response to null direction motion, which matches our findings for the calcium responses in T4c cells to null direction motion. We confirmed this finding by measuring the voltage response of VS-cells to gratings moving in different directions (Fig. 14*E*). The directional tuning measured in VS-cells with T4c/T5c blocked followed the tuning of the calcium signal measured in the terminal region of T4 cells. Thus, voltage to calcium transformation increases direction selectivity in T4/T5 cells which in turn enhances direction selectivity in downstream neurons.

In summary, our study provides evidence that the characteristics of voltage to calcium transformation are specifically tailored to the function of T4 cells within the motion processing pathway: instead of being a mere copy of the membrane voltage required for transmitter output at a chemical synapse, this transformation represents an important processing step that enhances direction selectivity in the output signal of motion-sensing T4 cells.

References

Aimon S, Katsuki T, Jia T, Grosenick L, Broxton M, Deisseroth K, Sejnowski TJ, Greenspan RJ (2019) Fast near-whole-brain imaging in adult *Drosophila* during responses to stimuli and behavior. PLoS Biol 17: e2006732.

Ammer G, Leonhardt A, Bahl A, Dickson BJ, Borst A (2015) Functional specialization of neural input elements to the *Drosophila* ON motion detector. Curr Biol 25:2247–2253.

Arenz A, Drews MS, Richter FG, Ammer G, Borst A (2017) The temporal tuning of the *Drosophila* motion detectors is determined by the dynamics of their input elements. Curr Biol 27:929–944.

Berens P (2009) CircStat: A MATLAB Toolbox for Circular Statistics. J Stat Soft 31(10):1–21.

Behnia R, Clark DA, Carter AG, Clandinin TR, Desplan C (2014) Processing properties of ON and OFF pathways for *Drosophila* motion detection. Nature 512:427–430.

Borst A, Helmstaedter M (2015) Common circuit design in fly and mammalian motion vision. Nat Neurosci 18:1067–1076.

Borst A, Haag J, Mauss AS (2019) How fly neurons compute the direction of visual motion. J Comp Physiol A Neuroethol Sens Neural Behav Physiol 206:109–124.

Borst A, Drews M, Meier M (2020) The neural network behind the eyes of a fly. Curr Opin Physiol 16:33–42.

Cao G, Platisa J, Pieribone VA, Raccuglia D, Kunst M, Nitabach MN (2013) Genetically targeted optical electrophysiology in intact neural circuits. Cell 154:904–913.

Chapman ER (2002) Synaptotagmin: a Ca2+ sensor that triggers exocytosis? Nat Rev Mol Cell Biol 3:498–508.

Chen TW, Wardill TJ, Sun Y, Pulver SR, Renninger SL, Baohan A, Schreiter ER, Kerr RA, Orger MB, Jayaraman V, Looger LL, Svoboda K, Kim DS (2013) Ultrasensitive fluorescent proteins for imaging neuronal activity. Nature 499:295–300.

Davis FP, Nern A, Picard S, Reiser MB, Rubin GM, Eddy SR, Henry GL (2020) A genetic, genomic, and computational resource for exploring neural circuit function. Elife 9:e50901.

Denk W, Strickler JH, Webb WW (1990) Two-photon laser scanning fluorescence microscopy. Science 248:73–76.

Di Maio V (2008) Regulation of information passing by synaptic transmission: a short review. Brain Res 1225:26–38.

Egelhaaf M, Borst A (1989) Transient and steady-state response properties of movement detectors. J Opt Soc Am A 6:116–127.

Eichner H, Joesch M, Schnell B, Reiff DF, Borst A (2011) Internal structure of the fly elementary motion detector. Neuron 70:1155–1164.

Fischbach KF, Dittrich APM (1989) The optic lobe of *Drosophila melanogaster*. I. A Golgi analysis of wild-type structure. Cell Tissue Res 258:441–475.

Fisher YE, Silies M, Clandinin TR (2015) Orientation selectivity sharpens motion detection in *Drosophila*. Neuron 88:390–402.

Gonzalez-Suarez AD, Zavatone-Veth JA, Chen J, Matulis CA, Badwan BA, Clark DA (2022) Excitatory and inhibitory neural dynamics jointly tune motion detection. Curr Biol 32:3659–3675.e8.

Gruntman E, Romani S, Reiser MB (2018) Simple integration of fast excitation and offset, delayed inhibition computes directional selectivity in *Drosophila*. Nat Neurosci 21:250–257.

Gruntman E, Romani S, Reiser MB (2019) The computation of directional selectivity in the *Drosophila* OFF motion pathway. Elife 8:e50706.

Groschner LN, Malis JG, Zuidinga B, Borst A (2022) A biophysical account of multiplication by a single neuron. Nature 603:119–123.

Gu H, Jiang SA, Campusano JM, Iniguez J, Su H, Hoang AA, Lavian M, Sun X O'Dowd DK (2009) Cav2-type calcium channels encoded by cac regulate AP-independent neurotransmitter release at cholinergic synapses in adult *Drosophila* brain. J Neurophysiol 101:42–53.

Haag J, Denk W, Borst A (2004) Fly motion vision is based on Reichardt detectors regardless of the signal-to-noise ratio. Proc Natl Acad Sci U S A 101:16333–16338.

Haag J, Arenz A, Serbe E, Gabbiani F, Borst A (2016) Complementary mechanisms create direction selectivity in the fly. Elife 5:e17421.

Haag J, Mishra A, Borst A (2017) A common directional tuning mechanism of *Drosophila* motion-sensing neurons in the ON and in the OFF pathway. Elife 6:e29044.

Iniguez J, Schutte SS, O'Dowd DK (2013) Cav3-type α1T calcium channels mediate transient calcium currents that regulate repetitive firing in *Drosophila* antennal lobe PNs. J Neurophysiol 110:1490–1496.

Isaacman-Beck J, Paik KC, Wienecke CFR, Yang HH, Fisher YE, Wang IE, Ishida IG, Maimon G, Wilson RI, Clandinin TR (2020) SPARC enables genetic manipulation of precise proportions of cells. Nat Neurosci 23:1168–1175.

Jia H, Rochefort NL, Chen X, Konnerth A (2011) In vivo two-photon imaging of sensory-evoked dendritic calcium signals in cortical neurons. Nat Protoc 6:28–35.

Jin L, Han Z, Platisa J, Wooltorton JRA, Cohen LB, Pieribone VA (2012) Single action potentials and subthreshold electrical events imaged in neurons with a fluorescent protein voltage probe. Neuron 75:779–785.

Joesch M, Schnell B, Raghu SV, Reiff DF, Borst A (2010) ON and OFF pathways in *Drosophila* motion vision. Nature 468:300–304.

Katz B, Miledi R (1967) Ionic requirements of synaptic transmitter release. Nature 215:651–651.

King GF (2007) Modulation of insect CaV channels by peptidic spider toxins. Toxicon 49:513–530.

Kohn JR, Portes JP, Christenson MP, Abbott LF, Behnia R (2021) Flexible filtering by neural inputs supports motion computation across states and stimuli. Curr Biol 31:5249–5260.e5.

Leong JC, Esch JJ, Poole B, Ganguli S, Clandinin TR (2016) Direction selectivity in *Drosophila* emerges from preferred-direction enhancement and null-direction suppression. J Neurosci 36:8078–8092.

Littleton JT, Ganetzky B (2000) Ion channels and synaptic organization: analysis of the *Drosophila* genome. Neuron 26:35–43.

Luo L (2020) Principles of neurobiology. New York: Garland Science.

Maisak MS, Haag J, Ammer G, Serbe E, Meier M, Leonhardt A, Schilling T, Bahl A, Rubin GM, Nern A, Dickson BJ, Reiff DF, Hopp E, Borst A (2013) A directional tuning map of *Drosophila* elementary motion detectors. Nature 500:212–216.

Mauss AS, Pankova K, Arenz A, Nern A, Rubin GM, Borst A (2015) Neural circuit to integrate opposing motions in the visual field. Cell 162:351–362.

Mazurek M, Kager M, Van Hooser SD (2014) Robust quantification of orientation selectivity and direction selectivity. Front Neural Circuits 8:92.

Murata Y, Iwasaki H, Sasaki M, Inaba K, Okamura Y (2005) Phosphoinositide phosphatase activity coupled to an intrinsic voltage sensor. Nature 435:1239–1243.

Pologruto TA, Sabatini BL, Svoboda K (2003) ScanImage: flexible software for operating laser scanning microscopes. Biomed Eng Online 2:1–9.

Salazar-Gatzimas E, Chen J, Creamer MS, Mano O, Mandel HB, Matulis CA, Pottackal J, Clark DA (2016) Direct measurement of correlation responses in *Drosophila* elementary motion detectors reveals fast timescale tuning. Neuron 92:227–239.

Serbe E, Meier M, Leonhardt A, Borst A (2016) Comprehensive characterization of the major presynaptic elements to the *Drosophila* OFF motion detector. Neuron 89:829–841.

Shinomiya K, et al. (2019) Comparisons between the ON- and OFF-edge motion pathways in the *Drosophila* brain. Elife 8:e40025.

Single S, Borst A (1998) Dendritic integration and its role in computing image velocity. Science 281:1848–1850.

Strother JA, Nern A, Reiser MB (2014) Direct observation of on and off pathways in the *Drosophila* visual system. Curr Biol 24:976–983.

Strother JA, Wu S, Wong AM, Nern A, Rogers EM, Le JQ, Rubin GM, Reiser MB (2017) The emergence of directional selectivity in the visual motion pathway of *Drosophila*. Neuron 94:168–182.

Takemura SY, Nern A, Chklovskii DB, Scheffer LK, Rubin GM, Meinertzhagen IA (2017) The comprehensive connectome of a neural substrate for 'ON' motion detection in *Drosophila*. Elife 6:e24394.

Virtanen P, et al. (2020) SciPy 1.0: fundamental algorithms for scientific computing in Python. Nat Methods 17:261–272.

Wienecke CFR, Leong JCS, Clandinin TR (2018) Linear summation underlies direction selectivity in *Drosophila*. Neuron 99:680–688.

Yang HH, Clandinin TR (2018) Elementary motion detection in *Drosophila*: algorithms and mechanisms. Annu Rev Vis Sci 4:143–163.

Yang HH, St-Pierre F, Sun X, Ding X, Lin MZ, Clandinin TR (2016) Subcellular imaging of voltage and calcium signals reveals neural processing in vivo. Cell 166:245–257.

3 DISCUSSION

In manuscript 2.1, my co-authors and I found that the elementary motion-sensitive neurons T4 and T5 in *Drosophila* regardless of their directional tuning and contrast preferences for ON or OFF stimuli implemented a preferred direction (PD) enhancement on the preferred side of their receptive field and a null direction (ND) suppression on the null side. This combination of PD enhancement and ND suppression increases the direction selectivity in T4 and T5 cells, the first cells where the direction selectivity emerges. In T4 cells, whole-cell patch clamp recordings revealed that while the preferred direction stimuli led to large membrane depolarizations, the null direction stimuli also evoked small, but significant responses (Groschner *et al.* 2022). The calcium recordings, however, had a large response to stimuli moving in the preferred direction and almost no response to stimuli moving in the null direction (Fisher *et al.* 2015; Maisak *et al.* 2013). In manuscript 2.2, we showed that the voltage-to-calcium transformation in addition to the synaptic mechanisms on the dendrites of the T4 neurons enhances the direction selectivity in the T4 neurons: the calcium signals in T4 cells had a significantly higher direction selectivity compared to the voltage signals, thus making T4 output signals more direction-selective.

3.1 FLY MOTION VISION

3.1.1 Models of motion detection

Classical algorithmic models for motion detection were developed based on the behavioral studies of beetles and other insects (Hassenstein & Reichardt 1956), and the studies of vertebrates' retinas (Barlow & Levick 1965). As discussed in section 1.4.3, the two algorithmic models: (i) the Hassenstein-Reichart (HR) correlator, and (ii) the Barlow-Levick (BL) detector, involve the interaction of two differentially filtered input signals from two spatially offset locations. The HR correlator enhances the responses to visual motion in the PD via a multiplication-like non-linearity, whereas the BL detector suppresses the responses in the ND via a division-like non-linearity (figure 6). Apparent motion stimuli were used to determine which of the two algorithms is being used by the direction-selective T4/T5 neurons (Haag *et al.* 2016). In apparent motion, stimuli are presented in discrete, consecutive steps instead of constant movement. Preferred direction enhancement occurs when the response to a stimulus moving in the preferred direction is larger than the added response when the stimulus is presented in isolation. In such cases, an HR correlator is used. However, if the response of a given cell is smaller when stimulated along the null direction compared to isolated stimulation, then the null direction suppression mechanism (BL detector) is active.

In the first manuscript, we showed that all four subtypes of both T4 and T5 cells use a combination of PD enhancement and ND suppression (a combination of the HR/BL model). This hybrid HR/BL detector has 3 input lines, two of which are filtered in time, and, lastly, at the non-linear stage, the signals are combined via multiplication on the preferred side and division on the null side. The HR or BL model alone produces weaker direction selectivity compared to the direction selectivity of the hybrid HR/BL model. Our finding explains the high degree of direction selectivity found already at the processing stage where direction-selective signals first emerge: it is not possible to achieve such a strong direction selectivity as observed experimentally with large responses for preferred motions and no responses for null motions in T4/T5 cells (Fisher *et al.* 2015; Maisak *et al.* 2013), by either enhancing signals for preferred motions or suppressing signals for null motions alone.

3.1.2 Cellular implementation of motion vision

How are PD enhancement and ND suppression implemented in T4 and T5 cells? Through decades of research, a complete connectome of motion vision circuitry has been assembled (Shinomiya *et al.* 2014, 2019; Takemura *et al.* 2008, 2017). A great deal of detail has been provided on the functional response properties (Arenz *et al.* 2017; Drews *et al.* 2020; Serbe *et al.* 2016; Strother *et al.* 2017) and transmitter phenotypes (Davis *et al.* 2020; Pankova & Borst 2017; Richter *et al.* 2018; Takemura *et al.* 2017) of the inputs to T4/T5 cells. Furthermore, it is also possible to visualize the endogenous expression of receptor proteins in T4 and T5 neurons. The subcellular distributions of the Acetylcholine (ACh) receptor subunit *Dα7*, the GABA receptor subunit *Rdl*, and the glutamate-gated chloride channel GluClα have been studied in T4 and T5 cells (Fendl *et al.* 2020).

In the T4 dendrites, GluClα receptors and the glutamatergic input Mi9 synapses are located on the distal part (the preferred side) of the dendrite (figure 7c, e). The ACh *Dα7* receptors and the cholinergic inputs Mi1 and Tm3 synapses are located at the center of the T4 dendrites. The GABA *Rdl* receptors and the GABAergic inputs Mi4, C3, and CT1 synapses are located on the proximal (the null side) of the T4 dendrites. The presence of the glutamate-gated chloride channels makes glutamate input from Mi9 inhibitory. Mi9 has an OFF center receptive field. Mi9 maintains an active state in the dark that abruptly ends when light stimulates its receptive field. The preferred direction enhancement or the multiplication-like nonlinearity arises from the coincidence of cholinergic excitation and release from glutamatergic inhibition (Groschner *et al.* 2022). The PD enhancement on the T4 dendrites is thus achieved by multiplying the release from Mi9 inhibitory glutamate input on the distal arm with an excitatory cholinergic input of Mi1 in the center. This 'multiplicative disinhibition' represents the opposite of divisive inhibition. GABAergic inhibitory inputs on the null sides Mi4, C3, and CT1 provide the divisive inhibition or the null direction suppression. Why are there multiple cells providing input on the null side and the specific contributions of each of these cells on the null side remain to be investigated.

There is still uncertainty regarding how PD enhancement and ND suppression are achieved in T5 dendrites. In the T5 dendrites, the ACh *Dα7* receptors and the cholinergic Tm1, Tm2, and Tm4 inputs synapses are located in the center of the dendrites (figure 7d, f). The GABA *Rdl* receptors and the GABAergic input CT1 synapses are located on the proximal part (the null side) of the dendrites. However, the GluClα receptors are absent in the case of T5 cells. The T5 dendrites on the distal part (the preferred side) receive input from cholinergic neuron Tm9 and also express ACh receptors. Hence, the implementation of PD enhancement in the case of T5 cells is most likely different from the implementation in the T4 cells. In addition, while 3 neurons (Mi4, C3, and CT1) provide GABAergic input to the null side of T4 dendrites, the T5 neurons receive inhibitory input on the null side only from CT1 neurons. As a result of these differences, the implementation of ND suppression in T5 cells may also be different in comparison to the T4 cells. These are some of the questions that need to be investigated further.

One possible approach to discern the individual contribution of the GABAergic input neurons Mi4, C3, and CT1 is to silence one of these neurons, while simultaneously recording neural activity from the T4 neurons. However, such blocking experiments come together with their own challenges. One such challenge is that the current blocking techniques are not connection-specific. In other words, silencing one type of cell will silence synaptic transmission to all of its postsynaptic targets. Especially in the fly visual system, where almost all of the medulla neurons are highly interconnected, this can be problematic (Takemura *et al.* 2017). For example, Mi4 and Mi9 cells have very strong reciprocal connections. Hence, silencing Mi4 neurons would also affect the neural activity in the Mi9 neurons. The effect thus observed downstream in T4 neurons is difficult to be attributed solely to Mi4. It is therefore possible to cause second-order effects if one cell type is blocked, resulting in a profound effect on the circuit overall. The development of connection-specific blockers could provide a solution to such confounding effects. Secondly, it is difficult to determine the effectiveness of a block. It is hard to say whether blocked cells have no effect or if the block was ineffective when there is no effect or negative results. Thirdly, does the stimulus being used test the distinct contribution of the cell to the response? If no effect or phenotype is observed and the block is effective, using another stimulus may result in an effect.

3.1.3 Mechanism for the temporal delay

Most major cells presynaptic to T4 and T5 have been characterized in detail in terms of their temporal response properties. Generally, inputs can be classified into two classes with respect to their temporal properties: transient band-pass filters and slow sustained low-pass filters (Arenz *et al.* 2017; Behnia *et al.* 2014; Serbe *et al.* 2016). In the ON pathway, while Mi9 and Mi4 show characteristics of a low-pass filter, Mi1 and Tm3 show characteristics

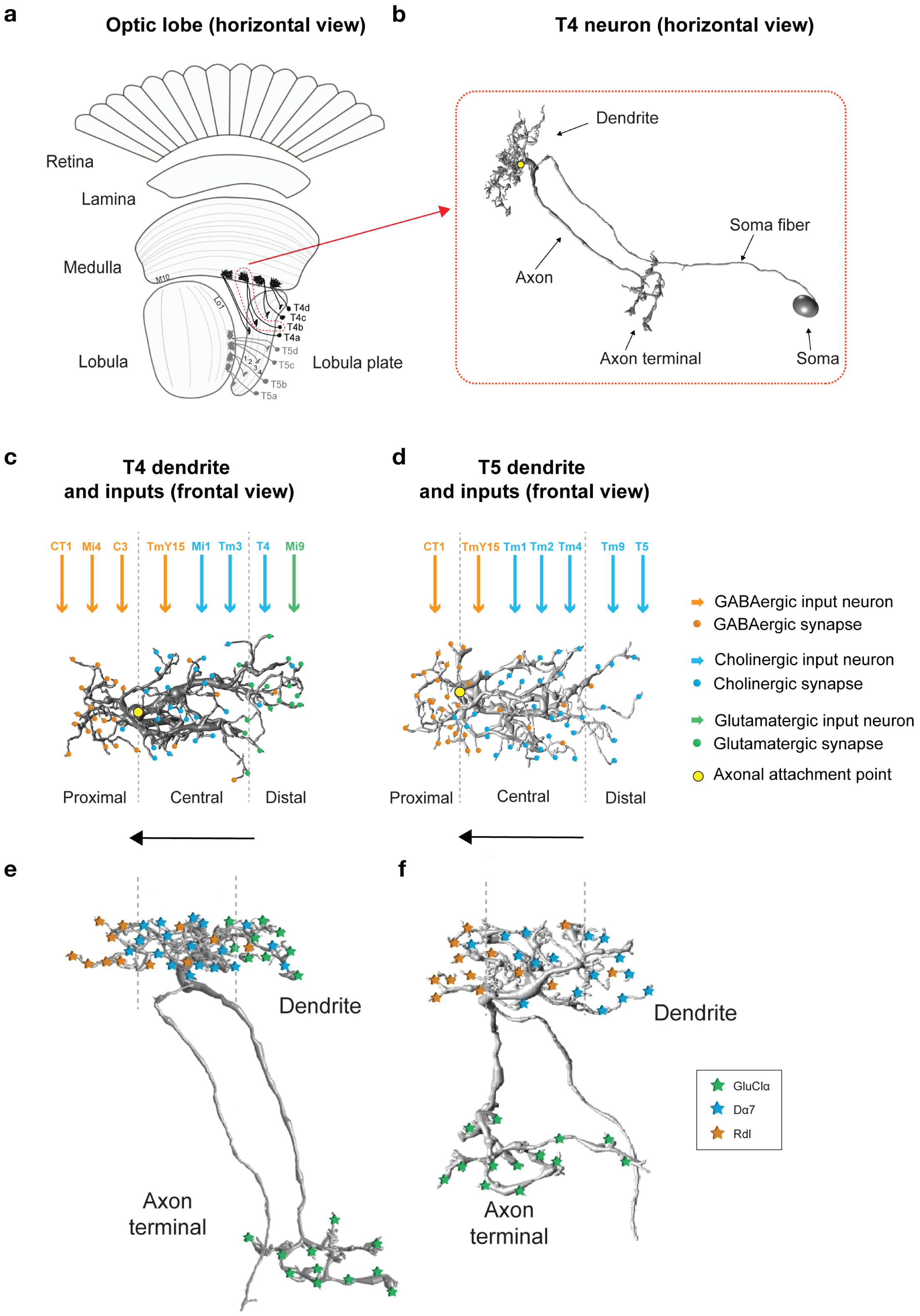
a
Optic lobe (horizontal view)
Retina
Lamina
Medulla
M10
Lo1
Lobula
Lobula plate
T4d
T4c
T4b
T4a
T5d
T5c
T5b
T5a
1
2
3
4
b
T4 neuron (horizontal view)
Dendrite
Soma fiber
Axon
Axon terminal
Soma
c
T4 dendrite
and inputs (frontal view)
CT1
Mi4
C3
TmY15
Mi1
Tm3
T4
Mi9
Proximal
Central
Distal
d
T5 dendrite
and inputs (frontal view)
CT1
TmY15
Tm1
Tm2
Tm4
Tm9
T5
Proximal
Central
Distal
GABAergic input neuron
GABAergic synapse
Cholinergic input neuron
Cholinergic synapse
Glutamatergic input neuron
Glutamatergic synapse
Axonal attachment point
e
Dendrite
Axon
terminal
f
Dendrite
Axon
terminal
GluClα
Dα7
Rdl

Figure 7: Distribution of the presynaptic partners, input synapses and receptors on the T4 and T5 dendrites: (a) A horizontal view of the optic lobe shows the retina, lamina, medulla, lobula, and lobula plate. Dendrites of T4 (darker gray) are found in layer 10 of the medulla, and those of T5 (lighter gray) are found in layer 1 of the lobula. (b) An EM-reconstructed T4 neuron showing the location of the dendrite, axon, and cell body. (c) An illustration of an individual T4 dendrite and its distribution of input synapses (frontal view). In this illustration, the dendrite points to the right, against its preferred right-to-left orientation (indicated by an arrow). (d) Same as in c, but for T5 cells. (e) Anatomic distribution of glutamate-gated chloride channels GluClα, acetylcholine receptors *Dα7*, and GABA receptors *Rdl* on T4 dendrites. (f) Same as in e, but for T5 cells. (Used and modified with permission from (Fendl *et al.* 2020))

of a band-pass filter. In the OFF pathway, Tm1, Tm2, and Tm4 revealed a band-pass characteristic, and Tm9 showed low-pass filter characteristics. The mechanisms underlying their diverse temporal properties, however, remain unknown. It is possible to implement a delay either intracellularly or synaptically. Simple mechanisms such as passive dendritic filtering can be used by cells. A neurite's length, diameter, and membrane resistance, for example, determine its conduction velocity. The time constant of a neuron, which describes its passive low-pass filtering properties, is linearly related to its input resistance. Therefore, slower medulla neurons may simply have higher resistances.

In addition to the cellular passive properties, voltage-gated ion channels can also delay electrical signals or render them more transient (Destexhe 1999). As an example, depolarizing synaptic inputs activate A-type potassium channels, but they quickly deactivate. The brief increase in potassium conductance prevents the membrane from reaching a threshold, causing a delay (Groschner *et al.* 2018). In the lateral geniculate nucleus of guinea pigs, a transient A-type potassium current has been hypothesized to explain the delayed visual response (McCormick 1991).

Synaptic transmission can have an important impact on a circuit's temporal dynamics in addition to cell-intrinsic mechanisms. The process of neurotransmitter release, diffusion, and binding to a receptor already imposes a delay of 2-3 milliseconds during chemical synaptic transmission. Additionally, postsynaptic receptor properties contribute to temporal filtering. Direct current can flow through ionotropic receptors, but metabotropic receptors initiate a second messenger cascade, which activates ionic conductances after a delay typically of tens to hundreds of milliseconds. All of these mechanisms are plausible since T4 and T5 neurons express a wide array of ionotropic and metabotropic neurotransmitter receptors and voltage-gated ion channels.

Mi9 and Tm9 with low-pass filter characteristics receive their major input from lamina cell L3, which exhibits slow temporal characteristics (Silies *et al.* 2013). L1 provides a major input to the faster cells Mi1 and Tm3 (Takemura *et al.* 2017). There are already fast band-pass characteristics in L1 (Clark *et al.* 2011; Drews *et al.* 2020; Reiff *et al.* 2010). Therefore, it is possible that medulla neurons inherit the temporal properties of their lamina inputs. Thus, the delay mechanism associated with ON and OFF motion detectors may be implemented between photoreceptors and lamina cells at the first synapse. In this scenario, motion blindness should be the result of flies with dysfunctional L3 cells. However, blocking synaptic transmission from L3 does not significantly affect fly optomotor activity (Bahl *et al.* 2015; Silies *et al.* 2013; Tuthill *et al.* 2013). The temporal filtering properties of a given neuron in the fly medulla are likely determined by several biophysical mechanisms.

3.1.4 Circuits downstream of T4 and T5 cells

How do downstream circuits use the motion direction information computed by the T4/T5 neurons in the optic lobe to guide fly behavior? The crucial roles of T4 and T5 cells in visually guided behaviors have been revealed through several studies inhibiting synaptic transmission from these cells. For fly optomotor behavior, T4 and T5 cells are required. Blocking the synaptic output of these cells led to motion blindness in flies (Bahl *et al.* 2013). Figure-ground discrimination (Fenk *et al.* 2014), avoidance of expanding stimuli, as well as landing responses (Schilling & Borst 2015) involve T4 and T5 cells. In what ways are direction-selective signals passed from T4/T5 cells to the central brain and to the motor areas? Lobula plate tangential cells provide the most direct link between motion-sensitive T4/T5 neurons and motor circuits.

In the lobula plate, T4 and T5 neurons provide excitatory inputs onto the tangential cells and lobula plate intrinsic neurons (Lpi). Monosynaptic, excitatory, and cholinergic connections exist between T4/T5 and tangential cells (Mauss *et al.* 2014). As discussed earlier (in section 1.4.2), the HS cells with dendrites in layer 1 depolarize during front-to-back motion and hyperpolarize during back-to-front motion, while VS cells with dendrites mainly in layer 4 depolarize primarily during downward motion and hyperpolarize during upward motion (Hopp *et al.* 2014; Schnell *et al.* 2010; Scott *et al.* 2002). In addition to abolishing the depolarization of tangential cells when stimulated along their preferred direction, blocking the output of T4 and T5 cells also affects the hyperpolarization when stimulated along their null direction (Schnell *et al.* 2012). Additionally, the tangential cells respond with a fast excitation, followed by inhibition when T4 and T5 cells are optically activated (Mauss *et al.* 2015). These results suggest that T4 and T5 cells provide tangential cells with both direct stimulation and indirect inhibition from adjacent lobula plate layers. Since LPi neurons bi-stratify in layer-specific ways, dendrites from one subtype reside exclusively in one layer, and axons in the neighboring layer, LPi are perfect candidates for this task (figure 8). T4/T5 cells in one layer provide feedforward glutamatergic inhibitory input via LPi via glutamate-gated chloride channels GluClα to tangential cell dendrites in the adjacent layer. Lpi neurons are direction-selective, and have the same preferred direction as the T4/T5 cells they receive the input from (figure 8g). These results taken together suggest that the T4/T5 cells depolarize the tangential cells during preferred direction motion directly via excitatory inputs, and hyperpolarize the tangential cells during null direction motion indirectly via inhibitory inputs from LPi neurons.

In manuscript 2.2, we showed that the voltage to calcium transformation in T4c neurons enhances their direction selectivity. The calcium signals in T4c cells had a significantly higher direction selectivity and tuning than the membrane voltage across different stimuli conditions. As calcium is required for neurotransmitter release, this is expected to increase the direction selectivity of T4 cells' output signals. In order to determine the direction selectivity of T4 cells' output signals, the neurons that are postsynaptic to T4 cells can be recorded. Upon silencing the LPi3-4 neurons' synaptic output via tetanus toxin, the VS neurons' depolarization response in the preferred direction did not change, but the null direction response was absent (figure 9) (Mauss *et al.* 2015). This suggests that T4/T5 cells do not release any transmitter in response to the null direction motion, which matches our findings for the calcium responses. Thus, the voltage to calcium transformation increases

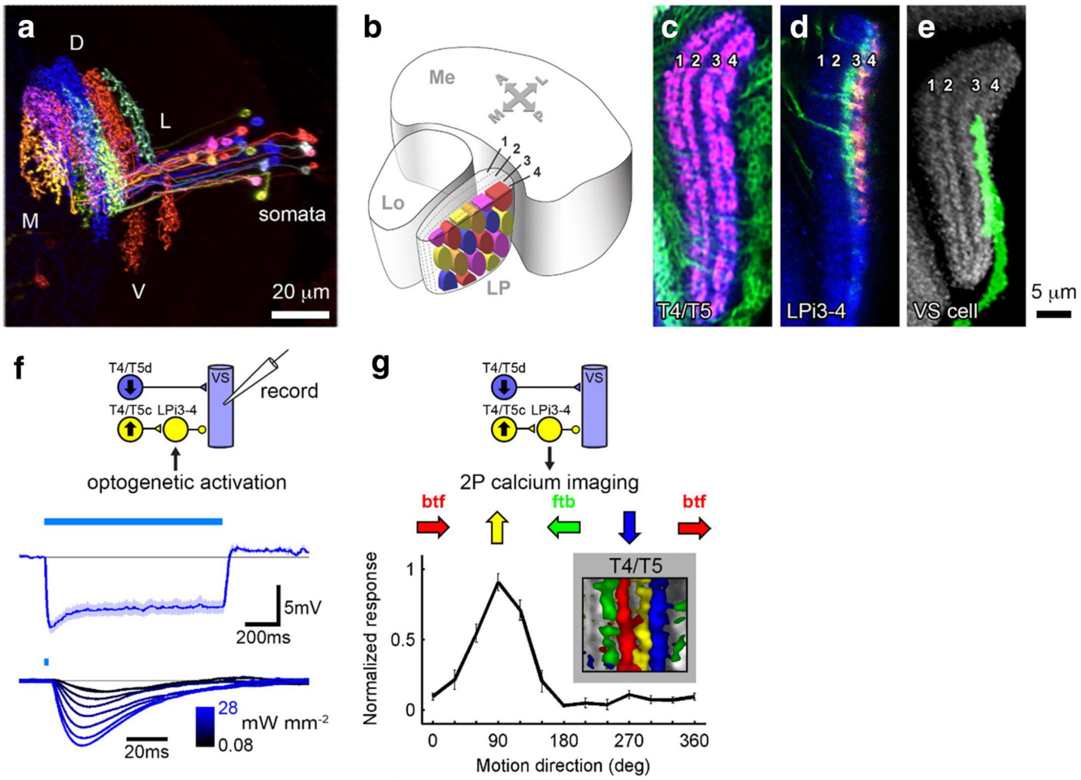
a
D
L
M
somata
V
20 μm
b
Me
A
L
M
P
1
2
3
4
Lo
LP
c
1 2 3 4
T4/T5
d
1 2 3 4
LPi3-4
e
1 2 3 4
VS cell
5 μm
f
T4/T5d
VS
record
T4/T5c LPi3-4
optogenetic activation
5mV
200ms
28
mW mm-2
0.08
20ms
g
T4/T5d
VS
T4/T5c LPi3-4
2P calcium imaging
btf
ftb
btf
T4/T5
Normalized response
1
0.5
0
0
90
180
270
360
Motion direction (deg)

Figure 8: Lobula plate intrinsic neurons (LPis): (a) Multi-color flip-out showing several LPi neurons in the lobula plate. D = dorsal, V = ventral, L = lateral, M = medial. (b) Dendritic fields of adjacent LPi neurons shown schematically. (c) The horizontal cross-section of the lobula plate shows GFP-expressing T4/T5 cells (green) and synaptotagmin-HA (red). (d) LPi neurons expressing GFP (green) and presynaptic synaptotagmin-HA (sytHA, red). Presynaptic specializations are restricted to layer 4 only, even though neurons ramify in layers 3 and 4. (e) GFP staining of a VS cell dendrite in layer 4 of the lobula plate. (f) Patch-clamp recordings from VS cells and optogenetic stimulation of LPi cells to study the synaptic connection between LPi and VS cells. A sustained hyperpolarizing potential is evoked by 1 s light stimulation of LPi neurons (upper recording trace). Light pulses (2 ms) are delivered in different strengths (bottom traces). (g) Direction-selectivity of Lpi cells. Visual activity in LPi3-4 neurons measured by calcium imaging in response to gratings moving in different directions. (Used with permission from (Borst *et al.* 2020b))

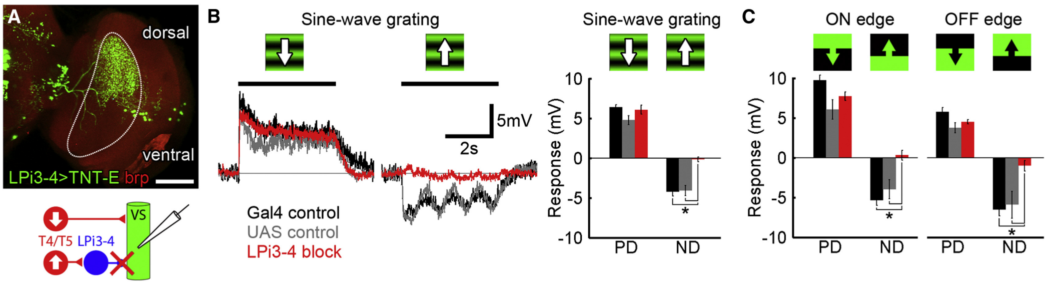

Figure 9: Tangential cells receive null direction responses from LPi neurons: (a) In LPi3-4 neurons, the tetanus toxin light chain suppresses synaptic release. The schematic below illustrates the experimental approach used to measure whole-cell voltages from VS cells in order to investigate LPi3-4 cell function. (b) Control flies respond to sine-wave gratings moving down (preferred direction [PD]) or up (null direction [ND]) by depolarizing or hyperpolarizing respectively. Hyperpolarizing responses to ND motion are selectively abolished in LPi3-4 block flies. (c) In LPi3-4 block flies, VS cell responses to moving ON and OFF edges are similarly affected with ND responses. (Used with permission from (Mauss *et al.* 2015))

direction selectivity in T4/T5 cells and this enhances direction selectivity in the T4/T5 cells' output signals.

3.2 THE EFFECT OF VOLTAGE-TO-CALCIUM TRANSFORMATION ON THE DIRECTION SELECTIVITY OF T4 CELLS

A neuron processes the input signals it receives from its presynaptic neurons and transforms them into a final transmitter output signal it provides to postsynaptic neurons. This signal flow comprises the following stages: (1) dendritic integration and processing of voltage signals; (2) transformation of voltage signals into calcium influx; and (3) transformation of calcium signals into transmitter release. Information processing can occur at different stages of this signaling cascade. In this study, we explored the transformation of voltage into calcium signals in T4 cells, the first direction-selective neurons in the Drosophila ON motion pathway. We showed that the voltage-to-calcium transformation enhances the direction selectivity of voltage signals computed in the dendrites. By recording from postsynaptic cells, we also demonstrated that this enhanced direction selectivity of the calcium signal is indeed reflected in an enhanced direction selectivity of the transmitter output signal of T4 cells.

We found that the voltage-to-calcium transformation in T4c neurons enhances their direction selectivity: calcium signals in T4c cells have a significantly higher direction selectivity and directional tuning index compared with membrane voltage across a large set of stimuli, including different speeds, different contrasts, different directions, and different spatial structures. Using a smaller stimulus set, a previous study on T5 cells also found the calcium signal to be more directionally selective than the voltage signal (Wienecke *et al.* 2018). Based on their experiments, the authors made a qualitative proposal for an adaptive supra linearity to account for the voltage-to-calcium transformation. In contrast, we demonstrate that a static supra linearity is sufficient to quantitatively match the experimental data derived from a comprehensive stimulus set covering a large range of speeds and contrasts. As calcium is required for neurotransmitter release, the voltage to calcium transformation is expected to increase the direction selectivity of T4/T5 cells' output signals. In the lobula plate, T4/T5 cells provide input to large lobula plate tangential cells that are depolarized during preferred and hyperpolarized during null direction motion. For example, vertical system (VS)-cells with dendrites in layer four receive direct excitatory inputs from downward-tuned T4d/T5d neurons causing depolarization during motion in the downward preferred direction. These VS cells also receive indirect inhibitory inputs from upward-tuned T4c/T5c neurons via glutamatergic LPi3-4 neurons projecting from layer three to layer four causing hyperpolarization in VS cells during motion in the upward null direction. Upon silencing LPi3-4 neurons' synaptic output via tetanus toxin, VS neurons' depolarization response in the preferred direction did not change, but the inhibition for the null direction was absent (Mauss *et al.* 2015). Furthermore, there was no depolarizing response to stimuli moving in the null direction. This suggests that T4/T5 do not release any transmitter in response to null direction motion, which matches our findings for the calcium responses in T4c cells to null direction motion. We confirmed this finding by measuring the voltage response of VS-cells to gratings moving in different directions. The directional tuning measured in VS-cells with T4c/T5c blocked followed the tuning of the calcium signal measured in the terminal region of T4 cells. Thus, voltage-to-calcium transformation increases direction selectivity in T4/T5 cells which in turn enhances direction selectivity in downstream neurons.

In summary, our study provides evidence that the characteristics of voltage-to-calcium transformation are specifically tailored to the function of T4 cells within the motion processing pathway: instead of being a mere copy of the membrane voltage required for transmitter output at a chemical synapse, this transformation represents an important processing step that enhances direction selectivity in the output signal of motion-sensing T4 cells.

3.3 THE FUNCTION OF THE VISUAL CIRCUIT DURING NATURAL BEHAVIOR

In this thesis, experiments were conducted on tethered flies whose movement is severely restricted. How do motion circuits operate during unrestrained behavior? State-dependent modulations are observed in the activity and tuning properties of visual circuits in mice and flies (Maimon 2011). During tethered flight or walking, tangential cells in the fly's lobula plate shift their temporal frequency tuning optimum towards higher frequencies (Chiappe *et al.* 2010; Jung *et al.* 2011; Maimon *et al.* 2010). In the ON motion vision pathway, the medulla neurons modulate their baseline calcium level according to their behavioral state, and octopaminergic neurons are needed to process fast-moving visual stimuli appropriately (Strother *et al.*

2018). Chlordimeform (CDM), an octopamine agonist, shifted the temporal tuning optima for T4 and T5 cells and all input elements towards higher frequencies (Arenz *et al.* 2017). Both mammalian and fly visual systems are affected by the general behavior state of the animal early on in the circuit and only a few synapses from photoreceptors.

A free-moving or flying fly experiences not only visual cues but also proprioceptive cues through its antennae and halteres (Mamiya *et al.* 2011; Sandeman & Markl 1980). Multiple cues are combined in higher multimodal circuits, usually in a non-linear way (Haag *et al.* 2010; Huston & Krapp 2009). As a result, the activity of visually responsive neurons during tethered flight might be completely different from that during free flight. Flies perform complex maneuvers during free flight, often involving multiple axes of rotation and translation. In a restrained environment, these maneuvers are hard or impossible to repeat. In order to fully understand the function of a visual circuit, it is ideally best to study it in its natural state. In larger animals that can carry head-mounted microscopes, head-stages, or fiber optics, this is easier, but in fruit flies, it is extremely challenging. Over the past years, substantial progress has been made toward achieving this goal. Fruit flies can be tracked online in 2D and 3D with high precision. An optical laser can be used to target the fly for thermogenetic or optogenetic activation of nerve cells using this information (Bath *et al.* 2014; Stowers *et al.* 2014; Straw *et al.* 2011). It is therefore possible to manipulate the activity of a subset of neurons when a fly performs a specific behavioral action or experiences a visual stimulus. Efforts are being made to perform functional imaging in freely walking flies (Grover *et al.* 2016). The combined use of these promising tools can give us a better understanding of how individual nerve cells and visual circuits operate under natural conditions.

3.4 COMPARISON WITH THE DIRECTION-SELECTIVE CIRCUITS IN THE MOUSE RETINA

Among the most striking similarities between the retina and the fly optic lobe is the early splitting of pathways into ON and OFF channels (figure 10). This allows for more efficient encoding of visual stimuli (Gjorgjieva *et al.* 2014). In the vertebrate retina, this splitting takes place right at the photoreceptor-bipolar synapse, whereas in the fly, it occurs one synapse later.

The photoreceptors of the mouse retina hyperpolarize in response to light, while in darkness they release glutamate onto their postsynaptic partners, the bipolar cells. The split between the ON and OFF pathways occurs at the synaptic level between photoreceptors and bipolar cells, resulting in the ON- and OFF-responsive bipolar cells. In the ON bipolar cells, the metabotropic inhibitory glutamate receptor mGluR6 causes a sign inversion and the ON channel is formed (Masu *et al.* 1995). The OFF bipolar cells, however, express ionotropic AMPA receptors that depolarize when glutamate binds (Euler *et al.* 2014). As in the fly optic lobe, there are fast and slow bipolar cells, similar to the medulla and transmedulla neurons.

In the fly, the split into the ON and OFF pathways occurs at the level of lamina cells. Vertebrates don't seem to have any equivalent to the lamina. The *Drosophila* photoreceptors depolarize under light and release histamine, which in turn inhibits lamina neurons via histamine-gated chloride channels (Hardie 1989). The cholinergic lamina neurons L2-L5 transmit photoreceptor signals to the medulla and transmedulla neurons. In the ON channel, L1 is the main input, while in the OFF channel, L2 is the main input (Joesch *et al.* 2010). The glutamatergic L1 neurons inhibit postsynaptic Mi1 and Tm3 neurons via the glutamate-gated chloride channel GluClα, implementing a sign inversion and creating an ON channel. Thus, the photoreceptors depolarize in response to the light, inhibiting L1 neurons, thereby disinhibiting Mi1 and Tm3 neurons, creating the ON-responses. Both GluClα and Rdl receptors are involved in this multi-synaptic sign inversion in the ON pathway (Molina-Obando *et al.* 2019). Both mouse and fly visual systems exhibit sign inversion in the ON pathway as a result of glutamatergic, inhibitory signaling. Fly uses the GluClα channel, which is unique to the invertebrates, instead of the mGluR6 receptor, which causes inhibition in the mouse retina.

Direction-selective T4/T5 cells in the flies are comparable to the starburst amacrine cells (SACs) in mammals and the lobula plate tangential cells are comparable to direction-selective ganglion cells (figure 10). The direction-selective retinal ganglion cells (DSGCs) were the first direction-selective cells to be described in the mammalian retina (H. B. Barlow & Hill 1963). Their four subtypes respond to movement in one of the four cardinal directions, similar to the elementary motion detectors in the fly (T4/T5 neurons) (Elstrott *et al.* 2008). Pharmacology and ablation experiments suggest that GABAergic starburst amacrine cells (SACs) are necessary for direction-selective responses in retinal ganglion cells (Yoshida *et al.* 2001). It is interesting to note that starburst amacrine cells are already direction-selective themselves in a centrifugal manner (Euler *et al.* 2002). Dendrites of these cells protrude radially, and they respond preferentially to stimuli from the base to the tip of the cell. The SACs, in turn, enable DSGCs to be direction selective by inhibiting the null side of their dendrites with asymmetric GABAergic inhibition (Briggman *et al.* 2011). How do the SACs become direction-selective? There are several hypotheses and lines of evidence about how bipolar cells providing excitatory glutamatergic input to both cell types shape their direction-selective responses. The starburst amacrine cells which respond to stimuli moving from the soma to the dendritic tips receive input from different types of bipolar cells, including those with fast and slow temporal dynamics (Baden *et al.* 2013). The different types of bipolar cells also exhibit space-time wiring specificity with starburst amacrine cells: slow bipolar cells wire with starburst amacrine cells proximally, whereas fast bipolar cells wire with the starburst amacrine cells distally (Kim *et al.* 2014). Thus, direction selectivity in flies and mammals may arise by similar mechanisms.

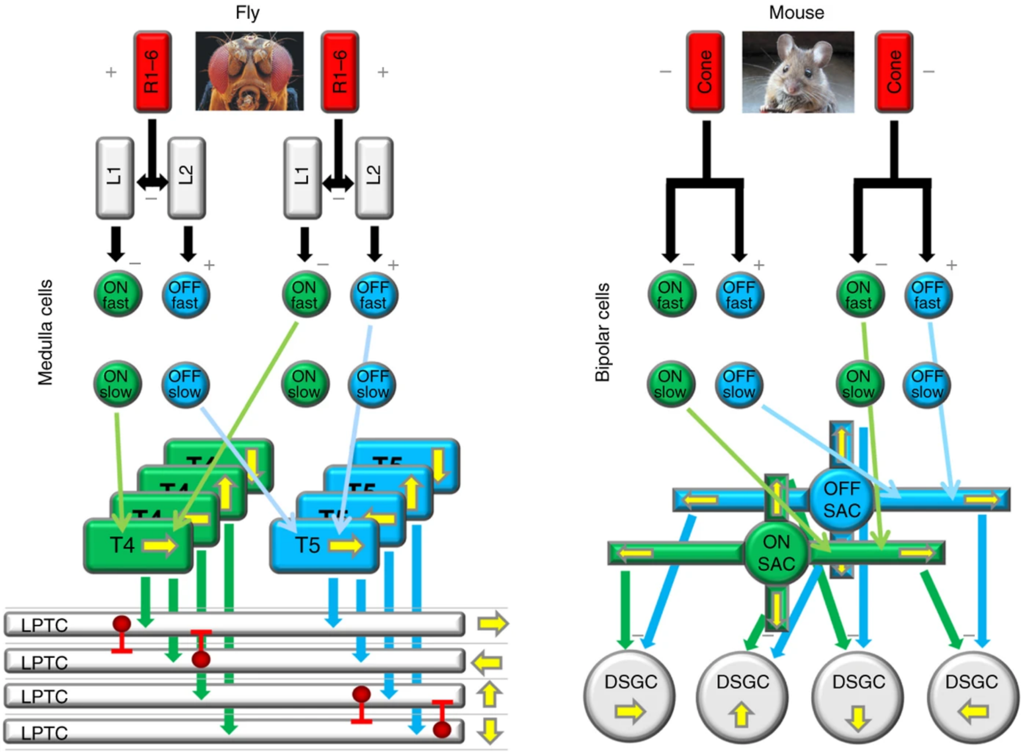
Fly
Mouse
R1–6
R1–6
Cone
Cone
L1
L2
L1
L2
Medulla cells
Bipolar cells
ON fast
OFF fast
ON slow
OFF slow
T4
T5
LPTC
LPTC
LPTC
LPTC
OFF SAC
ON SAC
DSGC
DSGC
DSGC
DSGC
+
–

Figure 10: Fly and mouse motion detection circuits: In the fly, the photoreceptors connect via sign-inverting synapses to the lamina monopolar cells L1 and L2, the entry to the ON and OFF pathway, respectively. The mouse retina lacks this additional layer of lamina cells and splits the signal directly between ON and OFF bipolar cells via two types of glutamate receptors. The T4 (ON) and T5 (OFF) neurons in the fly optic lobe and the ON and OFF SACs in the mouse retina are the first stages of direction-selective cells. Lobula plate tangential cells (LPTCs) in the fly and ON-OFF direction-selective ganglion cells (DSGCs) in the mouse integrate direction-selective information from these two pathways. (Used with permission from Borst & Helmstaedter 2015)

3.5 NEURONAL CALCIUM SIGNALING

In every eukaryotic cell, calcium (Ca^{2+}) regulates the most important activities. Neurons depend on it for the transmission of the depolarizing signal and for synaptic activity. A variety of neuronal processes including long-term potentiation of synaptic transmission or depression of synaptic transmission are controlled by Ca^{2+} signals. As a result, neurons have developed extensive and intricate calcium signaling pathways (Brini *et al.* 2014). Plasma membrane receptors and voltage-dependent ion channels facilitate calcium influx into neurons. Calcium is also released from intracellular stores, such as the endoplasmic reticulum, by intracellular channels. As Ca^{2+} is essential for cellular signaling, its background concentration within cells must be low enough to allow it to be significantly altered without consuming excessive energy.

There are three major groups of plasma membrane Ca^{2+} channels based on their mechanisms of opening: voltage-gated Ca^{2+} channels, receptor-operated Ca^{2+} channels (ROC), and store-operated Ca^{2+} entry channels (SOC), which are activated when the cellular Ca^{2+} stores are empty. There are five distinct subunits ($\alpha1$, $\alpha2$, β, γ, δ) encoded by different genes in the voltage-gated Ca^{2+} channels. They are divided into three subfamilies, namely, Cav1, Cav2, and Cav3 depending on the type of $\alpha1$ pore-forming subunit. According to the physiological and pharmacological properties of the type of current they carry, they can further be classified into six classes L, N, P, Q, R, and T. The $\alpha1$ subunit consists of four repeat domains (I-IV), each with six transmembrane segments (S1-S6). Within the pore-containing subunit, the S4 segments contain some positively charged residues that act as voltage sensors. The associated $\alpha2$, β, γ, and δ subunits have supplementary functions, including the control of channel expression and the modulation of current kinetics (Catterall 2000; Hofmann *et al.* 1999). In skeletal and cardiac muscle, the Cav1 subfamily mediates L-type currents and initiates excitation-contraction coupling. As a result of its activity in neuronal cells, Ca^{2+} transients are generated in dendrites and cell bodies, which in turn regulate processes like secretion and gene expression. Synaptic transmission, neurotransmitter release, and dendritic Ca^{2+} transients are mainly initiated by Cav2 channels, which generate N-, P/Q-, and R-type currents. Cav3 subfamily members are responsible for the T-type current, which is important for pacemaking in cardiac myocytes and repetitive action potential firing in the thalamus (Catterall 2011).

Extracellular ligands, such as neurotransmitters, activate receptor-operated Ca^{2+} channels (ROC). In mammals, L-Glutamate stimulates two classes of receptors: ionotropic receptors (iGluRs) and metabotropic receptors (mGluRs). The two principal types of ionotropic glutamate receptors are N-methyl-d-aspartate sensitive receptors (NMDARs) and Alpha-amino-3-hydroxy-5-methyl-4-isoxazole propionic acid-sensitive receptors (AMPARs). In the mammalian central nervous system, AMPARs transmit fast excitatory synaptic signals and are permeable to Na+ and K+, and may be permeable to Ca^{2+} ions. NMDARs are permeable to both Na^{+} and Ca^{2+}. Compared to AMPARs, NMDARs respond more slowly to glutamate. Not only glutamate is required for their activation (ligand-gating), but also membrane depolarization (voltage dependence) to remove Mg^{2+} that normally blocks them. The coincidence detection process that opens NMDAR channels is critical in learning and memory (Miyashita *et al.* 2012).

Store-operated Ca^{2+} entry channels (SOC) are activated when Ca^{2+} is released from the endoplasmic reticulum. Originally discovered in non-excitable cells, they are now being discovered in skeletal muscle and neurons as well. It was originally proposed that store-operated Ca^{2+} entry ensured the replenishment of intracellular stores after Ca^{2+} was released (Putney Jr 1986). There is evidence that Ca^{2+} influx through this pathway may directly signal targets located close to sites of Ca^{2+} entry, thus initiating specific signaling pathways (Feske 2011). A TRP channel is a type of channel that can either regulate intracellular Ca^{2+} concentration directly by acting as a Ca^{2+} entry pathway or indirectly by triggering voltage-dependent ion channel activation when cells are depolarized.

Considering the special importance of calcium signaling in neuronal function, the voltage-to-calcium transformation we studied in our second manuscript with a focus on direction selectivity may have a broader impact on other neuronal processes and should be investigated further.

3.5.1 Voltage-gated calcium channels

In manuscript 2.2, we built a model to capture the voltage-to-calcium transformation in T4c, Mi1, and Tm3 cells. A simple model with a single low-pass filter was able to reproduce the calcium responses in non-direction-selective Mi1 and Tm3 cells, whereas a more complex model combining the output of two low-pass filters via a multiplication was required to reproduce T4c calcium responses. The direction selectivity for the simple model signals for T4c was lower compared to the multiplicative model. This suggests that the voltage-to-calcium transformation in Mi1 and Tm3 cells is different from those in T4c cells.

Differential expression of voltage-gated calcium channels in these cells could explain the different voltage to calcium transformation. The voltage-gated calcium channels mediate depolarization-induced calcium influx that drives the release of neurotransmitters. The $\alpha 1$-subunit of the voltage-gated calcium channels form the ion-conducting pore, which makes it distinct from other calcium channels. Three families of genes encode $\alpha 1$ subunits. *Drosophila* genome has one $\alpha 1$ subunit gene in each family: $\alpha 1D$ (Ca_v1), cac (Ca_v2), and $\alpha 1T$ (Ca_v3) (King 2007; Littleton & Ganetzky 2000). In *Drosophila* antennal lobe projection neurons, cac (Ca_v2) type and $\alpha 1T$ (Ca_v3) type voltage-gated calcium channels are involved in sustained and transient calcium currents, respectively (Gu *et al.* 2009; Iniguez *et al.* 2013). According to a RNA-sequencing study (Davis *et al.* 2020), $\alpha 1T$ (Ca_v3) mRNA have higher expression in Mi1 (2050.16 Transcripts per Million (TPM)) compared to T4 (686.68 TPM) and Tm3 (336.45 TPM). While cac (Ca_v2) mRNA have higher expression in T4 (1298.53 TPM) compared to Mi1 (986.25 TPM) and Tm3 (817.61 TPM). Different expressions of voltage-gated calcium channels could cause the different voltage to calcium transformations in non-direction selective and direction-selective cells.

3.6 CONCLUSION

In the course of this work, I investigated neural computation in the *Drosophila* motion vision pathway. Together with my co-authors, we showed that both the preferred direction enhancement and null direction suppression are implemented in all four subtypes of T4 and T5 cells. Already at the first stage of direction selectivity computation, this combined strategy ensures a high degree of direction selectivity. Additionally, we showed that the voltage-to-calcium transformations further enhance direction selectivity in the output signals of T4 cells in addition to the synaptic mechanisms at the dendrites. We built a model to transform voltage signals into calcium signals. The model was more complex for the direction-selective T4 cells compared to non-direction selective cells Mi1 and Tm3. Future work will focus on the comparison of voltage-gated calcium channels in these neurons which might lead to the observed differences in the voltage-to-calcium transformations.

BIBLIOGRAPHY

Ammer, G., Vieira, R. M., Fendl, S. & Borst, A. Anatomical distribution and functional roles of electrical synapses in Drosophila. *Current Biology* **32** (2022). doi: 10.1016/j.cub.2022.03.040

Arenz, A., Drews, M. S., Richter, F. G., Ammer, G. & Borst, A. The temporal tuning of the Drosophila motion detectors is determined by the dynamics of their input elements. *Current Biology* **27,** 929–944 (2017). doi: 10.1016/j.cub.2017.01.051

Baden, T., Berens, P., Bethge, M. & Euler, T. Spikes in mammalian bipolar cells support temporal layering of the inner retina. *Current Biology* **23,** 48–52 (2013). doi: 10.1016/j.cub.2012.11.006

Bahl, A., Ammer, G., Schilling, T. & Borst, A. Object tracking in motion-blind flies. *Nature neuroscience* **16,** 730–738 (2013). doi: 10.1038/nn.3386

Bahl, A., Serbe, E., Meier, M., Ammer, G. & Borst, A. Neural mechanisms for Drosophila contrast vision. *Neuron* **88,** 1240–1252 (2015). doi: 10.1016/j.neuron.2015.11.004

Barlow, H. B. & Hill, R. M. Selective sensitivity to direction of movement in ganglion cells of the rabbit retina. *Science* **139,** 412–414 (1963). doi: 10.1126/science.139.3553.412

Barlow & Levick, W. R. The mechanism of directionally selective units in rabbit's retina. *The Journal of physiology* **178,** 477 (1965). doi: 10.1113/jphysiol.1965.sp007638

Bath, D. E. *et al.* FlyMAD: rapid thermogenetic control of neuronal activity in freely walking Drosophila. *Nature methods* **11,** 756–762 (2014). doi: 10.1038/nmeth.2973

Behnia, R., Clark, D. A., Carter, A. G., Clandinin, T. R. & Desplan, C. Processing properties of ON and OFF pathways for Drosophila motion detection. *Nature* **512,** 427–430 (2014). doi: 10.1038/nature13427

Bellen, H. J., Tong, C. & Tsuda, H. 100 years of Drosophila research and its impact on vertebrate neuroscience: a history lesson for the future. *Nature Reviews Neuroscience* **11,** 514–522 (2010). doi: 10.1038/nrn2839

Bennett, M. V. & Zukin, R. S. Electrical coupling and neuronal synchronization in the mammalian brain. *Neuron* **41,** 495–511 (2004). doi: 10.1016/S0896-6273(04)00043-1

Borst, A. Drosophila's view on insect vision. *Current biology* **19,** R36–R47 (2009). doi: 10.1016/j.cub.2008.11.001

Borst, A., Drews, M. & Meier, M. The neural network behind the eyes of a fly. *Current Opinion in Physiology* **16,** 33–42 (2020). doi: 10.1016/j.cophys.2020.05.004

Borst, A. & Egelhaaf, M. Principles of visual motion detection. *Trends in neurosciences* **12,** 297–306 (1989). doi: 10.1016/0166-2236(89)90010-6

Borst, A., Haag, J. & Mauss, A. S. How fly neurons compute the direction of visual motion. *Journal of Comparative Physiology A* **206,** 109–124 (2020). doi: 10.1007/s00359-019-01375-9

Borst, A. & Helmstaedter, M. Common circuit design in fly and mammalian motion vision. *Nature neuroscience* **18,** 1067–1076 (2015). doi: 10.1038/nn.4050

Boyden, E. S., Zhang, F., Bamberg, E., Nagel, G. & Deisseroth, K. Millisecond-timescale, genetically targeted optical control of neural activity. *Nature neuroscience* **8,** 1263–1268 (2005). doi: 10.1038/nn1525

Brand, A. H. & Perrimon, N. Targeted gene expression as a means of altering cell fates and generating dominant phenotypes. *Development* **118,** 401–415 (1993). doi: 10.1242/dev.118.2.401

Briggman, K. L., Helmstaedter, M. & Denk, W. Wiring specificity in the direction-selectivity circuit of the retina. *Nature* **471,** 183–188 (2011). doi: 10.1038/nature09818

Brini, M., Cal, T., Ottolini, D. & Carafoli, E. Neuronal calcium signaling: function and dysfunction. *Cellular and molecular life sciences* **71,** 2787–2814 (2014). doi: 10.1007/s00018-013-1550-7

Broussard, G. J., Liang, R. & Tian, L. Monitoring activity in neural circuits with genetically encoded indicators. *Frontiers in molecular neuroscience* **7,** 97 (2014). doi: 10.3389/fnmol.2014.00097

Buchner, E., Buchner, S. & Bülthoff, I. Deoxyglucose mapping of nervous activity induced inDrosophila brain by visual movement. *Journal of Comparative Physiology A* **155,** 471–483 (1984). doi: 10.1007/BF00611912

Cao, G. *et al.* Genetically targeted optical electrophysiology in intact neural circuits. *Cell* **154,** 904–913 (2013). doi: 10.1016/j.cell.2013.07.027

Card, G. & Dickinson, M. H. Visually mediated motor planning in the escape response of Drosophila. *Current Biology* **18,** 1300–1307 (2008). doi: 10.1016/j.cub.2008.07.094

Catterall, W. A. Structure and regulation of voltage-gated Ca2+ channels. *Annual review of cell and developmental biology* **16,** 521–555 (2000). doi: 10.1146/annurev.cellbio.16.1.521

Catterall, W. A. Voltage-gated calcium channels. *Cold Spring Harbor perspectives in biology* **3,** a003947 (2011). doi: 10.1101/cshperspect.a003947

Chapman, E. R. Synaptotagmin: a Ca2+ sensor that triggers exocytosis? *Nature Reviews Molecular Cell Biology* **3,** 498–508 (2002). doi: 10.1038/nrm855

Chen, P., Nordstrom, W., Gish, B. & Abrams, J. M. grim, a novel cell death gene in Drosophila. *Genes & development* **10,** 1773–1782 (1996). doi: 10.1101/gad.10.14.1773

Chen *et al.* Ultrasensitive fluorescent proteins for imaging neuronal activity. *Nature* **499,** 295–300 (2013). doi: 10.1038/nature12354

Chiappe, M. E., Seelig, J. D., Reiser, M. B. & Jayaraman, V. Walking modulates speed sensitivity in Drosophila motion vision. *Current Biology* **20,** 1470–1475 (2010). doi: 10.1016/j.cub.2010.06.072

Clark, D. A., Bursztyn, L., Horowitz, M. A., Schnitzer, M. J. & Clandinin, T. R. Defining the computational structure of the motion detector in Drosophila. *Neuron* **70,** 1165–1177 (2011). doi: 10.1016/j.neuron.2011.05.023

Covarrubias, M., Wei, A. & Salkoff, L. Shaker, Shal, Shab, and Shaw express independent K+ current systems. *Neuron* **7,** 763–773 (1991). doi: 10.1016/0896-6273(91)90279-9

Davis, F. P. *et al.* A genetic, genomic, and computational resource for exploring neural circuit function. *Elife* **9,** e50901 (2020). doi: 10.7554/eLife.50901

Denk, W. *et al.* Anatomical and functional imaging of neurons using 2-photon laser scanning microscopy. *Journal of neuroscience methods* **54,** 151–162 (1994). doi: 10.1016/0165-0270(94)90189-9

Denk, W., Strickler, J. H. & Webb, W. W. Two-photon laser scanning fluorescence microscopy. *Science* **248,** 73–76 (1990). doi: 10.1126/science.2321027

Destexhe, A. Biophysics of Computation: Information Processing in Single Neurons, by Christof Koch. *Trends in Cognitive Sciences* **3,** 444 (1999). doi: 10.1016/S1364-6613(99)01380-7

Di Maio, V. Regulation of information passing by synaptic transmission: a short review. *Brain research* **1225,** 26–38 (2008). doi: 10.1016/j.brainres.2008.06.016

Douglass, J. K. & Strausfeld, N. J. Visual motion-detection circuits in flies: parallel direction-and non-direction-sensitive pathways between the medulla and lobula plate. *Journal of Neuroscience* **16,** 4551–4562 (1996). doi: 10.1523/JNEUROSCI.16-15-04551.1996

Drews, M. S. *et al.* Dynamic signal compression for robust motion vision in flies. *Current Biology* **30,** 209–221 (2020). doi: 10.1016/j.cub.2019.10.035

Eichner, H., Joesch, M., Schnell, B., Reiff, D. F. & Borst, A. Internal structure of the fly elementary motion detector. *Neuron* **70,** 1155–1164 (2011). doi: 10.1016/j.neuron.2011.03.028

Elstrott, J. *et al.* Direction selectivity in the retina is established independent of visual experience and cholinergic retinal waves. *Neuron* **58,** 499–506 (2008). doi: 10.1016/j.neuron.2008.03.013

Euler, T., Detwiler, P. B. & Denk, W. Directionally selective calcium signals in dendrites of starburst amacrine cells. *Nature* **418,** 845–852 (2002). doi: 10.1038/nature00931

Euler, T., Haverkamp, S., Schubert, T. & Baden, T. Retinal bipolar cells: elementary building blocks of vision. *Nature Reviews Neuroscience* **15,** 507–519 (2014). doi: 10.1038/nrn3783

Fendl, S., Vieira, R. M. & Borst, A. Conditional protein tagging methods reveal highly specific subcellular distribution of ion channels in motion-sensing neurons. *Elife* **9,** e62953 (2020). doi: 10.7554/eLife.62953

Fenk, L. M., Poehlmann, A. & Straw, A. D. Asymmetric processing of visual motion for simultaneous object and background responses. *Current Biology* **24,** 2913–2919 (2014). doi: 10.1016/j.cub.2014.10.042

Feske, S. Immunodeficiency due to defects in store-operated calcium entry. *Annals of the New York Academy of Sciences* **1238,** 74–90 (2011). doi: 10.1111/j.1749-6632.2011.06240.x

Fischbach, K.-F. & Dittrich, A. The optic lobe of Drosophila melanogaster. I. A Golgi analysis of wild-type structure. *Cell and tissue research* **258,** 441–475 (1989). doi: 10.1007/BF00218858

Fisher, Y., Silies, M. & Clandinin, T. R. Orientation selectivity sharpens motion detection in Drosophila. *Neuron* **88,** 390–402 (2015). doi: 10.1016/j.neuron.2015.09.033

Gjorgjieva, J., Sompolinsky, H. & Meister, M. Benefits of pathway splitting in sensory coding. *Journal of Neuroscience* **34,** 12127–12144 (2014). doi: 10.1523/JNEUROSCI.1032-14.2014

Govorunova, E. G., Sineshchekov, O. A., Janz, R., Liu, X. & Spudich, J. L. Natural light-gated anion channels: A family of microbial rhodopsins for advanced optogenetics. *Science* **349,** 647–650 (2015). doi: 10.1126/science.aaa7484

Grether, M. E., Abrams, J. M., Agapite, J., White, K. & Steller, H. The head involution defective gene of Drosophila melanogaster functions in programmed cell death. *Genes & development* **9,** 1694–1708 (1995). doi: 10.1101/gad.9.14.1694

Grienberger, C., Giovannucci, A., Zeiger, W. & Portera-Cailliau, C. Two-photon calcium imaging of neuronal activity. *Nature Reviews Methods Primers* **2,** 1–23 (2022). doi: 10.1038/s43586-022-00147-1

Groschner, L. N., Hak, L. C. W., Bogacz, R., DasGupta, S. & Miesenböck, G. Dendritic integration of sensory evidence in perceptual decision-making. *Cell* **173,** 894–905 (2018). doi: 10.1016/j.cell.2018.03.075

Groschner, L. N., Malis, J. G., Zuidinga, B. & Borst, A. A biophysical account of multiplication by a single neuron. *Nature* **603,** 119–123 (2022). doi: 10.1038/s41586-022-04428-3

Grover, D., Katsuki, T. & Greenspan, R. J. Flyception: imaging brain activity in freely walking fruit flies. *Nature methods* **13,** 569–572 (2016). doi: 10.1038/nmeth.3866

Gruntman, E., Romani, S. & Reiser, M. B. Simple integration of fast excitation and offset, delayed inhibition computes directional selectivity in Drosophila. *Nature neuroscience* **21,** 250–257 (2018). doi: 10.1038/s41593-017-0046-4

Gu, H. *et al.* Cav2-type calcium channels encoded by cac regulate AP-independent neurotransmitter release at cholinergic synapses in adult Drosophila brain. *Journal of neurophysiology* **101,** 42–53 (2009). doi: 10.1152/jn.91103.2008

Gutman, G. A. *et al.* International Union of Pharmacology. LIII. Nomenclature and molecular relationships of voltage-gated potassium channels. *Pharmacological reviews* **57,** 473–508 (2005). doi: 10.1124/pr.57.4.10

Haag, J., Arenz, A., Serbe, E., Gabbiani, F. & Borst, A. Complementary mechanisms create direction selectivity in the fly. *Elife* **5,** e17421 (2016). doi: 10.7554/eLife.17421

Haag, J. & Borst, A. Active membrane properties and signal encoding in graded potential neurons. *Journal of Neuroscience* **18,** 7972–7986 (1998). doi: 10.1523/JNEUROSCI.18-19-07972.1998

Haag, J., Mishra, A. & Borst, A. A common directional tuning mechanism of Drosophila motion-sensing neurons in the ON and in the OFF pathway. *Elife* **6,** e29044 (2017). doi: 10.7554/eLife.29044

Haag, J., Wertz, A. & Borst, A. Central gating of fly optomotor response. *Proceedings of the National Academy of Sciences* **107,** 20104–20109 (2010). doi: 10.1073/pnas.1009381107

Hamada, F. N. *et al.* An internal thermal sensor controlling temperature preference in Drosophila. *Nature* **454,** 217–220 (2008). doi: 10.1038/nature07001

Hamill, O. P., Marty, A., Neher, E., Sakmann, B. & Sigworth, F. J. Improved patch-clamp techniques for high-resolution current recording from cells and cell-free membrane patches. *Pflügers Archiv* **391,** 85–100 (1981). doi: 10.1007/BF00656997

Hardie, R. C. A histamine-activated chloride channel involved in neurotransmission at a photoreceptor synapse. *Nature* **339,** 704–706 (1989). doi: 10.1038/339704a0

Hardie, R. C. & Juusola, M. Phototransduction in drosophila. *Current opinion in neurobiology* **34,** 37–45 (2015). doi: 10.1016/j.conb.2015.01.008

Hardie, R. C. & Raghu, P. Visual transduction in Drosophila. *Nature* **413,** 186–193 (2001). doi: 10.1038/35093002

Hassenstein, B. & Reichardt, W. Systemtheoretische analyse der zeit-, reihenfolgen-und vorzeichenauswertung bei der bewegungsperzeption des rüsselkäfers chlorophanus. *Zeitschrift für Naturforschung B* **11,** 513–524 (1956). doi: 10.1515/znb-1956-9-1004

Hausen, K. Functional characterization and anatomical identification of motion sensitive neurons in the lobula plate of the blowfly Calliphora erythrocephala. *Zeitschrift für Naturforschung c* **31,** 629–634 (1976). doi: 10.1515/znc-1976-9-1001

Hodgkin, A. L. & Huxley, A. F. A quantitative description of membrane current and its application to conduction and excitation in nerve. *The Journal of physiology* **117,** 500 (1952). doi: 10.1113/jphysiol.1952.sp004764

Hofmann, F., Lacinova, L. & Klugbauer, N. Voltage-dependent calcium channels: from structure to function. *Reviews of Physiology, Biochemistry and Pharmacology, Volume 139,* 33–87 (1999). doi: 10.1007/BFb0033648

Hopp, E., Borst, A. & Haag, J. Subcellular mapping of dendritic activity in optic flow processing neurons. *Journal of Comparative Physiology A* **200,** 359–370 (2014). doi: 10.1007/s00359-014-0893-3

Huston, S. J. & Krapp, H. G. Nonlinear integration of visual and haltere inputs in fly neck motor neurons. *Journal of Neuroscience* **29,** 13097–13105 (2009). doi: 10.1523/JNEUROSCI.2915-09.2009

Iniguez, J., Schutte, S. S. & O'Dowd, D. K. Cav3-type $\alpha 1$T calcium channels mediate transient calcium currents that regulate repetitive firing in Drosophila antennal lobe PNs. *Journal of neurophysiology* **110,** 1490–1496 (2013). doi: 10.1152/jn.00368.2013

Jenett, A. *et al.* A GAL4-driver line resource for Drosophila neurobiology. *Cell reports* **2,** 991–1001 (2012). doi: 10.1016/j.celrep.2012.09.011

Jin, L. *et al.* Single action potentials and subthreshold electrical events imaged in neurons with a fluorescent protein voltage probe. *Neuron* **75,** 779–785 (2012). doi: 10.1016/j.neuron.2012.06.040

Joesch, M., Plett, J., Borst, A. & Reiff, D. F. Response properties of motion-sensitive visual interneurons in the lobula plate of Drosophila melanogaster. *Current Biology* **18,** 368–374 (2008).
doi: 10.1016/j.cub.2008.02.022

Joesch, M., Schnell, B., Raghu, S. V., Reiff, D. F. & Borst, A. ON and OFF pathways in Drosophila motion vision. *Nature* **468,** 300–304 (2010).
doi: 10.1038/nature09545

Joesch, M., Weber, F., Eichner, H. & Borst, A. Functional specialization of parallel motion detection circuits in the fly. *Journal of Neuroscience* **33,** 902–905 (2013). doi: 10.1523/JNEUROSCI.3374-12.2013

Johns, D. C., Marx, R., Mains, R. E., O'Rourke, B. & Marbán, E. Inducible genetic suppression of neuronal excitability. *Journal of Neuroscience* **19,** 1691–1697 (1999). doi: 10.1523/JNEUROSCI.19-05-01691.1999

Jung, S. N., Borst, A. & Haag, J. Flight activity alters velocity tuning of fly motion-sensitive neurons. *Journal of Neuroscience* **31,** 9231–9237 (2011). doi: 10.1523/JNEUROSCI.1138-11.2011

Kim *et al.* Space–time wiring specificity supports direction selectivity in the retina. *Nature* **509,** 331–336 (2014). doi: 10.1038/nature13240

King, G. F. Modulation of insect CaV channels by peptidic spider toxins. *Toxicon* **49,** 513–530 (2007). doi: 10.1016/j.toxicon.2006.11.012

Kirschfeld, K. Die Projektion der optischen Umwelt auf das Raster der Rhabdomere im Komplexauge von Musca. *Experimental Brain Research* **3,** 248–270 (1967). doi: 10.1007/BF00235588

Kitamoto, T. Conditional modification of behavior in Drosophila by targeted expression of a temperature-sensitive shibire allele in defined neurons. *Journal of neurobiology* **47,** 81–92 (2001). doi: 10.1002/neu.1018

Krapp, H. G., Hengstenberg, B. & Hengstenberg, R. Dendritic structure and receptive-field organization of optic flow processing interneurons in the fly. *Journal of neurophysiology* **79,** 1902–1917 (1998). doi: 10.1152/jn.1998.79.4.1902

Land, M. F. Visual acuity in insects. *Annual review of entomology* **42,** 147–177 (1997). doi: 10.1146/annurev.ento.42.1.147

Littleton, J. T. & Ganetzky, B. Ion channels and synaptic organization: analysis of the Drosophila genome. *Neuron* **26,** 35–43 (2000).
doi: 10.1016/s0896-6273(00)81135-6

Liu, Q. *et al.* Gap junction networks in mushroom bodies participate in visual learning and memory in Drosophila. *Elife* **5,** e13238 (2016). doi: 10.7554/eLife.13238

Luan, H., Peabody, N. C., Vinson, C. R. & White, B. H. Refined spatial manipulation of neuronal function by combinatorial restriction of transgene expression. *Neuron* **52,** 425–436 (2006). doi: 10.1016/j.neuron.2006.08.028

Luo, L. *Principles of Neurobiology* (Garland Science, 2020). doi: 10.1201/9781003053972

Maimon, G. Modulation of visual physiology by behavioral state in monkeys, mice, and flies. *Current opinion in neurobiology* **21,** 559–564 (2011). doi: 10.1016/j.conb.2011.05.001

Maimon, G., Straw, A. D. & Dickinson, M. H. Active flight increases the gain of visual motion processing in Drosophila. *Nature neuroscience* **13,** 393–399 (2010). doi: 10.1038/nn.2492

Maisak, M. S. *et al.* A directional tuning map of Drosophila elementary motion detectors. *Nature* **500,** 212–216 (2013). doi: 10.1038/nature12320

Mamiya, A., Straw, A. D., Tómasson, E. & Dickinson, M. H. Active and passive antennal movements during visually guided steering in flying Drosophila. *Journal of Neuroscience* **31,** 6900–6914 (2011). doi: 10.1523/JNEUROSCI.0498-11.2011

Masland, R. H. The neuronal organization of the retina. *Neuron* **76,** 266–280 (2012). doi: 10.1016/j.neuron.2012.10.002

Masu, M. *et al.* Specific deficit of the ON response in visual transmission by targeted disruption of the mGIuR6 gene. *Cell* **80,** 757–765 (1995). doi: 10.1016/0092-8674(95)90354-2

Mauss, A. S., Busch, C. & Borst, A. Optogenetic neuronal silencing in Drosophila during visual processing. *Scientific reports* **7,** 1–12 (2017). doi: 10.1038/s41598-017-14076-7

Mauss, A. S., Meier, M., Serbe, E. & Borst, A. Optogenetic and pharmacologic dissection of feedforward inhibition in Drosophila motion vision. *Journal of Neuroscience* **34,** 2254–2263 (2014). doi: 10.1523/JNEUROSCI.3938-13.2014

Mauss, A. S. *et al.* Neural circuit to integrate opposing motions in the visual field. *Cell* **162,** 351–362 (2015). doi: 10.1016/j.cell.2015.06.035

McCormick, D. A. Functional properties of a slowly inactivating potassium current in guinea pig dorsal lateral geniculate relay neurons. *Journal of Neurophysiology* **66,** 1176–1189 (1991). doi: 10.1152/jn.1991.66.4.1176

Meier, M. & Borst, A. Extreme compartmentalization in a Drosophila amacrine cell. *Current Biology* **29,** 1545–1550 (2019). doi: 10.1016/j.cub.2019.03.070

Miyashita, T. *et al.* Mg2+ block of Drosophila NMDA receptors is required for long-term memory formation and CREB-dependent gene expression. *Neuron* **74,** 887–898 (2012). doi: 10.1016/j.neuron.2012.03.039

Mohammad, F. *et al.* Optogenetic inhibition of behavior with anion channelrhodopsins. *Nature methods* **14,** 271–274 (2017). doi: 10.1038/nmeth.4148

Molina-Obando, S. *et al.* ON selectivity in the Drosophila visual system is a multisynaptic process involving both glutamatergic and GABAergic inhibition. *Elife* **8,** e49373 (2019). doi: 10.7554/eLife.49373

Murata, Y., Iwasaki, H., Sasaki, M., Inaba, K. & Okamura, Y. Phosphoinositide phosphatase activity coupled to an intrinsic voltage sensor. *Nature* **435,** 1239–1243 (2005). doi: 10.1038/nature03650

Nagai, T., Sawano, A., Park, E. S. & Miyawaki, A. Circularly permuted green fluorescent proteins engineered to sense Ca2+. *Proceedings of the National Academy of Sciences* **98,** 3197–3202 (2001). doi: 10.1073/pnas.051636098

Nagel, G. *et al.* Light activation of channelrhodopsin-2 in excitable cells of Caenorhabditis elegans triggers rapid behavioral responses. *Current Biology* **15,** 2279–2284 (2005). doi: 10.1016/j.cub.2005.11.032

Otsuna, H. & Ito, K. Systematic analysis of the visual projection neurons of Drosophila melanogaster. I. Lobula-specific pathways. *Journal of Comparative Neurology* **497,** 928–958 (2006). doi: 10.1002/cne.21015

Pankova, K. & Borst, A. Transgenic line for the identification of cholinergic release sites in Drosophila melanogaster. *Journal of Experimental Biology* **220,** 1405–1410 (2017). doi: 10.1242/jeb.149369

Papazian, D. M., Schwarz, T. L., Tempel, B. L., Jan, Y. N. & Jan, L. Y. Cloning of genomic and complementary DNA from Shaker, a putative potassium channel gene from Drosophila. *Science* **237,** 749–753 (1987). doi: 10.1126/science.2441470

Pavlou, H. J. & Goodwin, S. F. Courtship behavior in Drosophila melanogaster: towards a 'courtship connectome'. *Current opinion in neurobiology* **23,** 76–83 (2013). doi: 10.1016/j.conb.2012.09.002

Pfeiffer, B. D. *et al.* Refinement of tools for targeted gene expression in Drosophila. *Genetics* **186,** 735–755 (2010). doi: 10.1534/genetics.110.119917

Pfeiffer, B. D. *et al.* Tools for neuroanatomy and neurogenetics in Drosophila. *Proceedings of the National Academy of Sciences* **105,** 9715–9720 (2008). doi: 10.1073/pnas.0803697105

Piggott, B. J. *et al.* Paralytic, the Drosophila voltage-gated sodium channel, regulates proliferation of neural progenitors. *Genes & development* **33,** 1739–1750 (2019). doi: 10.1101/gad.330597.119

Pulver, S. R., Pashkovski, S. L., Hornstein, N. J., Garrity, P. A. & Griffith, L. C. Temporal dynamics of neuronal activation by Channelrhodopsin-2 and TRPA1 determine behavioral output in Drosophila larvae. *Journal of neurophysiology* **101,** 3075–3088 (2009). doi: 10.1152/jn.00071.2009

Putney Jr, J. W. A model for receptor-regulated calcium entry. *Cell calcium* **7,** 1–12 (1986). doi: 10.1016/0143-4160(86)90026-6

Raji, J. I. & Potter, C. J. The number of neurons in Drosophila and mosquito brains. *PLoS One* **16,** e0250381 (2021). doi: 10.1371/journal.pone.0250381

Ready, D. F., Hanson, T. E. & Benzer, S. Development of the Drosophila retina, a neurocrystalline lattice. *Developmental biology* **53,** 217–240 (1976). doi: 10.1016/0012-1606(76)90225-6

Reiff, D. F., Plett, J., Mank, M., Griesbeck, O. & Borst, A. Visualizing retinotopic half-wave rectified input to the motion detection circuitry of Drosophila. *Nature neuroscience* **13,** 973–978 (2010). doi: 10.1038/nn.2595

Richter, F. G., Fendl, S., Haag, J., Drews, M. S. & Borst, A. Glutamate signaling in the fly visual system. *IScience* **7,** 85–95 (2018). doi: 10.1016/j.isci.2018.08.019

Rivera-Alba, M. *et al.* Wiring economy and volume exclusion determine neuronal placement in the Drosophila brain. *Current Biology* **21,** 2000–2005 (2011). doi: 10.1016/j.cub.2011.10.022

Rubin, G. M. & Spradling, A. C. Genetic transformation of Drosophila with transposable element vectors. *Science* **218,** 348–353 (1982). doi: 10.1126/science.6289436

Ryu, L., Kim, S. Y. & Kim, A. J. From Photons to Behaviors: Neural Implementations of Visual Behaviors in Drosophila. *Frontiers in Neuroscience* **16** (2022). doi: 10.3389/fnins.2022.883640

Sandeman, D. C. & Markl, H. Head movements in flies (Calliphora) produced by deflexion of the halteres. *Journal of Experimental Biology* **85,** 43–60 (1980). doi: 10.1242/jeb.85.1.43

Schilling, T. & Borst, A. Local motion detectors are required for the computation of expansion flow-fields. *Biology open* **4,** 1105–1108 (2015). doi: 10.1242/bio.012690

Schnell, B., Raghu, S. V., Nern, A. & Borst, A. Columnar cells necessary for motion responses of wide-field visual interneurons in Drosophila. *Journal of Comparative Physiology A* **198,** 389–395 (2012). doi: 10.1007/s00359-012-0716-3

Schnell, B. *et al.* Processing of horizontal optic flow in three visual interneurons of the Drosophila brain. *Journal of neurophysiology* **103,** 1646–1657 (2010). doi: 10.1152/jn.00950.2009

Scott, E. K., Raabe, T. & Luo, L. Structure of the vertical and horizontal system neurons of the lobula plate in Drosophila. *Journal of Comparative Neurology* **454,** 470–481 (2002). doi: 10.1002/cne.10467

Serbe, E., Meier, M., Leonhardt, A. & Borst, A. Comprehensive characterization of the major presynaptic elements to the Drosophila OFF motion detector. *Neuron* **89,** 829–841 (2016). doi: 10.1016/j.neuron.2016.01.006

Shinomiya, K. *et al.* Candidate neural substrates for off-edge motion detection in Drosophila. *Current Biology* **24,** 1062–1070 (2014). doi: 10.1016/j.cub.2014.03.051

Shinomiya, K. *et al.* Comparisons between the ON-and OFF-edge motion pathways in the Drosophila brain. *Elife* **8,** e40025 (2019). doi: 10.7554/eLife.40025

Silies, M. *et al.* Modular use of peripheral input channels tunes motion-detecting circuitry. *Neuron* **79,** 111–127 (2013). doi: 10.1016/j.neuron.2013.04.029

Stebbings, L. A. *et al.* Gap junctions in Drosophila: developmental expression of the entire innexin gene family. *Mechanisms of development* **113,** 197–205 (2002). doi: 10.1016/S0925-4773(02)00025-4

Stowers, J. R. *et al.* Reverse engineering animal vision with virtual reality and genetics. *Computer* **47,** 38–45 (2014). doi: 10.1109/MC.2014.190

Strausfeld, N. J. The organization of the insect visual system (Light microscopy). *Zeitschrift für Zellforschung und mikroskopische Anatomie* **121,** 377–441 (1971). doi: 10.1007/BF00337640

Strausfeld, N. J. & Lee. Neuronal basis for parallel visual processing in the fly. *Visual neuroscience* **7,** 13–33 (1991). doi: 10.1017/S0952523800010919

Straw, A. D., Branson, K., Neumann, T. R. & Dickinson, M. H. Multi-camera real-time three-dimensional tracking of multiple flying animals. *Journal of The Royal Society Interface* **8,** 395–409 (2011). doi: 10.1098/rsif.2010.0230

Strother, J. A., Nern, A. & Reiser, M. B. Direct observation of ON and OFF pathways in the Drosophila visual system. *Current Biology* **24,** 976–983 (2014). doi: 10.1016/j.cub.2014.03.017

Strother, J. A. *et al.* Behavioral state modulates the ON visual motion pathway of Drosophila. *Proceedings of the National Academy of Sciences* **115,** E102–E111 (2018). doi: 10.1073/pnas.1703090115

Strother, J. A. *et al.* The emergence of directional selectivity in the visual motion pathway of Drosophila. *Neuron* **94,** 168–182 (2017). doi: 10.1016/j.neuron.2017.03.010

Svoboda, K. & Yasuda, R. Principles of two-photon excitation microscopy and its applications to neuroscience. *Neuron* **50,** 823–839 (2006). doi: 10.1016/j.neuron.2006.05.019

Sweeney, S. T., Broadie, K., Keane, J., Niemann, H. & O'Kane, C. J. Targeted expression of tetanus toxin light chain in Drosophila specifically eliminates synaptic transmission and causes behavioral defects. *Neuron* **14,** 341–351 (1995). doi: 10.1016/0896-6273(95)90290-2

Takemura, S.-y., Lu, Z. & Meinertzhagen, I. A. Synaptic circuits of the Drosophila optic lobe: the input terminals to the medulla. *Journal of Comparative Neurology* **509,** 493–513 (2008). doi: 10.1002/cne.21757

Takemura, S.-y. *et al.* Cholinergic circuits integrate neighboring visual signals in a Drosophila motion detection pathway. *Current biology* **21,** 2077–2084 (2011). doi: 10.1016/j.cub.2011.10.053

Takemura, S.-y. *et al.* The comprehensive connectome of a neural substrate for 'ON'motion detection in Drosophila. *Elife* **6,** e24394 (2017). doi: 10.7554/eLife.24394

Tuthill, J. C., Nern, A., Holtz, S. L., Rubin, G. M. & Reiser, M. B. Contributions of the 12 neuron classes in the fly lamina to motion vision. *Neuron* **79,** 128–140 (2013). doi: 10.1016/j.neuron.2013.05.024

Wienecke, C. F., Leong, J. C. & Clandinin, T. R. Linear summation underlies direction selectivity in Drosophila. *Neuron* **99,** 680–688 (2018). doi: 10.1016/j.neuron.2018.07.005

Wilson, R. I., Turner, G. C. & Laurent, G. Transformation of olfactory representations in the Drosophila antennal lobe. *Science* **303,** 366–370 (2004). doi: 10.1126/science.1090782

Wu, M. *et al.* Visual projection neurons in the Drosophila lobula link feature detection to distinct behavioral programs. *Elife* **5,** e21022 (2016). doi: 10.7554/eLife.21022

Yang, H. H. *et al.* Subcellular imaging of voltage and calcium signals reveals neural processing in vivo. *Cell* **166,** 245–257 (2016). doi: 10.1016/j.cell.2016.05.031

Yoshida, K. *et al.* A key role of starburst amacrine cells in originating retinal directional selectivity and optokinetic eye movement. *Neuron* **30,** 771–780 (2001). doi: 10.1016/S0896-6273(01)00316-6

Zhu, Y. The Drosophila visual system: From neural circuits to behavior. *Cell adhesion & migration* **7,** 333–344 (2013). doi: 10.4161/cam.25521

ACKNOWLEDGEMENTS

First and foremost, I would like to thank Axel for giving me the opportunity to work in his lab. He provided excellent supervision, guidance, and support when I needed it the most. As I worked on my scientific ideas and projects, he always gave me freedom but also guided me in the right direction when necessary. Thank you Axel for constantly motivating me throughout my Ph.D. It would not have been possible for me to complete my Ph.D. without your consistent support over the past five years. Next, I would like to thank Jürgen Haag (Bulle) for providing me with direct supervision and being a co-author of both of my research papers. Without your support, I could not have published these papers. I also want to thank him for helping me build the two-photon microscope setup and troubleshooting the recurring problems at the setup. I would like to thank Lukas Groschner and Bulle for reviewing my thesis.

Thanks to the Graduate School of Systemic Neurosciences (GSN) team for organizing a variety of scientific and non-scientific events. Additionally, I am grateful to my TAC members Ruben Portugues and Laura Busse for their useful advice and stimulating discussions regarding my projects. I want to thank all the members of the Borst lab for creating a wonderful environment of work in the lab. I would like to thank Michael Drews for helping with the software for the stimulus arena and establishing the analysis pipeline. I want to thank members of the P7 office Florian Richter, Michael Drews, Nadya Pirogova, and Anna Schützenberger for creating a wonderful atmosphere when I had newly joined the lab.

I want to thank my parents Arjunanand Mishra and Indu Mishra for all the personal sacrifices they made to support me throughout my academic journey. I also want to thank my brother Ashish and sister Anjali. Last but not the least, I want to thank my wife Manvi for providing support in the final year of my Ph.D. I would always be thankful to my family. Without their patience and support, I would not have been able to pursue my Ph.D.

CURRICULUM VITAE

EDUCATION

- 2017–present: PhD student at Graduate School for Systemic Neurosciences (LMU Munich)/Max-Planck-Institute for Neurobiology, Germany; supervised by Prof. Dr. Alexander Borst
- 2011–2016: B.Tech/M.Tech in Biotechnology and Biochemical Engineering at the Indian Institute of Technology (IIT) Kharagpur, India

RESEARCH INTERNSHIPS

- 2015: University of British Columbia, Vancouver, Canada
- 2014: University of Alberta, Edmonton, Canada
- 2013: Indian Institute of Science, Bangalore, India

MAJOR AWARDS/FELLOWSHIPS

- Graduate school of systemic neurosciences (GSN-LMU) fast-track Ph.D. fellowship *2016*
- MITACS Globalink fellowship, Canada *2015*
- University of Alberta research experience fellowship *2014*
- Indian Academy of Sciences summer research fellowship *2013*

PERSONAL INFORMATION

- Birthday: 20th April 1992
- Languages: Hindi (native), Nepali (native), English (fluent), German (beginner)

PUBLICATIONS

- Haag, J., **Mishra, A.**, and Borst, A. "A common directional tuning mechanism of *Drosophila* motion-sensing neurons in the ON and in the OFF pathway" *eLife* (2017)

- **Mishra, A.**, Serbe-Kamp, E., Borst, A., and Haag, J. “Voltage to calcium transformation enhances direction selectivity in *Drosophila* T4 neurons" J. Neuroscience (2023)

AFFIDAVIT

Hiermit versichere ich an Eides statt, dass ich die vorliegende Dissertation **Neural information processing in the *Drosophila* motion vision pathway** selbstständig angefertigt habe, mich außer der angegebenen keiner weiteren Hilfsmittel bedient und alle Erkenntnisse, die aus dem Schrifttum ganz oder annähernd übernommen sind, als solche kenntlich gemacht und nach ihrer Herkunft unter Bezeichnung der Fundstelle einzeln nachgewiesen habe.

I hereby confirm that the dissertation **Neural information processing in the *Drosophila* motion vision pathway** is the result of my own work and that I have only used sources or materials listed and specified in the dissertation.

....	....
München, 12.10.2022	Abhishek Mishra
Munich, 12.10.2022	Unterschrift
	Signature

CONTRIBUTIONS

- Juergen Haag, **Abhishek Mishra** and Alexander Borst (2017). A common directional tuning mechanism of *Drosophila* motion-sensing neurons in the ON and in the OFF pathway. *eLife* 6:e29044.
    - Juergen Haag, Conceptualization, Data curation, Software, Investigation, Visualization, Writing, review and editing; Abhishek Mishra, Software, Investigation (collected and analysed data for figure 4), Visualization (figure 4); Alexander Borst, Conceptualization, Funding acquisition, Writing original draft, Project administration, Writing, review and editing
- **Abhishek Mishra**, Alexander Borst, and Juergen Haag (2022). Voltage to Calcium Transformation Enhances Direction Selectivity in *Drosophila* T4 neurons. *bioRxiv*.
    - Abhishek Mishra, Conceptualization, Investigation, Data curation, Software, Visualization, Writing original draft, review and editing; Juergen Haag, Conceptualization, Data curation, Software, Investigation, review and editing; Alexander Borst, Conceptualization, Funding acquisition, Project administration, Review and editing

……………………	……………………
Abhishek Mishra	Juergen Haag Co-author

……………………
Prof. Dr. Alexander Borst
Supervisor